Shape characterisation of tool path motion

by

Luke Chanda

A thesis submitted to the
Faculty of Engineering of
The University of Birmingham
for the degree of
DOCTOR OF PHILOSOPHY

Geometric Modelling Group
Department of Mechanical Engineering
School of Engineering
The University of Birmingham
Edgbaston
Birmingham B15 2TT
UK

January 2018

UNIVERSITY OF
BIRMINGHAM

University of Birmingham Research Archive

e-theses repository

This unpublished thesis/dissertation is copyright of the author and/or third parties. The intellectual property rights of the author or third parties in respect of this work are as defined by The Copyright Designs and Patents Act 1988 or as modified by any successor legislation.

Any use made of information contained in this thesis/dissertation must be in accordance with that legislation and must be properly acknowledged. Further distribution or reproduction in any format is prohibited without the permission of the copyright holder.

Synopsis

The dominant approach to regulate tool path motion is to allow the controller of a given machine to autonomously adjust both the intended shape and kinematics. For a given application, the autonomous regulation of motion can produce undesirable and unknown machining conditions. Parameters may therefore need to be optimised using machinist experience. Indeed, the methods employed are often iterative and informed by empirical evidence from machining trials. Such *a posteriori* attempts to obtain suitable machining conditions are heuristic and time intensive.

A shape characterisation of tool path motion is postulated by enforcing constraints on the general vector equations describing velocity, acceleration and jerk. The resulting description of tool path motion depends only upon the kinematic limits of a machine and the intrinsic shape properties of a tool path. Both sets of parameters may be identified prior to physical machining.

The shape characteristic equations describing tool path motion are consolidated into a series of diagrams, referred as shape schematics. These shape schematics provide a complete illustration of the distinctive features of each of the kinematic vectors. Kinematic profiles, derived from a series of test tool path motions are compared with the shape schematics in order to provide supportive empirical evidence.

The main contribution of this thesis is to demonstrate *a priori* shape characterisation of tool path motion. This characterisation is achieved without knowledge of the motion control algorithms implemented by a given machine's controller. The characterisation may be employed to inform the selection of machining parameters and thereby reduce the time and the number of machining trials.

To my aunt

Sophia

Acknowledgements

I would like to express my sincere gratitude to my supervisor Dr Robert J. Cripps. I am truly grateful for his endless patience, unwavering support and thoughtful advice throughout my PhD. I feel extremely fortunate and privileged to have had his supervision both in my undergraduate and postgraduate degrees.

I would also like to acknowledge all the members of the Geometric Modelling Group. In particular, I would like to thank Dr Benjamin Cross and Dr Xiaogeng Jiang. Both always made time for me. They were always willing to share their advice and own experiences in research.

Many thanks also go to Mr Andrew Loat, Dr Oluremi Olatunbosun and Dr Richard Hood for their generous help with my experiments.

Contents

List of Publications

The following articles have been published as a result of the research presented in this thesis.

1. Title: Toolpath Geometry and High Speed Machine Axis Motion

   Authors: L. Chanda and R. J. Cripps

   Conference: Proceedings of the 14th International Conference on Manufacturing Research

   Year: 2016

   Volume: 3

   Pages: 7–12

2. Title: Characterising the effects of shape on tool path motion

   Authors: R. J. Cripps and L. Chanda

   Journal: International Journal of Machine Tools and Manufacture

   Year: 2018

   Volume: 132

   Pages: 17–35

List of Figures

List of Tables

Nomenclature

α	Gradient of the curvature profile
$\bar{\Psi}$	Average centripetal acceleration
β	Initial curvature
δ	Angle between the workpiece's unit surface normal vector that passes through the cutter contact point and the unit vector that passes through the cutter location point
ε	Interpolation error
Γ_0	An osculating curve to a tool path
Γ_λ	A family of curves which intersect a tool path at a given point
$\hat{a}$	Acceleration in the frequency domain
κ	Scalar curvature
κ_c	Constant curvature
κ_g	Geodesic curvature
κ_i	Test curvature value

κ_n Normal curvature

κ_α Transition curvature

κ_{max} Maximum curvature

κ_{min} Minimum curvature

$\hat{\mathbf{b}}$ Unit binormal vector

$\hat{\mathbf{N}}$ Unit surface normal vector

$\hat{\mathbf{n}}$ Principal unit normal vector

$\hat{\mathbf{n}}_0$ Unit vector that passes through the cutter contact point and is directed perpendicular to the workpiece's surface

$\hat{\mathbf{n}}_1$ Unit vector that passes through the cutter location point and is directed parallel to the spindle axis

$\hat{\mathbf{T}}$ Unit bi-tangent vector

$\hat{\mathbf{t}}$ Unit tangent vector

$\boldsymbol{\kappa}$ Curvature vector

$\mathbf{a}$ Acceleration vector

$\mathbf{F}$ Resultant force

$\mathbf{F}_1$ Frenet frame

$\mathbf{F}_2$ Darboux frame

$\mathbf{j}$	Jerk vector
$\mathbf{r}$	Position vector
$\mathbf{v}$	Velocity vector
Ω	Winding angle
ϕ	Angle between the Frenet and Darboux frames
$\prod_c$	Cleaver plane
$\prod_n$	Normal plane
$\prod_o$	Osculating plane
$\prod_r$	Rectifying plane
$\prod_t$	Tangent plane
Ψ_1	Constant commanded feed rate
Ψ_2	Centripetal acceleration limit
σ_Ψ	Standard deviation of centripetal acceleration values
τ	Scalar torsion
τ_g	Geodesic torsion
θ_0	Initial angle made by the path with x-axis
Υ	Servomotor torque
Υ_{max}	Servomotor maximum torque

ε_B Integration error bound

a_n Centripetal acceleration

a_x $x-$ Axis acceleration

a_y $y-$ Axis acceleration

f_s Frequency

G^0 Position continuity

G^1 Tangent continuity

G^2 Curvature continuity

H Hermite blend

I Axis inertia

j_b Scalar binormal jerk

j_n Scalar normal jerk

j_t Scalar tangential jerk

K Constant curvature

L Total length of the path

L_{arc} Circular arc segment length

L_{line} Linear segment length

L_{min} Minimum segment length

m	Mass
N	Number of samples
P	Servomotor power
P_{max}	Servomotor maximum power
r	Radius of circle
s	Arc length
s_x	$x-$ Axis displacement
s_y	$y-$ Axis displacement
s_{max}	Upper arc length limit
s_{min}	Lower arc length limit
T	Total motion time
t	Time
t_a	Achieved time
t_i	Discrete time value
T_m	Time taken to process and execute a cutting tool's movement between consecutive positions
T_p	Controller minimum processing time
t_r	Requested time

t_{av} Average time

u Arbitrary parameter

v Feed rate

v_a Achieved feed rate

v_b Backward integration velocity

v_c Constant feed rate

v_f Forward integration velocity

v_x $x-$ Axis velocity

v_y $y-$ Axis velocity

v_{max} Maximum feed rate

x_0 Initial x-axis position

y_0 Initial y-axis position

Chapter 1

Introduction

Unknown controller regulation of tool path motion can produce unacceptable manufactured components [1]. Such instances can call for the heuristic and iterative modification of the machining parameters associated with cutting tool and workpiece movements [2]. This in turn diminishes material and energy resources, thus reducing the efficiency and productivity of the manufacturing process [2]. This thesis addresses the issue by developing a shape characterisation of tool path motion that provides a description of motion that is independent of the motion control algorithms implemented by a given machine. The resulting shape schematics may be employed in a pre-processing manner to inform the selection of parameters without the need for physical machining [1].

To develop and verify this *a priori* approach to motion characterisation, this thesis begins the introductory chapter by providing an overview of the *Computer-aided Design and Manufacturing process* (CAD/CAM). A tool path and its function within CAD/CAM are then defined

and discussed. This is then followed by a review of the current approaches employed by machine controllers to regulate motion. The effects of shape on tool path motion are emphasised throughout the literature review. This then motivates the research aim which is stated in section 1.4. The chapter concludes with a brief discussion of the possible impact of the research.

1.1 Computer-aided Design and Manufacturing

Computers can be used to help manufacture components [3]. The sequential steps through which a conceptual design becomes a physical component are collectively referred to as the CAD/CAM [3]. This thesis is concerned with the use of CAD/CAM in the context of controlled material removal processes, specifically milling. The general aims of CAD/CAM in subtractive manufacturing are to produce components in smaller time periods, to a higher dimensional accuracy and with as little financial expense as possible [3].

The first step in the process is to create a computerised description of a design. The numerical nature of the description enables the design to be interrogated by computer software that facilitate CAD/CAM [4, 5]. Many commercial CAD software systems are available. Solidworks and AutoCAD, developed by Dassault Systèmes and Autodesk respectively, being two popular examples [4, 5]. Such software enables engineers to model and refine designs using an integrated graphical user interface (GUI).

Empirical and *ab initio* designs are the two main types of design that are modelled using CAD software. The shapes of some designs are arrived at iteratively by experimental evaluation of

the processes undertaken by the resulting components during their service times. These types of designs are referred to as *empirical* designs [6]. Examples are mechanical and structural components whose aesthetic appearance need not affect their operation, like compressor blades, engine manifolds and surgical implants. Many modern CAD systems provide dynamic analysis tools that can improve the efficiency of this iterative modelling process [4]. The shapes of other designs depend on both aesthetic and functional requirements. These are frequently termed *ab initio* designs [6]. Examples are the skin of car bodies, aircraft fuselages and ship hulls. The appearance of such designs may be perceived, by the resulting product's consumers, to be linked to physical performance characteristics and as a result affect sales [7]. Their designs therefore cannot be formulated entirely in terms of quantitative criteria, but must be resolved by a judicious combination of computational and heuristic methods [6].

CAD systems commonly represent both empirical and *ab initio* designs using Non-Uniform Rational B-Spline (NURBS) curves and surfaces [6, 8]. These parameterised rational curves and surfaces form the primitive elements from which a given design is constructed. Multiple curves and surfaces may be joined together to form complex designs. For example, multiple curves may be joined together to from a composite curve and individual surfaces may be joined together to form a composite surface, where each surface is then referred to as a patch.

The properties of NURBS allow engineers to manipulate the shape of a design in an intuitive and predictable manner. The engineer does not require an understanding of the underlying mathematics to manipulate the shape of the design. Consider a degenerate form of NURBS curve, the Bézier curve. Although it can be expressed as a recursive algorithm, it can also be expressed as a *weighted* summation of control points, $\mathbf{P}_0$, $\mathbf{P}_1$, ..., $\mathbf{P}_{n-1}$, $\mathbf{P}_n$ [8]. The weights,

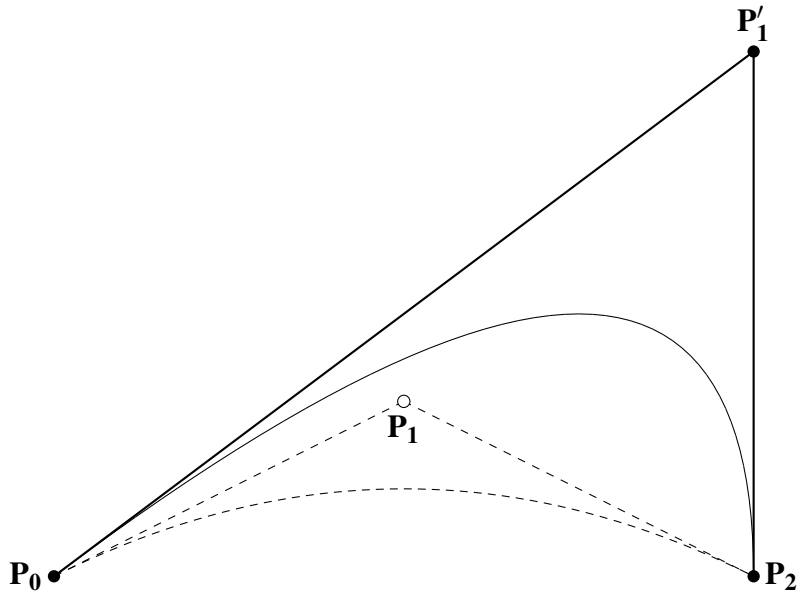

Figure 1.1: Intuitive shape manipulation

referred to as the Bernstein polynomials, are employed as coefficients of the control points in order to affect the shape of the resulting curve [8]. Further, since the Bernstein polynomials are non negative and sum to unity, they provide the convex hull property [8]. This may be interpreted geometrically, in the planar case, that the curve must lie within the convex polygon whose vertices are formed by the control points. Moving control point $\mathbf{P}_1$ to $\mathbf{P'}_1$ (in Fig. 1.1) therefore has the effect of *stretching* the curve towards $\mathbf{P'}_1$ and being contained in the convex polygon formed by control points $\mathbf{P}_0$, $\mathbf{P'}_1$ and $\mathbf{P}_2$. By extension, the control points of a surface, collectively referred to as the control polyhedron, can be manipulated to change the shape of the surface.

Once an appropriate shape for a given design is achieved, the CAD model is imported into CAM software. Here the machining process, defined as controlled material removal from a raw material to form a desired final shape, can be simulated, analysed and refined [9]. This simulated machining can reduce the amount of physical machining trials and so less material is

wasted and fewer interruptions are required in production [4, 5, 9].

Simulation requires the definition of workpiece, cutting tools and their movements. Once the workpiece material and its dimensions are specified, cutting tools suitable for removing material are chosen. Different cutting tools are used for different stages of the machining process. To initially remove high volumes of material per unit time (rough cutting), a tool with serrated teeth may be used as this can help to break chips into smaller pieces. Typically, the resulting machined surfaces are relatively rough. Removing a lower volume of material per unit time (finishing cutting), can improve the surface finish. This can then be achieved by using a cutting tool with relatively more teeth, that need not be serrated, since the presence of more teeth reduces the total volume of the space between teeth and so less material is removed per unit time.

Material removal requires the cutting tool's teeth to move relative to the workpiece surface. This motion can be defined in CAM software by specifying the rate at which the tool rotates about the spindle axis (spindle speed), the speed at which the entire tool moves relative to the workpiece surface (feed rate) and the path traversed on the workpiece surface (tool path).

When a machining strategy suitable for the given application has been established, CAM software is able to produce numerical instructions (G-Code) that can be used to manufacture the design. This is achieved via a language definition file, called a post processor, that modifies generic G-Code to adapt it to the particular computer numerically controlled (CNC) machine being used. The resulting instructions are then transferred to the controller of the CNC machine in the form a numerical control (NC) file.

The CNC machine's controller then translates NC file instructions into motion commands for the machine's axes servomotors. Once the automated machine motion starts, the engineer has little further effect on the manufacture of the component and in turn the resulting component quality. It is therefore imperative that the instructions presented to the controller are appropriate for the given application and achievable within the machine's physical capabilities. For example, the motions imposed by tool path shape should not exceed the maximum kinematics permissible by the machine's servomotors.

The actual motions produced derive from the machine's attempts to provide the desired relative movements between tool and workpiece defined in the NC file. As discussed above, a given motion is defined by the spindle speed, feed rate and tool path. If the selected parameters do not account for the kinematic constraints of the machine, the desired motions may not be realised in practice. For a given workpiece material, cutting tool manufacturers recommend particular values for feed rate and spindle speed. Also, in general, the maximum feed rate and spindle speed for a given machine are clearly stated in the literature. Assuming proper selection of feed rate and spindle speed, the emphasis therefore lies on constructing suitable paths for the cutting tool to traverse relative to the workpiece.

1.2 Tool paths

Change in position and/or orientation of a cutting tool relative to the workpiece coordinate system, in a finite time period, is considered a motion. A given position and orientation are collectively referred to as a tool pose (or tool posture). A *tool path* is therefore defined as the

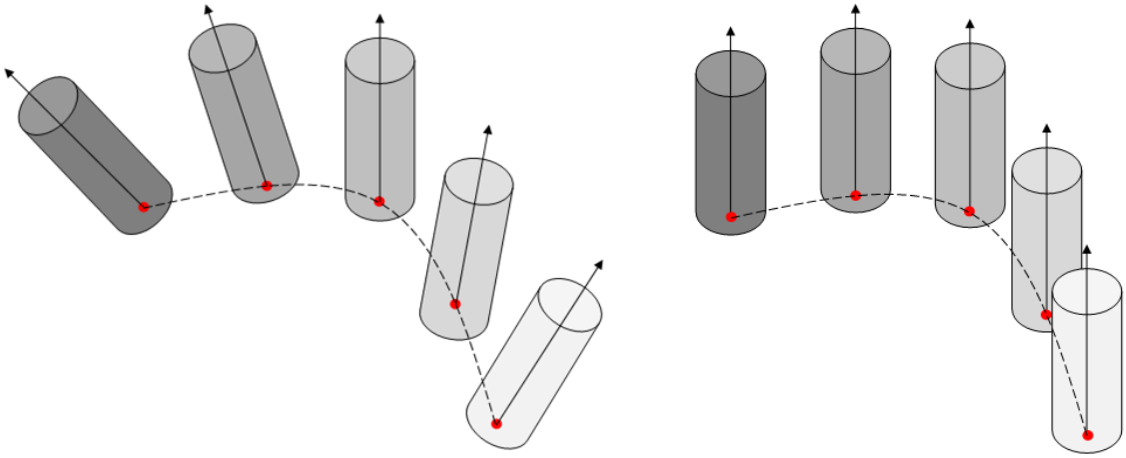

(a) Locus of poses (b) Locus of positions

Figure 1.2: Tool path definitions

continuous locus of poses associated with a given motion (Fig. 1.2a). A tool path can also be considered as a continuous locus of positions when a desired motion does not require changes in orientation (Fig. 1.2b).

The locus of positions correspond to those of a given point on a cutting tool. The choice of point is immaterial provided that the point's position is fixed with respect to the machine's spindle axis. The point is therefore confined to lie on the axis of rotation of the spindle. Typically the top or bottom point of the cutting tool is chosen to represent the location of a tool on a tool path. This cutter location point, CL, need not be the same as the point in contact with the workpiece at a given instance in time. Such a point is commonly referred to as the cutter contact point, CC. A key distinction between the two is that the CL point remains fixed for a given motion and the CC point does not. The point on the cutting tool corresponding to the CC point changes as the tool rotates about the spindle axis.

The orientation of the cutting tool in the workpiece coordinate system is defined as the angle, δ,

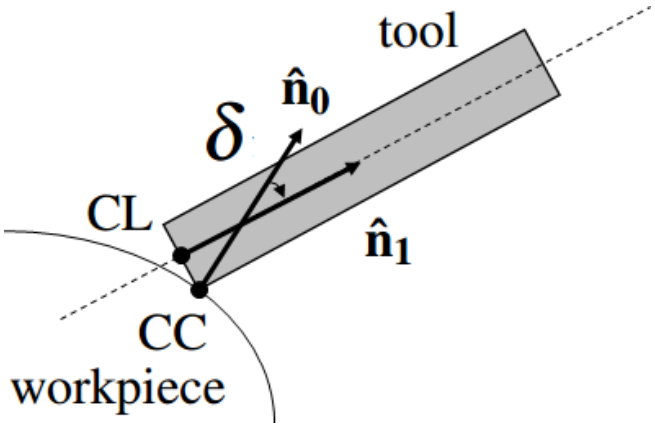

Figure 1.3: Cutting tool orientation

between the workpiece's unit surface normal vector that passes through the CC point, $\hat{\mathbf{n}}_0$, and the unit vector that passes through the CL point and is directed parallel to the spindle axis, $\hat{\mathbf{n}}_1$ (See Fig. 1.3).

By definition, consecutive poses of a continuous tool path are different. Either the position, orientation or both change. It then follows that an infinite number of poses are required to exactly describe a given tool path. Such descriptions cannot be presented to the controller of a CNC machine, since each pose must be interpreted into motion commands for the machine's servomotors. Each interpretation occurs over a finite period of time, therefore an infinite amount of time would be necessary to traverse a given tool path.

In practice a finite number of appropriate poses must be selected from the desired continuous tool path. These discrete poses are then interpolated to form an approximation to the desired tool path. Linear and circular interpolation have traditionally been employed [3]. Consider a portion of a planar tool path, $\mathbf{C}$, shown in Fig. 1.4. Since the path is planar, the orientations of the path's poses do not change, therefore the path may be considered as a locus of positions. Let $\mathbf{P_0}$ and $\mathbf{P}_1$ denote the start and end positions of this portion. By linearly interpolating from

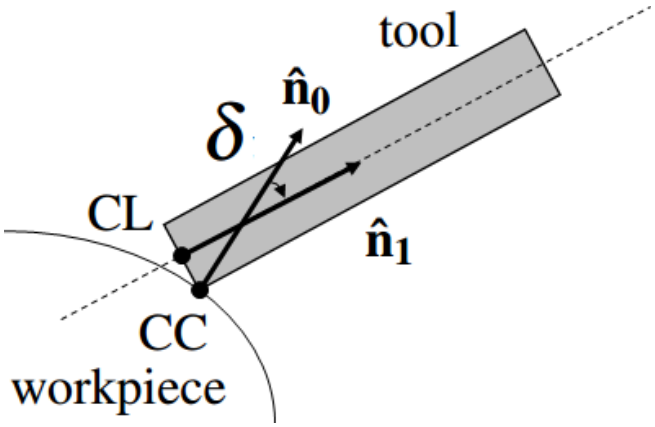

Figure 1.3: Cutting tool orientation

between the workpiece's unit surface normal vector that passes through the CC point, $\hat{\mathbf{n}}_0$, and the unit vector that passes through the CL point and is directed parallel to the spindle axis, $\hat{\mathbf{n}}_1$ (See Fig. 1.3).

By definition, consecutive poses of a continuous tool path are different. Either the position, orientation or both change. It then follows that an infinite number of poses are required to exactly describe a given tool path. Such descriptions cannot be presented to the controller of a CNC machine, since each pose must be interpreted into motion commands for the machine's servomotors. Each interpretation occurs over a finite period of time, therefore an infinite amount of time would be necessary to traverse a given tool path.

In practice a finite number of appropriate poses must be selected from the desired continuous tool path. These discrete poses are then interpolated to form an approximation to the desired tool path. Linear and circular interpolation have traditionally been employed [3]. Consider a portion of a planar tool path, $\mathbf{C}$, shown in Fig. 1.4. Since the path is planar, the orientations of the path's poses do not change, therefore the path may be considered as a locus of positions. Let $\mathbf{P_0}$ and $\mathbf{P}_1$ denote the start and end positions of this portion. By linearly interpolating from

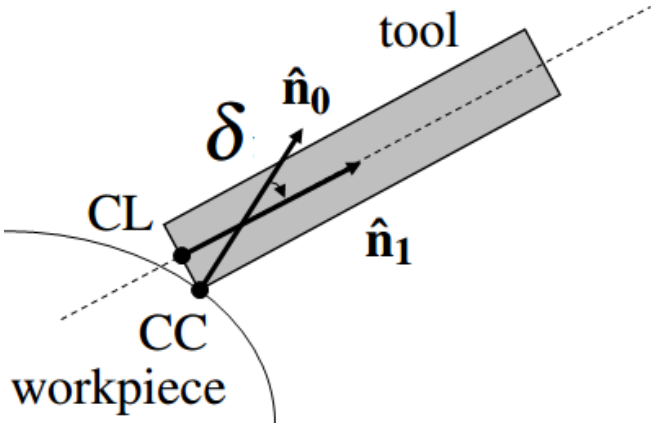

Figure 1.3: Cutting tool orientation

between the workpiece's unit surface normal vector that passes through the CC point, $\hat{\mathbf{n}}_0$, and the unit vector that passes through the CL point and is directed parallel to the spindle axis, $\hat{\mathbf{n}}_1$ (See Fig. 1.3).

By definition, consecutive poses of a continuous tool path are different. Either the position, orientation or both change. It then follows that an infinite number of poses are required to exactly describe a given tool path. Such descriptions cannot be presented to the controller of a CNC machine, since each pose must be interpreted into motion commands for the machine's servomotors. Each interpretation occurs over a finite period of time, therefore an infinite amount of time would be necessary to traverse a given tool path.

In practice a finite number of appropriate poses must be selected from the desired continuous tool path. These discrete poses are then interpolated to form an approximation to the desired tool path. Linear and circular interpolation have traditionally been employed [3]. Consider a portion of a planar tool path, $\mathbf{C}$, shown in Fig. 1.4. Since the path is planar, the orientations of the path's poses do not change, therefore the path may be considered as a locus of positions. Let $\mathbf{P_0}$ and $\mathbf{P}_1$ denote the start and end positions of this portion. By linearly interpolating from

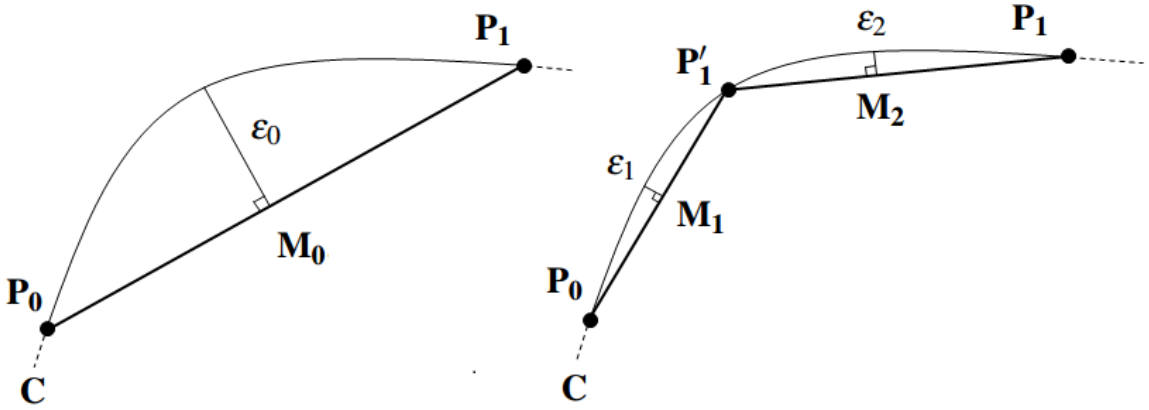

Figure 1.4: Interpolation error, ε

$\mathbf{P}_0$ to $\mathbf{P}_1$ the desired path is approximated by a single chord, $\overline{\mathbf{P}_0\mathbf{P}_1}$. The error of this type of interpolation, ε_0, may be defined as the length of a perpendicular line segment connecting the midpoint, $\mathbf{M}_0$, of the chord, $\overline{\mathbf{P}_0\mathbf{P}_1}$, to the tool path, $\mathbf{C}$. By selecting another point, $\mathbf{P'}_1$, on $\mathbf{C}$ between $\mathbf{P}_0$ and $\mathbf{P}_1$ two chords, $\overline{\mathbf{P}_0\mathbf{P'}_1}$ and $\overline{\mathbf{P'}_1\mathbf{P}_1}$, form an alternative linear approximation to the portion of the desired tool path, $\mathbf{C}$. Points $\mathbf{M}_1$ and $\mathbf{M}_2$ denote the midpoints of $\overline{\mathbf{P}_0\mathbf{P'}_1}$ and $\overline{\mathbf{P'}_1\mathbf{P}_1}$ respectively. Given the direction of the desired path, $\mathbf{C}$, changes monotonically between points $\mathbf{P}_0$ and $\mathbf{P}_1$ the error of each chord, ε_1 and ε_2 respectively, is less that the error of the original single chord, ε_0; $\varepsilon_1, \varepsilon_2 < \varepsilon_0$.

The greater the number of positions selected, the smaller the interpolation error for a given chord and so the closer the shape of the discretised tool path is to the desired continuous tool path. A greater number of positions also decreases the distances between consecutive positions. If the time taken to process and execute a cutting tool's movement between consecutive positions, T_m, is less than the controller's minimum processing time, T_p, the tool will rest at the end position and wait or *dwell* for the next motion command to be generated by the controller. When $T_m < T_p$, the machine's servomotors are effectively deprived of motion data. This phe-

nomenon is commonly referred to as *data starvation* [10]. A compromise must therefore be made between the number of positions selected and the magnitudes of the interpolation errors associated with the discretised tool path. Conventional CAM software does not automatically account for the effects of data starvation. It is generally the responsibility of the engineer to heuristically determine and specify a suitable trade-off.

An alternative to the conventional linear and circular interpolation methods is parametric (or spline) interpolation [11]. Many modern controllers are able to process tool paths expressed as parameterised polynomial curves [11, 12]. The most common type of parametric curve employed are NURBS [11, 12]. Since CAD models can be described with NURBS, (see section 1.1) the geometric information of a model may be transferred to a machine's controller exactly. It is then the responsibility of the controller to select appropriate poses. Further, less information is generally required to define a tool path if NURBS are used compared to conventional interpolation [12]. Only critical parameters, like control points, need be specified in a NC file for a given NURBS tool path. Particularly with larger NC files, that may require many linear interpolation segments, parametric interpolation can consolidate tool path descriptions using less information thereby reducing the risk of data starvation.

Whether the discretisation occurs in CAM software or in the controller, the shape of the resulting tool path imposes particular kinematic demands on the machine. The controller attempts to provide the requested kinematics by coordinating the movements of the machine's independent translational and/or rotational axes. Should the demands exceed the capabilities of the machine's servomotors, controller regulation intervenes to provide permissible tool path motion that is deemed, by motion control algorithms, to be an appropriate alternative to the desired tool

path motion.

1.3 Tool path motions

Tool path motion is governed by motions of the machine's axes. The inertia of each axis, I, and the finite torque, Υ_{max}, and power, P_{max}, capacities of the corresponding servomotors limit the achievable tool path kinematics [13]. Consider, for example, circular tool path motion resulting from the simple harmonic motions of two orthogonal linear axes. For a given feed rate, v, the shape of the circle, defined by its radius, r, imposes a maximum acceleration of magnitude v^2/r on each axis. The smaller the radius the greater the acceleration required to traverse the circular path at a given feed rate. It is shown in appendix A that the maximum feed rate, v_{max}, attainable for a given radius, with servomotors of limited power is

$$v_{max} = \left(\frac{P_{max}}{I} \right)^{\frac{1}{3}} r \ .$$

Similarly, when servomotor torque is the limiting factor it is shown that

$$v_{max} = \left(\frac{\Upsilon_{max}}{I} \right)^{\frac{1}{2}} r \ .$$

The axes of a given machine commonly have the same kinematic limits, as implied above, although many modern controllers provide the functionality of defining separate limits for each

axis should a particular application require it [12].

In order to adhere to the kinematic limits of a given machine, the controller may command the machine's axes to divert from both the intended feed rate and tool path shape.

Consider a planar, point continuous, G^0, tool path composed of linear segments (Fig. 1.5). At the junction of consecutive segments the tangent vector, $\hat{\mathbf{t}}$, is not unique (Fig. 1.5). Its direction changes instantaneously. Change in the direction of the tangent vector with respect to the distance travelled along the path, s, is defined as curvature, $\kappa(s)$ [14]. It then follows that a singularity in the tool path's curvature function exists at the junction of consecutive linear segments (Fig. 1.6). Traversal at a given feed rate, where $v > 0$, of such a tool path shape requires an instantaneous change in direction of the velocity vector. Such a motion is not possible in practice. The cutting tool must come to rest at the junction if the path is to be followed exactly. Changes in acceleration are required for this intermittent motion. The rate of change of acceleration, with respect to time, is defined as jerk [15]. The resulting jerk can change resultant forces on the cutting tool, causing deflection marks on the surface of the machined component [16]. Further, feed rate, acceleration and jerk fluctuations increase numerical control cycle time and prematurely wear the cutting tool, in turn reducing productivity [17].

In general, to reduce fluctuations in kinematic properties of tool path motion, CNC controllers can permit cutting tools to follow alternative trajectories that deviate from programmed tool paths by given tolerances [17]. These new trajectories may be considered to *smooth* motion since less fluctuations in higher feed rates are generally attainable with reduced accelerations and jerks [18].

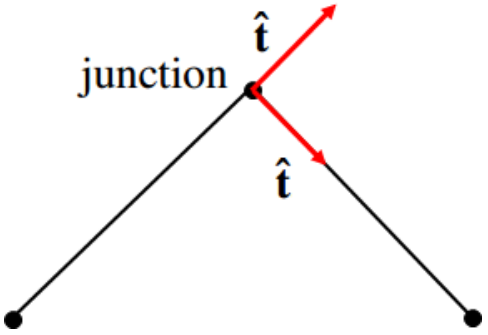

Figure 1.5: Undefined tangent vector

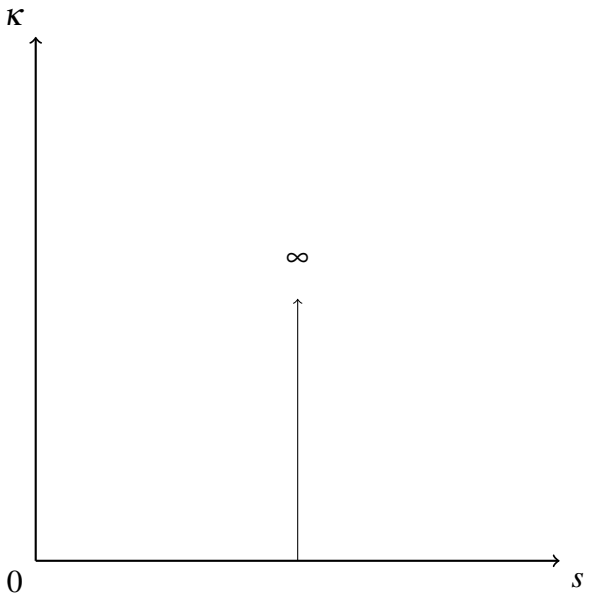

Figure 1.6: G^0 linear segments. Piecewise impulse curvature profile

The precise nature of an amended tool path motion may not be known prior to machining. This is mainly due to machine manufacturers regarding their motion control algorithms as giving them commercial advantage so that they do not disclose the ways in which these algorithms operate. The specifics of these control algorithms are therefore not generally accessible. This has not deterred academia, nor should it, from proposing novel algorithms to be implemented in machine controllers [18–21].

Consider again, the tangent discontinuous linearly segmented tool path. The segment junctions impose impractical kinematic demands on any machine. Controller regulation is therefore required. The general approach of many of the proposed algorithms is to first fit an appropriate path between consecutive linear segments. This path removes the infinite acceleration imposed by the junction whilst still adhering to the desired positional tolerances [19]. The algorithms then plan the feed rate profile across the revised path accounting for machine kinematic limits [19].

For example, the junction may be replaced by a circular arc that joins each linear segment with tangent continuity, G^1 (Fig. 1.7) [20]. The direction of the tangent vector no longer changes instantaneously, thus enabling a continuous feed rate profile. The curvature singularity is replaced by a non zero constant curvature segment (Fig. 1.8). This piecewise constant curvature profile corresponds to instantaneous changes in curvature at the start and end of the circular arc (Fig. 1.9). Traversing such a path at a constant feed rate, v_c, would require an instant increase in acceleration, from 0 to v_c^2/r, at the beginning of the arc in order to change direction and follow the circular arc and an instant decrease in acceleration, from v_c^2/r to 0, at the end of the arc in order to stop changing direction and follow the linear path. Despite the revised tool path

improving the motion, in the sense that traversal no longer requires an infinite acceleration, constant feed rate motion still cannot be realised. The new tool path's piecewise constant curvature imposes infinite jerk at the beginning and end of the arc. A jerk limited feed rate profile can then be used to allow the cutting tool to follow the revised tool path exactly [18, 21].

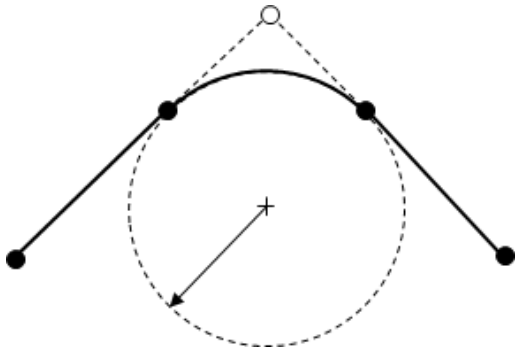

Figure 1.7: G^1 circular arc

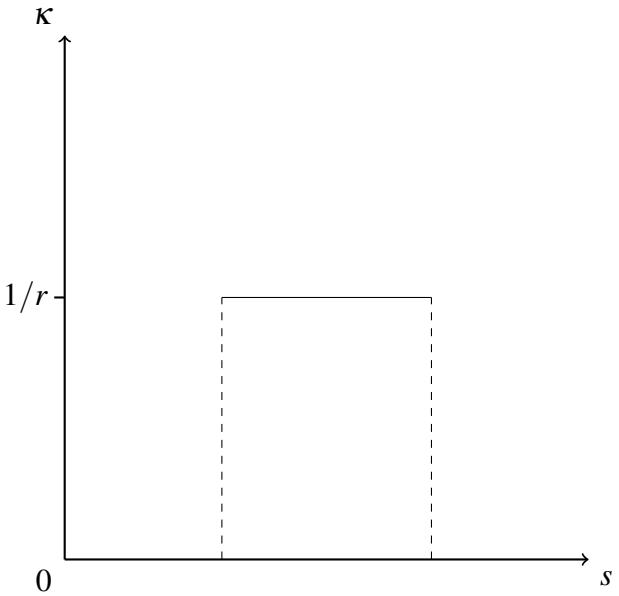

Figure 1.8: G^1 circular arc. Piecewise constant curvature profile

By replacing the circular arc with two Cornu spirals (Fig. 1.10), curvature continuity, G^2, may be achieved across the linear and spiral segments, thus enabling a continuous acceleration profile [22]. A Cornu spiral is a planar path, defined by a linear curvature profile, $\kappa(s) = \alpha s + \beta$,

$0 \leq s \leq L$, where L is the total length of the path and α, $\beta \in \mathbb{R}$ and α is the gradient of the curvature profile and β is the initial curvature of the associated path [23]. The piecewise constant curvature profile can therefore be replaced by a continuous linear curvature profile (Fig. 1.11). The curvature at each point on the path is well defined and unique. It then follows that traversal no longer requires instantaneous changes in acceleration. The shape of the tool path now only imposes a finite jerk at each position. The gradient of the curvature profile describes the rate at which curvature changes with respect to the distance travelled along the path, $d\kappa(s)/ds$. Fig. 1.12 illustrates that this curvature derivative is piecewise continuous. It then follows that $d^2\kappa(s)/ds^2$ can be shown by Fig. 1.13. The figure indicates that $d^2\kappa(s)/ds^2$ is undefined at each segment transition point. It can be shown such shape properties correspond to instantaneous changes in jerk [1]. The rate at which jerk changes with respect to time is defined as jounce [15]. The shape of the G^2 Cornu spiral smoothing tool path thus imposes infinite jounce at each transition point. Such kinematic demands cannot be realised. In practice, the feed rate must fluctuate in order to follow the tool path exactly. Further, direct implementation of Cornu spirals within CAD/CAM is impractical since positional evaluation requires numerical methods and thus must be approximated [24].

As discussed previously, NURBS tool paths can be implemented directly within CAD/CAM. Motion control algorithms within controllers may use NURBS tool paths to avoid the impractical kinematic demands of linear and circular segments [12, 25–27]. For example, two quartic polynomial splines can be used to achieve continuous curvature cornering within user specified tolerances [12]. A single G^2 quintic Bézier can be used to ensure axis acceleration limits are adhered to [25]. Many other proposed algorithms use B-splines as they offer flexibility in locally changing the shape of a tool path [26, 27]. However the rational nature of NURBS means that

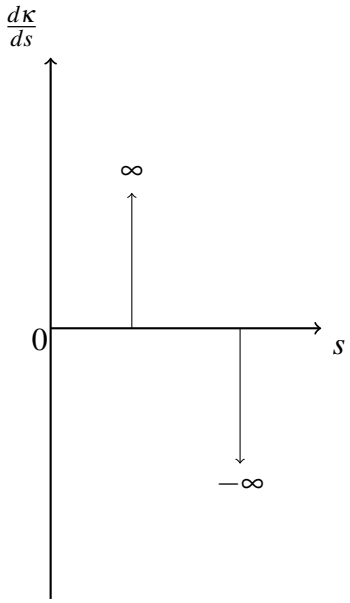

Figure 1.9: G^1 circular arc. Piecewise impulse curvature derivative profile

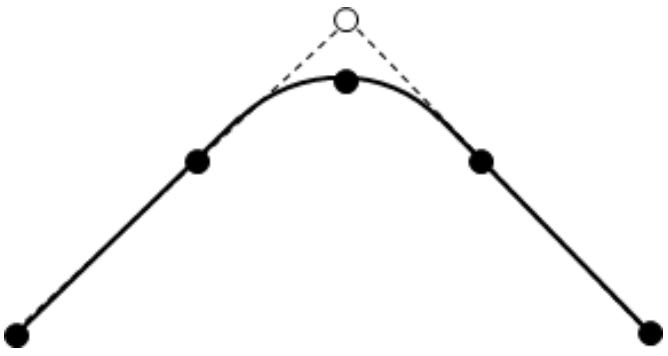

Figure 1.10: G^2 Cornu spirals

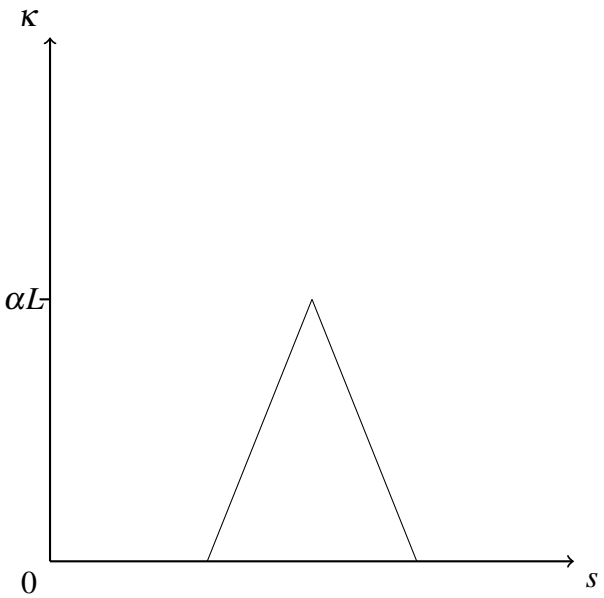

Figure 1.11: G^2 Cornu spiral curvature profile

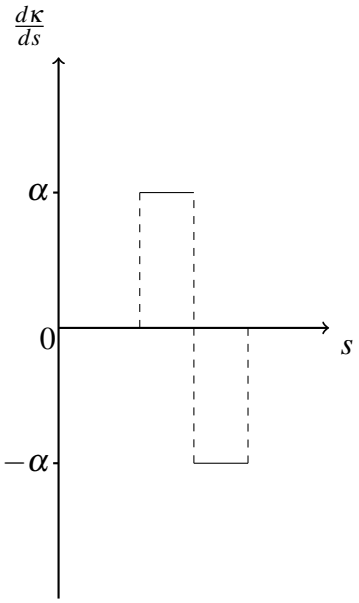

Figure 1.12: G^2 Cornu spiral curvature derivative profile

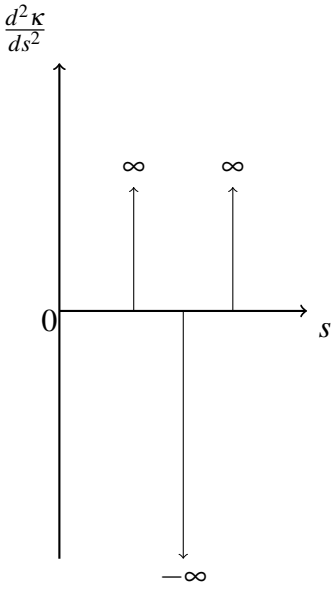

Figure 1.13: G^2 Cornu spiral curvature second derivative profile

tool paths can experience undulating oscillations in curvature which in turn impose fluctuations in the kinematic properties of tool path motion [8, 28].

1.4 Research aim

The discussion above suggests that the current dominant approach to regulate tool path motion is to allow the controller of a given machine to autonomously adjust both the intended shape and kinematics. Such autonomy is machine specific. The control algorithms implemented on one machine need not be the same as those implemented on another. Execution of a given NC file can therefore result in different sets of conditions depending on the machine being used. A given design, machined on different machines, can result in manufactured components of different qualities.

For a given application, the autonomous regulation of kinematics by a controller may produce undesirable and unknown machining conditions. For example, a commanded feed rate may have been specified in order to achieve particular conditions, such as certain material removal rates or surface finish. However, the kinematics imposed by the shapes of the specified tool paths exceed the machine capabilities and therefore controller regulation results in a manufactured component outside of tolerance. Therefore, in practice, parameters need to be *optimised* for a given application. A series of machining trials may be conducted to refine the machining parameters for the given application.

For a given workpiece material, cutting tool manufacturers recommend particular values for parameters such as feed rate, depth of cut, and spindle speed. These suggested values are however, often based on assumptions of simple components with tool paths describing simple motions, predominately linear. Paths with varying curvature profiles, referred to in this thesis as free-form paths, place a greater burden on control algorithms to generate resulting motions. As a result the recommended values for the machining parameters are, in general, not achieved on free-form tool paths. In such instances the experience of the machinist is used to identify suitable parameters for the given application [2]. The methods employed may be iterative and informed by empirical evidence from machining trials. Such *a posteriori* attempts to obtain suitable machining conditions are often heuristic and time intensive.

The main aim of this thesis is to present a methodology for assessing the kinematic capabilities of any CNC machine, in terms of a tool path's intrinsic shape properties. Two key objectives must be met in order to achieve this aim.

- To enable the methodology to be applicable for any CNC machine, it must be independent of a given machine's motion control algorithms. As discussed earlier in this section, dependence on a specific motion control algorithm only enables tool path motion description for a machine upon which the algorithm is used. Further, machine and controller manufacturers tend not to disclose the ways in which these algorithms operate. This in turn limits the applicability of many of the current proposed methods.

- The methodology must also provide a means of identifying the kinematic limits of a given machine. Since the aim specifies that the assessment must be conducted in terms of a path's intrinsic shape properties, the approach must attempt to isolate the contribution of a tool path's shape properties to the actual kinematics produced in a given motion.

Such a methodology would produce a characterisation of tool path motion that would only depend upon the intrinsic shape properties of a desired tool path and a machine's kinematic limits. These are two of the very few conditions that are identifiable without undergoing the iterative machining trial procedure. The methodology would therefore provide *a priori* shape characterisation of tool path motion. The characterisation may be employed in a pre-processing manner to inform the selection of NC file tool path motions. This can therefore help to reduce the time and number of machining trials and so improve the efficiency and productivity of the manufacturing process by reducing the material and energy resources being consumed.

A resulting characterisation may be used in at least two ways. Firstly, a proposed tool path motion may be checked to see whether its shape imposed kinematics are likely to be achieved on a given machine. Secondly, having identified the maximum magnitudes of the kinematics vectors achievable by the machine, given the shape of the tool path, the commanded feed rate

and desired tool path shape may be adapted in order to accommodate the machine's kinematic limits.

1.5 Contents outline

This introductory chapter began by providing an overview of the CAD/CAM process. The definition of a tool path and its role within CAD/CAM were then detailed. This was then followed by a study of the effects of shape on tool path motion and a review of the current approaches employed by machine controllers to regulate motion. Motivation and a statement of the research aim were then provided, followed by a brief discussion of the possible impact of the research.

The following chapter establishes the foundations of the mathematical theory required in Chapter 3 to characterise tool path motion in terms of shape. By considering the motion of a local orthogonal frame, the tool path's intrinsic shape properties are linked to the kinematic properties of the corresponding motion.

Chapter 3 then considers the effects of these intrinsic shape properties on a machine, with kinematic limits, in order to postulate a shape characteristic model.

Chapter 4 employs a test methodology to identify the kinematic limits of any conventional CNC machine. Empirical evidence obtained from three example machines is used to establish the maximum permissible kinematics for given shape properties.

Chapter 5 furthers the investigation by considering motion along free-form paths.

Chapter 6 analyses the empirical data gathered from chapters 4 and 5, compares the evidence with the characteristic model derived in chapter 3 and discusses the results.

Chapter 7 begins by presenting an overview of the research tasks undertaken. This is then followed by discussions on the contributions and limitations of the research presented. The chapter then concludes the thesis by suggesting areas for future research.

Chapter 2

Shape properties of motion

As discussed in the previous chapter, the motion of a cutting tool relative to a workpiece surface is defined by three parameters, namely spindle speed, tool path shape and feed rate (section 1.1). Since spindle speed, however important to material removal, does not affect movements of the machine's axes, it is from here onwards omitted from motion analysis. The first section (section 2.1) of this chapter investigates tool path shape. The intrinsic shape properties, curvature and torsion, are introduced and discussed within the context of motion. Section 2.2 then describes the relationships between the shape properties of CAD model surfaces and the tool paths that lie on them. Sections 2.3, 2.4 and 2.5 then relate the kinematic properties, velocity, acceleration and jerk, to tool path shape.

2.1 Tool path shape

The path traversed by a specified point on a cutting tool during a given tool path motion may be represented as a parametric space curve $\mathbf{r}(u)$, where u is an arbitrary parameter [11]. By assuming the path is differentiable and continuous, analysis of motion may be simplified by expressing the tool path as a time, t, parameterised function in three dimensional Euclidean space $\mathbb{E}^3$. It then follows that $\mathbf{r}(t) = \langle x(t),\ y(t),\ z(t)\rangle$, where $0 \leq t \leq T$, $x(t)$, $y(t)$ and $z(t) \in \mathbb{R}$ and T is the total time for the motion.

A local coordinate system is employed to facilitate describing each position in terms of the shape properties of a tool path. A local affine coordinate system, with origin $\mathbf{r}(t)$, may be formed from the first three derivatives of $\mathbf{r}(t)$, with respect to parameter t, ($\mathbf{r}'(t)$, $\mathbf{r}''(t)$ and $\mathbf{r}'''(t)$) (Fig. 2.1) [8]. The resulting vectors may be orthonormalised, using the Gram-Schmidt process, to form a local Cartesian system called the Frenet frame, with origin $\mathbf{r}(t)$ and axes $\hat{\mathbf{t}}(t)$, $\hat{\mathbf{n}}(t)$ and $\hat{\mathbf{b}}(t)$, where the unit tangent vector, $\hat{\mathbf{t}}(t) = \mathbf{r}'(t)/\|\mathbf{r}'(t)\|$, the principal unit normal vector, $\hat{\mathbf{n}}(t) = \hat{\mathbf{t}}'(t)/\|\hat{\mathbf{t}}'(t)\|$ and the binormal vector, $\hat{\mathbf{b}}(t) = \hat{\mathbf{t}}(t) \wedge \hat{\mathbf{n}}(t)$ (Fig. 2.1) [29]. This frame further defines local planes (Fig. 2.2). At a given point, $\mathbf{r}(t)$, on the tool path, $\prod_n := \hat{\mathbf{n}}(t) \wedge \hat{\mathbf{b}}(t)$, $\prod_r := \hat{\mathbf{b}}(t) \wedge \hat{\mathbf{t}}(t)$ and $\prod_o := \hat{\mathbf{t}}(t) \wedge \hat{\mathbf{n}}(t)$ define the normal, rectifying and osculating planes respectively.

Insight into the effects of shape on tool path motion may be gained by considering changes in frame orientation as time increases. It is assumed the distance travelled along the path, arc length, s, increases monotonically with time. Frame motion may then be expressed in terms of the path's intrinsic shape properties if a reparameterisation to arc length is made. Since arc

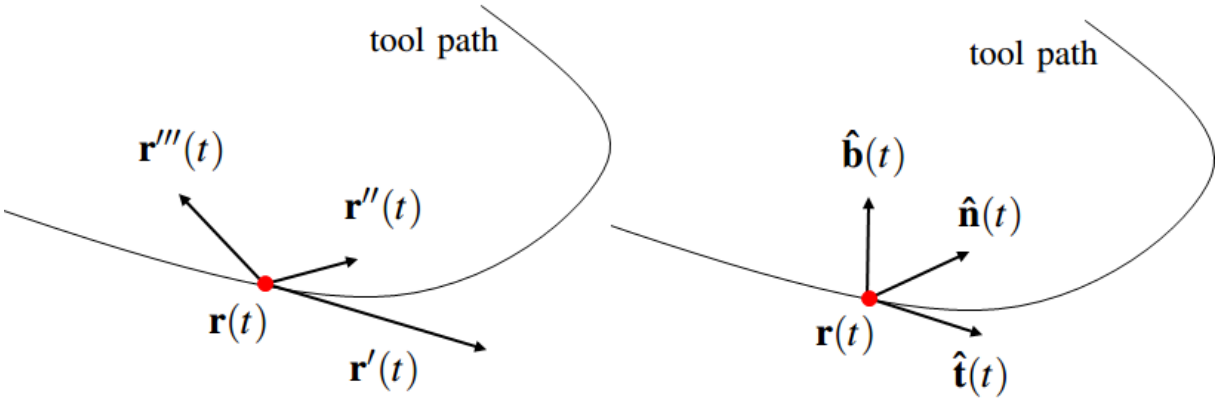

Figure 2.1: Local affine system (left) and Frenet frame (right) [8]

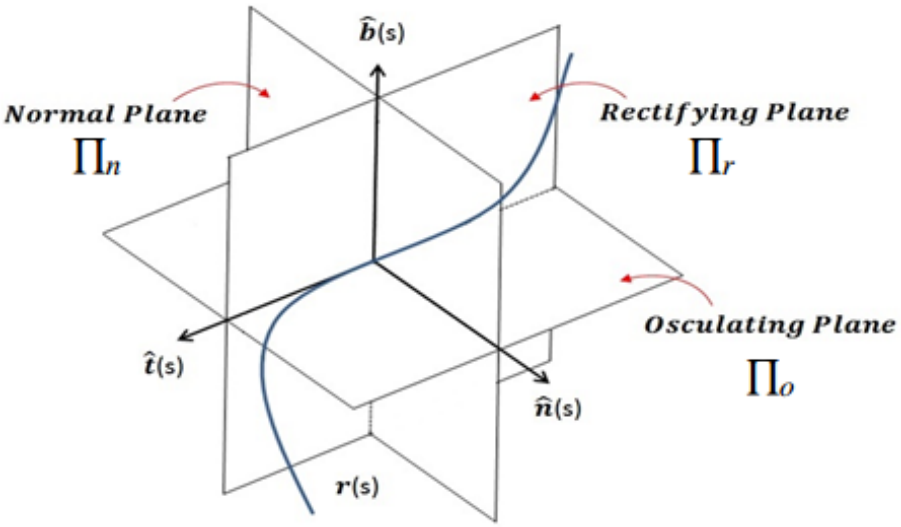

Figure 2.2: The local planes

length is an intrinsic shape property, a reparameterisation does not change the shape of the tool path [8]. Assuming $s = s(t)$ is differentiable and the inverse, $t = t(s)$, exists, it follows that $\mathbf{r}(s) \equiv \mathbf{r}(t)$. Such a parameterisation, $s(t) = \int \left\| \dot{\mathbf{r}}(t) \right\| dt$, enables frame motion to be described using the following equations,

$$\frac{d\hat{\mathbf{t}}(s)}{ds} = \kappa(s)\hat{\mathbf{n}}(s) \ , \tag{2.1}$$

$$\frac{d\hat{\mathbf{n}}(s)}{ds} = -\kappa(s)\hat{\mathbf{t}}(s) + \tau(s)\hat{\mathbf{b}}(s) \ , \tag{2.2}$$

and

$$\frac{d\hat{\mathbf{b}}(s)}{ds} = -\tau(s)\hat{\mathbf{n}}(s) \ . \tag{2.3}$$

The above Frenet-Serret relations contain the functions $\kappa(s)$ and $\tau(s)$, which refer to the shape properties, curvature and torsion respectively [14]. Formally they are defined by Eq. (2.1) and Eq. (2.3). Curvature describes the rate at which the tangent vector changes direction, as the frame traverses the path with respect to arc length. The more the path *bends* the greater the magnitude of the curvature. Torsion measures the rate at which the binormal vector changes direction with respect to arc length. Intuitively, torsion may be considered to describe how much the tool path *twists* out of the osculating plane.

The shape of the desired engineering component's CAD model has some influence on the curvature and torsion of the resulting tool paths used in machining. Particularly in the finishing stages of the machining process, the actual paths traversed by the cutting tool closely follow

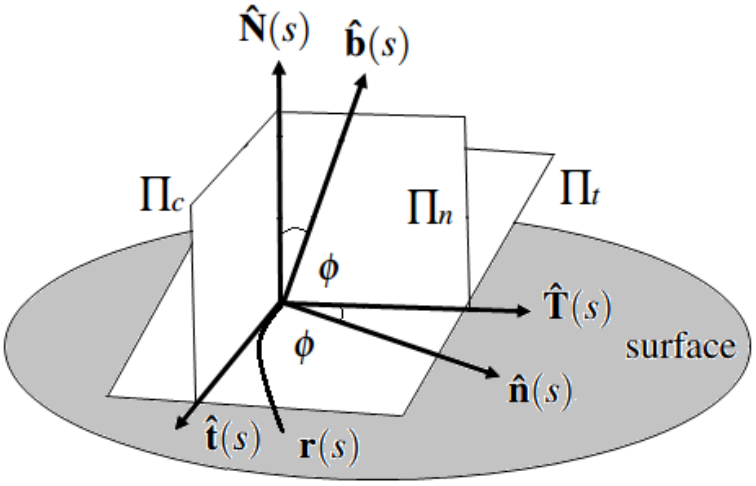

Figure 2.3: Surface Frame [30]

the surfaces of the original CAD model [3]. Indeed, in the finishing stages, the desired tool paths are derived from the surfaces on which they lie (see section 1.2). The following section therefore describes the relationships between the shape properties of the CAD model surfaces and the desired tool paths used in the corresponding machining process.

2.2 Tool paths on surfaces

Consider a tool path lying on a surface. In addition to the Frenet frame, $\mathbf{F}_1(s)$, it is possible to assign another frame, the Darboux frame, $\mathbf{F}_2(s)$, at each point on the tool path (Fig. 2.3) [30]. At a given point there is only one unit surface normal vector, $\hat{\mathbf{N}}(s)$, and an infinity of tangent vectors. These tangent vectors lie in the tangent plane that is orthogonal to $\hat{\mathbf{N}}(s)$. The tool path's unit tangent vector and the surface's unit normal vector can together be used to form a vector that is orthogonal to both, referred to in this thesis as the bi-tangent vector, $\hat{\mathbf{T}}(s)$, $\hat{\mathbf{T}}(s) = \hat{\mathbf{N}}(s) \wedge \hat{\mathbf{t}}(s)$ [30].

Both orthogonal frames, $\mathbf{F}_1(s)$ and $\mathbf{F}_2(s)$, share the tool path's unit tangent vector, $\hat{\mathbf{t}}(s)$, $\hat{\mathbf{n}}(s) \wedge \hat{\mathbf{b}}(s) \equiv \hat{\mathbf{T}}(s) \wedge \hat{\mathbf{N}}(s)$ (Fig. 2.3). It then follows that $\hat{\mathbf{n}}(s)$, $\hat{\mathbf{T}}(s)$, $\hat{\mathbf{b}}(s)$ and $\hat{\mathbf{N}}(s)$ all lie in the normal plane of $\mathbf{F}_1(s)$. Further, at a given point, $\mathbf{r}(s)$, on the tool path, vectors $\hat{\mathbf{t}}(s)$ and $\hat{\mathbf{T}}(s)$ define the tangent plane, $\prod_t := \hat{\mathbf{t}}(s) \wedge \hat{\mathbf{T}}(s)$ and the vectors $\hat{\mathbf{N}}(s)$ and $\hat{\mathbf{t}}(s)$ define the cleaver plane, $\prod_c := \hat{\mathbf{N}}(s) \wedge \hat{\mathbf{t}}(s)$ (Fig. 2.3) [30].

Rotating $\mathbf{F}_1(s)$ about $\hat{\mathbf{t}}(s)$, by an angle ϕ, converts it into $\mathbf{F}_2(s)$ (Fig. 2.3). ϕ is dependent on the given orientation of $\mathbf{F}_1(s)$ at a given s. It then follows that the angle of rotation is a function of arc length, $\phi(s)$. From the figure observe that,

$$\hat{\mathbf{T}}(s) = cos(\phi(s))\hat{\mathbf{n}}(s) + sin(\phi(s))\hat{\mathbf{b}}(s)$$

and

$$\hat{\mathbf{N}}(s) = -sin(\phi(s))\hat{\mathbf{n}}(s) + cos(\phi(s))\hat{\mathbf{b}}(s) \ .$$

The structure of the above expressions suggest that the connection between $\mathbf{F}_1(s)$ and $\mathbf{F}_2(s)$ may be expressed concisely in matrix form [30],

$$\begin{pmatrix} \hat{\mathbf{t}}(s) \\ \hat{\mathbf{T}}(s) \\ \hat{\mathbf{N}}(s) \end{pmatrix} = \begin{pmatrix} 1 & 0 & 0 \\ 0 & cos(\phi(s)) & sin(\phi(s)) \\ 0 & -sin(\phi(s)) & cos(\phi(s)) \end{pmatrix} \begin{pmatrix} \hat{\mathbf{t}}(s) \\ \hat{\mathbf{n}}(s) \\ \hat{\mathbf{b}}(s) \end{pmatrix} \ .$$

As the surface tool path is traversed the surface frame's orientation and position changes. The rate at which the surface frame changes with respect to arc length may be expressed as

$$\begin{pmatrix} \hat{\mathbf{t}}'(s) \\ \hat{\mathbf{T}}'(s) \\ \hat{\mathbf{N}}'(s) \end{pmatrix} = \begin{pmatrix} 0 & \kappa_g & \kappa_n \\ -\kappa_g & 0 & \tau_g \\ -\kappa_n & -\tau_g & 0 \end{pmatrix} \begin{pmatrix} \hat{\mathbf{t}}(s) \\ \hat{\mathbf{T}}(s) \\ \hat{\mathbf{N}}(s) \end{pmatrix} ,$$

where $\kappa_g = \kappa(s)cos(\phi(s))$, $\kappa_n = \kappa(s)sin(\phi(s))$ and $\tau_g = \tau(s) + \phi'(s)$ [30]. In the above anti-symmetric matrix, κ_g is called the surface's geodesic curvature, κ_n is called the surface's normal curvature and τ_g is called the surface's geodesic torsion. In equation form,

$$\frac{d\hat{\mathbf{t}}(\mathbf{s})}{ds} = \kappa_g \hat{\mathbf{T}}(s) + \kappa_n \hat{\mathbf{N}}(s) ,$$

$$\frac{d\hat{\mathbf{T}}(\mathbf{s})}{ds} = -\kappa_g \hat{\mathbf{t}}(s) + \tau_g \hat{\mathbf{N}}(s) ,$$

$$\frac{d\hat{\mathbf{N}}(\mathbf{s})}{ds} = -\kappa_n \hat{\mathbf{t}}(s) - \tau_g \hat{\mathbf{T}}(s) ,$$

are known as the Bonnet-Kovalevski relations [30]. They may therefore be considered to relate the shape of the tool path to the shape of the surface on which it lies.

From the definitions of κ_g and κ_n it is possible to derive expressions that describe, at a given point, the shape of a tool path lying on a surface [30]. It can be shown that the path's curvature is [30]

$$\kappa = \pm\sqrt{\kappa_g^2 + \kappa_n^2} .$$

The sign of κ is equal to the sign of κ_g in the interval $-\pi/2 < \phi < \pi/2$. The corresponding torsion of the tool path is [30]

$$\tau = \tau_g - \frac{\triangle}{\kappa^2} ,$$

where $\triangle$ is the determinant,

$$\triangle = \begin{vmatrix} \kappa_g & \kappa_g' \\ \kappa_n & \kappa_n' \end{vmatrix}.$$

A given tool path therefore does not lose its identity when it lies on a surface [30]. The Frenet frame, $\mathbf{F}_1(s)$, is retained at each point on the path [30]. Further, from the fundamental theorem of space curves, the shape of a tool path is completely defined by its curvature and torsion profiles [31]. The following analysis of tool path motion is therefore conducted independently of surface shape, and solely in terms of the path's intrinsic shape properties.

Frame motion and in turn the motion of any object that moves with the frame, for example a cutting tool, may be described in terms of curvature and torsion. For example, $\kappa(s)$ and $-\tau(s)$ describe the angular velocities of the unit tangent and binormal vectors as the Frenet frame traverses a tool path [8].

Other intrinsic shape properties also offer a kinematic interpretation. As a consequence of unit feed rate traversal of a tool path, the parameters, arc length and time, may be considered identical, $s \equiv t$ ($ds/dt = 1 \Rightarrow \int_0^s ds = \int_0^t dt \therefore s = t$). It then follows that $d\mathbf{r}(s)/ds \equiv d\mathbf{r}(t)/dt$. The unit tangent is thus equivalent to the velocity vector. Also, $d\hat{\mathbf{t}}(s)/ds \equiv d\mathbf{v}(t)/dt$. The curvature vector is thus equivalent to the acceleration vector. Further, $d\kappa(s)/ds \equiv d\mathbf{a}(t)/dt$. The rate at which the curvature vector changes with respect to arc length is therefore equivalent to the jerk vector.

Investigating unit feed rate traversal is useful for helping to develop initial insight into the shape properties of motion, but general motion, at an arbitrary speed, requires further effort. The

following sections derive the velocity, acceleration and jerk equations for tool path traversal at an arbitrary feed rate.

2.3 Velocity

2.3.1 Definition

The derivative of the position vector, $\mathbf{r}(s)$, with respect to time, t, produces the velocity vector, $\mathbf{v}(t)$,

$$\mathbf{v}(t) = \frac{ds}{dt}\frac{d\mathbf{r}(s)}{ds} \ .$$

Therefore,

$$\mathbf{v}(t) = \frac{ds}{dt}\hat{\mathbf{t}}(s) \ . \tag{2.4}$$

Dimensional analysis reveals that this kinematic vector may be described in terms of the base quantities, length and time, $length/time$. Using the International System of Units (SI), magnitudes of velocity are expressed in m/s [32].

2.3.2 Feed rate

The rate at which the arc length of a tool path changes with respect to time quantifies the magnitude of the velocity vector. The magnitude of velocity is perhaps more appropriately referred to as feed rate within the context of machining. The velocity vector lies in the direction of a first order *osculant* to the tool path at a given point [31]. A member, Γ_0, of a family of curves, Γ_λ, which intersect the tool path, at a given point, is called an *osculating curve of the family* to the tool path, if the degree of contact with Γ_0, at the point, is greater than or equal to the degree of contact of the tool path with any other of the curves from Γ_λ [31]. It then follows for the velocity vector, a first order osculant is a line that best approximates the path in the vicinity of a given point [31].

2.4 Acceleration

2.4.1 Definition

The derivative of the velocity vector, $\mathbf{v}(t)$, with respect to time, t, produces the acceleration vector, $\mathbf{a}(t)$,

$$\mathbf{a}(t) = \frac{d\mathbf{v}(t)}{dt} .$$

Its dimensions are $length/time^2$. Commonly used units to express accelerations are mm/min^2

and the SI units, m/s^2 [32].

2.4.2 Tangential and normal components

From Eq. (2.4) it follows that,

$$\mathbf{a}(t) = \frac{d}{dt}\left\{\frac{ds}{dt}\hat{\mathbf{t}}(s)\right\}$$

$$= \frac{d^2s}{dt^2}\hat{\mathbf{t}}(s) + \left\{\frac{ds}{dt}\right\}^2 \frac{d\hat{\mathbf{t}}(s)}{ds} \ .$$

Substituting Eq. (2.1) into the above equation produces an expression for the acceleration vector in terms of its tangent and normal components:

$$\mathbf{a}(t) = \frac{d^2s}{dt^2}\hat{\mathbf{t}}(s) + \left\{\frac{ds}{dt}\right\}^2 \kappa(s)\hat{\mathbf{n}}(s) \ . \tag{2.5}$$

The second derivative of arc length with respect to time defines tangential acceleration. It is therefore the rate at which feed rate changes along the tool path. The normal component of acceleration is expressed in terms of curvature. The rate at which the normal component of acceleration changes with respect to time is directly proportional to the path's curvature. It can be shown that this normal acceleration acts towards the centre of the circle of curvature [14]. At each point on the tool path, the corresponding circle of curvature is a second order

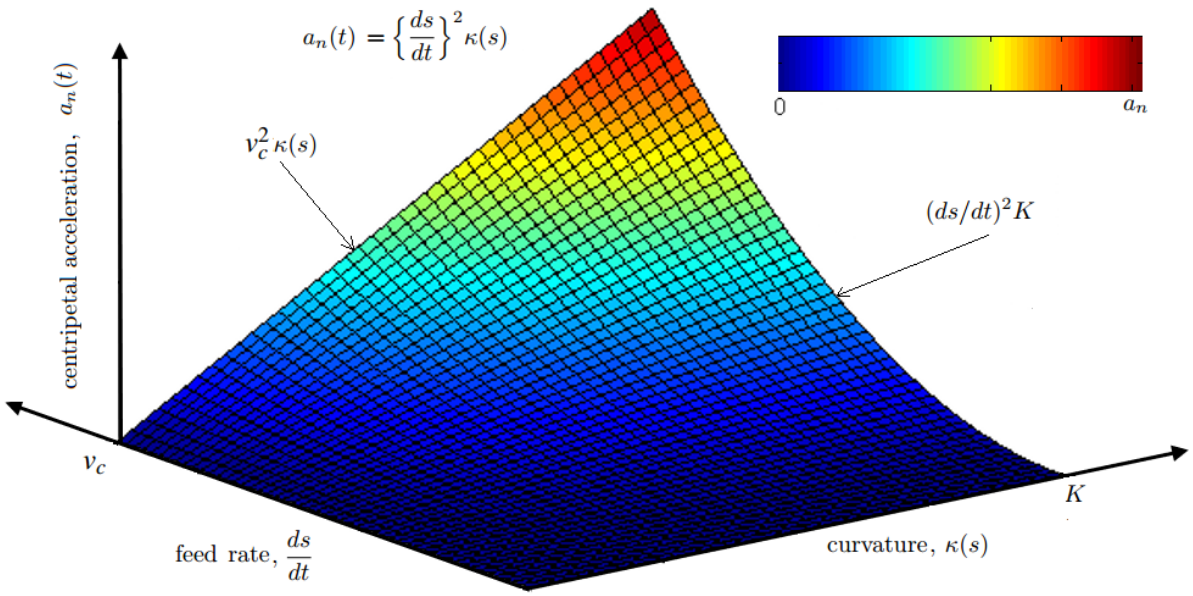

Figure 2.4: Centripetal acceleration surface

osculant, whose derivatives, up to and including order two, agree with those of the path [14]. Subsequently, normal acceleration is commonly referred to as centripetal acceleration [33].

From Eq. (2.5) it follows that normal acceleration consists of time and shape dependent elements, feed rate, ds/dt, and curvature, $\kappa(s)$, respectively. The surface, shown in Fig. (2.4), illustrates the effect of each element on centripetal acceleration, $a_n(t)$. The surface is mathematically expressed explicitly in terms of ds/dt and $\kappa(s)$, $a_n(t) = (ds/dt)^2\kappa(s)$. Centripetal acceleration (Fig. 2.5) increases linearly with curvature, $a_n(t) = v_c^2\kappa(s)$, for a constant feed rate, v_c. Centripetal acceleration increases parabolically with feed rate, $a_n(t) = (ds/dt)^2 K$, for a constant curvature, K.

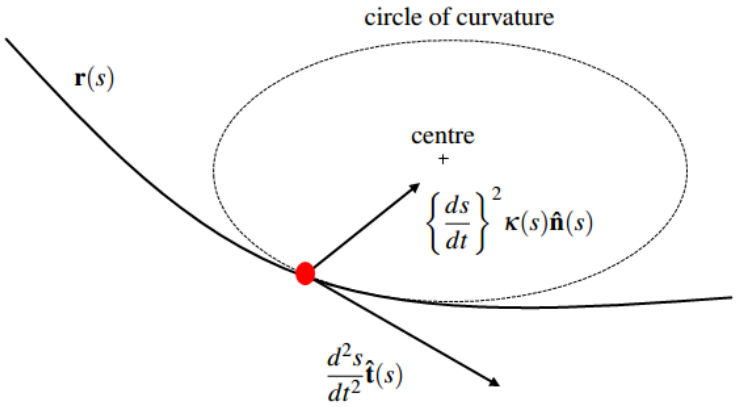

Figure 2.5: Acceleration vector components

2.5 Jerk

2.5.1 Definition

The derivative of acceleration with respect to time is defined as jerk,

$$\mathbf{j}(t) = \frac{d\mathbf{a}(t)}{dt} \,. \tag{2.6}$$

This kinematic vector may be described in terms of the base quantities, length and time, $length/time^3$. Using SI units, magnitudes of jerk are expressed in m/s^3 [32]. Other common units are g/s (standard gravity per second) and mm/min^3 [32].

2.5.2 Geometric interpretation

It follows from the above definition that jerk is the third derivative of displacement with respect to time,

$$\frac{d\mathbf{a}(t)}{dt} \equiv \frac{d^2\mathbf{v}(t)}{dt^2} \equiv \frac{d^3\mathbf{r}(t)}{dt^3} \ .$$

Jerk is the rate of change, of the rate of change, of the rate of change of displacement with respect to time. Such an explicit temporal (time-related) interpretation may not be the most intuitive and so it can be difficult to gain insight into problems relating to this kinematic vector. By analysing the relationships between force and motion, this section provides a geometric interpretation of jerk that may be of more practical engineering use.

Consider Newton's second law. *"Lex II: Mutationem motus proportionalem esse vi motirici impressae, et fieri secundum lineam reactum qua vis illa imprimitu"* [34]. A modern translation, accounting for Newton's use of terminology, is "Law II: A change in motion is proportional to the motive force impressed and takes place along the straight line in which that force is impressed" [35]. Commonly this law is expressed mathematically as $\mathbf{F}(t) = m\mathbf{a}(t)$, where $\mathbf{F}(t)$ is the *motive force impressed* on a body of mass m causing an acceleration $\mathbf{a}(t)$. This motive force (or resultant force) may be seen as a force which acts over a period of time, an impulse [35]. It then follows that, assuming the body's mass is unchanged, acceleration is not constant. A description for the rate at which the acceleration changes with respect to time can be obtained

from differentiating the equation describing the law,

$$\frac{d\mathbf{F}(t)}{dt} = m\frac{d\mathbf{a}(t)}{dt} \ .$$

Because of Eq. (2.6),

$$\frac{d\mathbf{F}(t)}{dt} = m\mathbf{j}(t) \ .$$

Jerk experienced, by a body of given mass, is therefore directly proportional to the rate at which the resultant force acting on the body changes over a period of time. Jerk may therefore be thought of as the first derivative of force, opposed to the third derivative of displacement, with respect to time.

The resultant force, of a given motion, need not act in a manner that changes the magnitude of the velocity vector. Provided the force acts perpendicular to the direction of travel, no component of it will lie parallel to the velocity vector and so will not affect its magnitude. This force will only affect the rate at which the direction of the velocity vector changes. The force is therefore directly proportional to curvature and so is confined to lie along the line of intersection of the rectifying and osculating planes.

2.5.3 Vector components

From the three kinematic properties discussed in this chapter, jerk has perhaps received comparatively little attention since it does not appear directly in mathematical expressions of fundamental engineering concepts likes energy, force and momentum. Trends of high speed ma-

chining and increased part shape complexity, have however led to jerk becoming an important parameter that should be well considered [28]. For example, it has been shown that jerk can influence vibrations of industrial high-speed systems [36]. Significant investigations have been undertaken to consider jerk when planning machine motion [19, 37–39]. It is for this reason that the effects of shape on jerk are considered in this thesis.

By taking the derivative of Eq. (2.5) with respect to time and making substitutions with Frenet-Serret formulae (Eqs. (2.1)–(2.3)), it can be shown that jerk can be described as the sum of three orthogonal components (see appendix B).

$$\mathbf{j}(t) = j_t(t)\hat{\mathbf{t}}(s) + j_n(t)\hat{\mathbf{n}}(s) + j_b(t)\hat{\mathbf{b}}(s) \; ; \tag{2.7}$$

where

$$j_t(t) = \frac{d^3 s}{dt^3} - \left\{\frac{ds}{dt}\right\}^3 \{\kappa(s)\}^2 \; ,$$

$$j_n(t) = 3\frac{ds}{dt}\frac{d^2 s}{dt^2}\kappa(s) + \left\{\frac{ds}{dt}\right\}^3 \frac{d\kappa(s)}{ds} \; ,$$

and

$$j_b(t) = \left\{ \frac{ds}{dt} \right\}^3 \kappa(s)\tau(s) \ .$$

The normal component of jerk can also be expressed in terms of an affine differential invariant of plane paths, namely *aberrancy* [40]. The local asymmetry of a path with respect to the path's normal at a given point is measured by aberrancy [40]. It can be shown that the normal component of jerk, at a given point on a path, is related to a unique parabola whose Cartesian derivatives, up to and including order three, agree with those of the path [15]. This parabola may be reffered to as the osculating parabola [15].

2.6 Chapter summary

Using the Frenet-Serret relations, section 2.1 introduced the shape properties, curvature and torsion, and discussed them within the context of tool path shape. The following section (2.2) then considered their connection to the shape properties of CAD model surfaces. It was shown that the effects of shape on tool path motion can be investigated without reference to the shape properties of the corresponding CAD model. This then enabled, in sections 2.3, 2.4 and 2.5, the general kinematic vector equations of tool path motion to expressed in terms of the tool path's intrinsic shape properties. Establishing the kinematic vector equations in this manner has facilitated the task of deriving the shape characteristic model in the following chapter.

Chapter 3

Shape characterisation of bounded motion

Any given machine must operate within the confines of its physical abilities [13]. For example, tool path motion is bound by a machine's kinematic limits [1, 13, 41–43]. This chapter provides a description of tool path motion accounting for such limits. A shape characterisation of tool path motion is postulated by enforcing constraints on the general kinematic vector equations developed in the previous chapter (Eqs. (2.4), (2.5) and (2.7)). The resulting description of tool path motion depends only upon the kinematic limits of the machine and the intrinsic shape properties of the tool path. Both sets of parameters (kinematic limits and shape properties) may be identified prior to physical machining. The curvature and torsion of a tool path may be found from interrogation of the derivatives of the path with respect to the path's given parameterisation [8, 14]. The maximum magnitudes of the velocity, acceleration and jerk vectors may be found using the techniques discussed in the following chapter.

This chapter therefore demonstrates an *a priori* approach to describing and assessing tool path

motion. The first section begins by establishing the behaviour of the velocity, acceleration and jerk vectors when a tool path is traversed at a constant feed rate. This is then followed by analysis of the effects of a given machine adhering to its maximum centripetal acceleration limit. Once the characteristic equations describing bounded tool path motion have been expressed in terms of shape, the chapter concludes by presenting a series of shape schematics. These diagrams illustrate the permissible magnitudes for kinematic vectors given the shape of a tool path.

3.1 Velocity limited phase

Eqs. (2.4), (2.5) and (2.7) show that constant feed rate traversal of a tool path, with an arbitrary shape, imposes a particular set of kinematic demands on a given machine. A constant commanded feed rate of Ψ_1 implies that the rate at which the arc length, s, along a tool path changes with respect to time, t, is constant, $ds/dt = \Psi_1$. From Eq. (2.4) it follows that the velocity vector required for traversal can be expressed as

$$\mathbf{v}(t) = \Psi_1 \hat{\mathbf{t}}(s) \; . \tag{3.1}$$

From Eq. (2.5) it can be seen that a description of the acceleration necessary to provide constant feed rate requires the evaluation of the second derivative of arc length with respect to time. Since $ds/dt = \Psi_1$ which is assumed constant, it follows that,

$$\frac{d^2s}{dt^2} = \frac{d^3s}{dt^3} = 0 \, .$$

No component of the acceleration vector thus lies in the direction of travel. The acceleration is parallel to the curvature vector and is thus referred to as centripetal acceleration. Substitution of the above expression into Eq. (2.5) gives,

$$\mathbf{a}(t) = \Psi_1^2 \kappa(s) \hat{\mathbf{n}}(s) \, . \tag{3.2}$$

For a given feed rate, acceleration is directly proportional to the curvature of the path. For a given curvature, the magnitude of the acceleration vector increases parabolically with feed rate. Eq. (3.2) shows that the acceleration vector changes both its direction and magnitude as it traverses a tool path at a constant feed rate, Ψ_1. Tool path motion therefore requires the existence of a jerk vector. Substituting the first three derivatives of arc length with respect to time into Eq. (2.7) produces the following expression for the jerk vector occurring during constant feed rate traversal,

$$\mathbf{j}(t) = \Psi_1^3 \left[\frac{d\kappa(s)}{ds} \hat{\mathbf{n}}(s) - \{\kappa(s)\}^2 \hat{\mathbf{t}}(s) \right] \, . \tag{3.3}$$

3.2 Acceleration limited phase

Eq. (3.2) shows that at a constant feed rate acceleration is directly proportional to curvature. The magnitude of acceleration increases linearly with curvature. As discussed in the introductory chapter, this growth cannot be sustained indefinitely. At a given point on the tool path, its curvature will impose a magnitude of the centripetal acceleration vector that exceeds the machine's limits. It is at this point that controller regulation must intervene to provide an alternative motion to that requested in the NC file. As argued previously, the nature of the control algorithms have some dependence on the mechatronic attributes of the given machine and so different machines can respond differently to an imposed breach of the kinematic limits.

A possible action is to continue to provide the maximum centripetal acceleration permitted by a machine, Ψ_2, despite curvature imposing a greater magnitude [1]. Such an action will cause the machine to transition from a velocity to an acceleration limited phase of tool path motion. The point on a given tool path where this phase transition occurs may be identified by the path's curvature, which is therefore referred to as the *transition curvature*, κ_α [1]. The curvature, κ_α, at which a commanded feed rate, Ψ_1, requires a machine's maximum centripetal acceleration, Ψ_2, can be found from Eq. (3.2). It follows that $\kappa_\alpha = \Psi_2/\Psi_1^2$.

By enforcing a limit on the centripetal acceleration, the normal component of the general expression for the acceleration vector, Eq. (2.5), may be equated to Ψ_2,

$$\left\{\frac{ds}{dt}\right\}^2 \kappa(s(t)) = \Psi_2 \ .$$

It then follows that feed rate during the acceleration limited phase of motion may be expressed as,

$$\frac{ds}{dt} = \sqrt{\frac{\Psi_2}{\kappa(s)}} \, . \tag{3.4}$$

The magnitude of velocity is thus inversely proportional to the square root of curvature,

$$\mathbf{v}(t) = \sqrt{\frac{\Psi_2}{\kappa(s)}} \hat{\mathbf{t}}(s) \, . \tag{3.5}$$

As curvature increases past κ_α, the feed rate decreases. A tangential deceleration must therefore occur. The nature of this deceleration can be characterised by the derivative of Eq. (3.4), since this corresponds to the tangential component of Eq. (2.5). The second derivative of arc length with respect to time is thus,

$$\frac{d^2s}{dt^2} = \sqrt{\Psi_2} \frac{d}{ds} \left\{ \sqrt{\frac{1}{\kappa(s)}} \right\} \frac{ds}{dt} \, .$$

It then follows that,

$$\frac{d^2s}{dt^2} = -\frac{1}{2} \sqrt{\frac{\Psi_2}{\{\kappa(s)\}^3}} \frac{d\kappa(s)}{ds} \frac{ds}{dt} \, .$$

Substituting Eq. (3.4), into the above equation enables the tangential acceleration component to be expressed as

$$\frac{d^2s}{dt^2} = -\frac{1}{2}\Psi_2 \frac{1}{\{\kappa(s)\}^2}\frac{d\kappa(s)}{ds} \,. \tag{3.6}$$

Thus the complete acceleration vector is given by

$$\mathbf{a}(t) = \Psi_2 \left[\hat{\mathbf{n}}(s) - \frac{1}{2}\frac{1}{\{\kappa(s)\}^2}\frac{d\kappa(s)}{ds}\hat{\mathbf{t}}(s)\right] \,. \tag{3.7}$$

Given a tool path whose curvature increases at a constant rate, the magnitude of the tangential deceleration required to adhere to the centripetal acceleration limit increases. Further, by definition, the normal component of acceleration is constant.

Eq. (2.7) shows that the tangential component of the general jerk vector contains the third derivative of arc length with respect to time, d^3s/dt^3. Taking the derivative of Eq. (3.6) with respect to time gives,

$$\begin{aligned} \frac{d^3s}{dt^3} &= -\frac{1}{2}\Psi_2 \frac{d}{ds}\left[\frac{1}{\{\kappa(s)\}^2}\frac{d\kappa(s)}{ds}\right]\frac{ds}{dt} \\ &= -\frac{1}{2}\Psi_2 \frac{1}{\{\kappa(s)\}^2}\left[\frac{d^2\kappa(s)}{ds^2} - 2\frac{1}{\kappa(s)}\left\{\frac{d\kappa(s)}{ds}\right\}^2\right]\frac{ds}{dt} \,. \end{aligned} \tag{3.8}$$

An alternative form of Eq. (3.4) is

$$\frac{ds}{dt} = \frac{\sqrt{\Psi_2}\sqrt{\kappa(s)}}{\kappa(s)} \,. \tag{3.9}$$

Substituting this expression into Eq. (3.8) gives,

$$\frac{d^3s}{dt^3} = -\frac{1}{2}\Psi_2\sqrt{\Psi_2}\sqrt{\kappa(s)}\frac{1}{\{\kappa(s)\}^3}\left[\frac{d^2\kappa(s)}{ds^2} - 2\frac{1}{\kappa(s)}\left\{\frac{d\kappa(s)}{ds}\right\}^2\right] .$$

The alternative expression for feed rate can also be substituted into the other term of tangential jerk to give,

$$\left\{\frac{ds}{dt}\right\}^3 \{\kappa(s)\}^2 = \Psi_2\sqrt{\Psi_2}\sqrt{\kappa(s)} \,.$$

Substituting the above two expressions into Eq. (2.7) characterises the tangential jerk experienced during the acceleration limited phase of tool path motion,

$$j_t(t) = -\frac{\Psi_2\sqrt{\Psi_2}\sqrt{\kappa(s)}}{2\{\kappa(s)\}^3}\left[\frac{d^2\kappa(s)}{ds^2} - 2\frac{1}{\kappa(s)}\left\{\frac{d\kappa(s)}{ds}\right\}^2 + 2\{\kappa(s)\}^3\right] . \tag{3.10}$$

Substituting Eqs. (3.4) and (3.6) into the normal component of Eq. (2.7), provides a means of characterising the normal component of jerk in the acceleration limited phase of tool path

motion,

$$j_n(t) = -\frac{\Psi_2\sqrt{\Psi_2}\sqrt{\kappa(s)}}{2\{\kappa(s)\}^2}\frac{d\kappa(s)}{ds} \ . \tag{3.11}$$

3.3 Shape schematics

Having described the characteristics of bounded tool path motion in terms of shape, this section consolidates the corresponding equations into a series of diagrams, referred to in this thesis as *shape schematics*. Curvature alone describes the shape of a planar tool path [14]. By plotting the magnitude of each kinematic vector with respect to curvature, each of the shape schematics provide a complete illustration of the effects of planar tool path shape on a given kinematic vector. Further, by considering a constant curvature derivative, the shape of the profiles are independent of any derivative of curvature with respect to arc length, $d^n\kappa(s)/ds^n$, $n \geq 1$. Within the context of the schematics, these derivatives simply correspond to the rates at which the profiles are rendered. For simplicity, it is assumed that the schematics are rendered at a constant rate, specifically $d\kappa(s)/ds = 1$ and so $d^n\kappa(s)/ds^n = 0$, $n \geq 2$ (Figs. 3.1, 3.2, 3.3 and 3.4). For a tool path where the $d\kappa(s)/ds$ is not constant, the appropriate magnitudes must be substituted into the relevant equations when constructing the corresponding shape schematics. A non constant curvature derivative changes the magnitudes of the normal component of jerk during the velocity limited phase of motion (Eq. 3.11), as well as the tangential acceleration and both components of the jerk vector during the acceleration limited phase of motion (Eq. 3.7 and Eqs. 3.10 and 3.11 respectively).

At κ_α an instantaneous tangential deceleration is required in order to adhere to the centripetal acceleration limit. γ_1, shown in Fig. 3.2, may be quantified by substituting κ_α into Eq. (3.6). $\because d^2s/dt^2\big|_{\kappa(s)=\kappa_\alpha} \equiv \gamma_1$ and $d\kappa(s)/ds = 1$ and so,

$$\gamma_1 = -\frac{1}{2}\Psi_2\frac{1}{\kappa_\alpha^2} \ .$$

The normal component of the jerk vector changes direction instantaneously at κ_α. The value of this component in the acceleration limited phase is denoted by γ_2 and can be quantified by evaluating Eq. (3.11) when $\kappa(s) = \kappa_\alpha$. γ_2 is thus,

$$\gamma_2 = -\frac{\Psi_2\sqrt{\Psi_2}\sqrt{\kappa_\alpha}}{2\kappa_\alpha^2} \ .$$

γ_3 and γ_4 are labels for the tangential jerks at κ_α. Approaching κ_α from the velocity limited phase to the acceleration limited phase, requires an instantaneous increase in magnitude from $|\gamma_3|$ to $|\gamma_4|$. Approaching κ_α from the acceleration limited phase to the velocity limited phase, requires an instantaneous decrease in magnitude from $|\gamma_4|$ to $|\gamma_3|$. Evaluation of Eq. (3.3) therefore expresses γ_3,

$$\gamma_3 = -\Psi_1^3\kappa_\alpha^2 \ ,$$

and evaluating Eq. (3.10) gives γ_4,

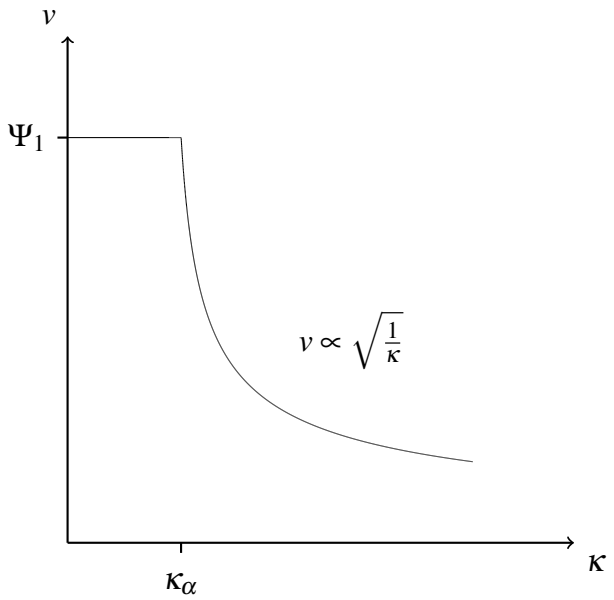

Figure 3.1: Velocity schematic

$$\gamma_4 = \Psi_2\sqrt{\Psi_2}\left\{\sqrt{\frac{1}{\kappa_\alpha^7}} - \sqrt{\kappa_\alpha}\right\}.$$

In the acceleration limited phase of motion γ_5, shown in Fig. 3.4, denotes the point at which the direction of the tangential jerk vector changes again. The value of γ_5 can be found by equating Eq. (3.10) to zero and accounting for $\kappa \geq \kappa_\alpha$.

The discontinuities illustrated in Figs. 3.2, 3.3 and 3.4 are a result of ignoring acceleration and deceleration from and to rest. In practice these discontinuities, that occur at the transition curvature, refer to the discrete time period where a machine transitions from one limited phase to another [1]. The actual curvature at which this transition begins must therefore be less than the theoretical transition curvature [1].

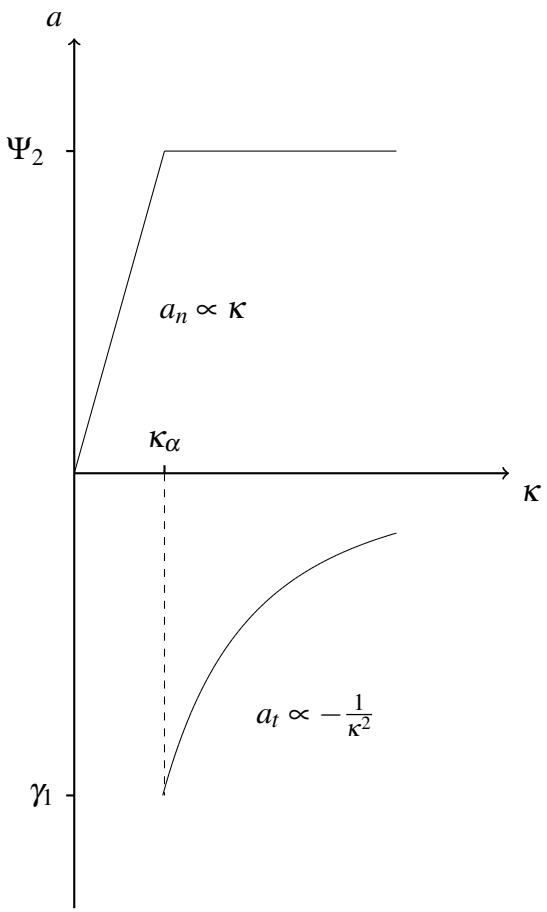

Figure 3.2: Acceleration schematic

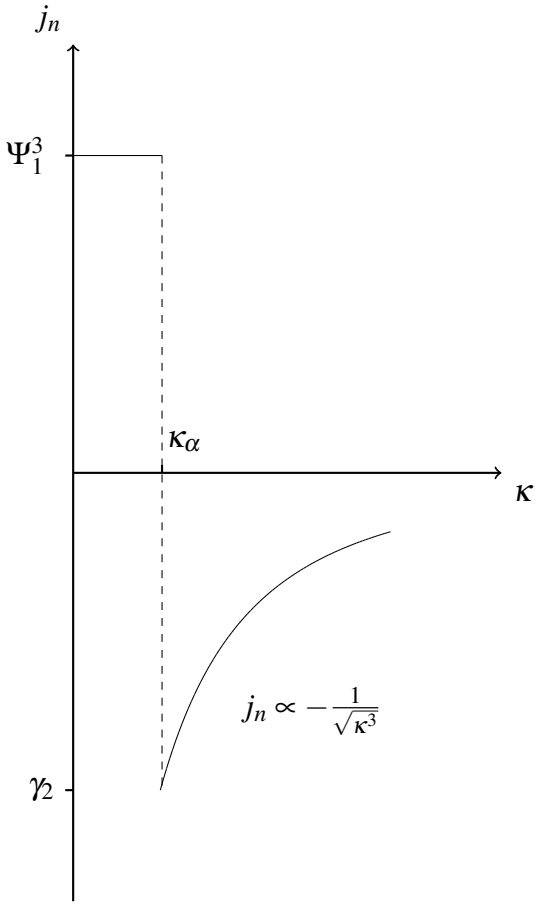

Figure 3.3: Normal jerk schematic

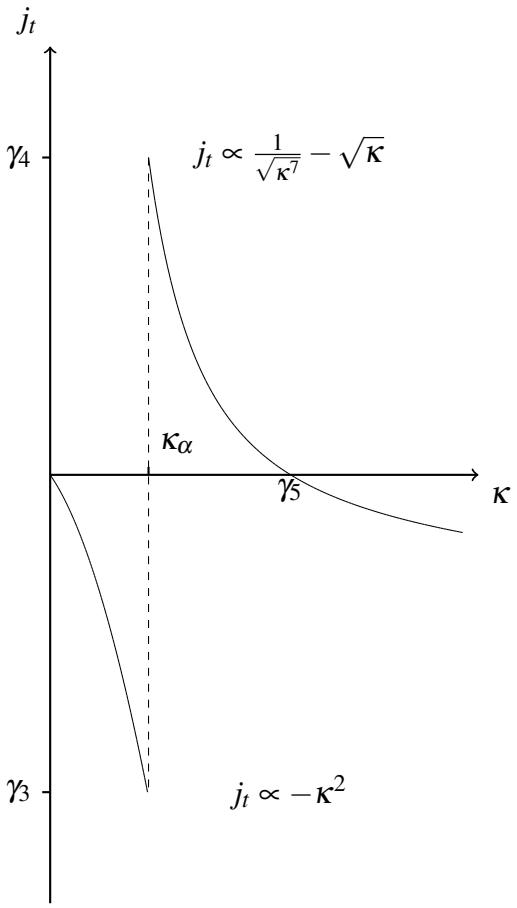

Figure 3.4: Tangential jerk schematic

3.4 Chapter summary

This chapter has characterised tool path motion in terms of the path's intrinsic shape properties. Two distinct phases of motion originated as a result of enforcing limits on the velocity, acceleration and jerk vectors.

The velocity limited phase enforced the constraint of constant feed rate traversal, Eq. (3.1). In order to maintain a constant feed rate it was shown that, at a given point, the magnitude of the acceleration vector must be directly proportional to the curvature of the tool path, Eq. (3.2). Analysis of the change in both the direction and magnitude of this acceleration vector revealed the behaviour of the jerk vector, Eq. (3.3). It was shown that the normal component of jerk is directly proportional to the rate at which the curvature changes with respect to arc length. Further, the magnitude of the tangential component increases parabolically with curvature but is directed opposite to the direction of travel.

The acceleration limited phase enforced the constraint of a maximum magnitude on the centripetal acceleration vector. It was shown that in order to adhere to this limit, the feed rate is required to decrease as the path's curvature increases. Specifically, Eq. (3.4), shows that the feed rate is inversely proportional to the square root of the path's curvature. This change in feed rate was shown to require a negative tangential acceleration, a deceleration, that is described by Eq. (3.6). Finally, the behaviour of the tangential and normal components of the corresponding jerk vector are described by Eqs. (3.10) and (3.11).

Direct interpretation of the above mentioned equations (Eqs. (3.1)–(3.3), (3.5), (3.7), (3.10) and

(3.11)) may not be the most intuitive or insightful. Consider for example, the expression for the tangential component of the jerk vector during the acceleration limited phase of motion,

$$-\frac{\Psi_2\sqrt{\Psi_2}\sqrt{\kappa(s)}}{2\{\kappa(s)\}^3}\left[\frac{d^2\kappa(s)}{ds^2}-2\frac{1}{\kappa(s)}\left\{\frac{d\kappa(s)}{ds}\right\}^2+2\{\kappa(s)\}^3\right].$$

The shape schematics (Figs. 3.1, 3.2, 3.3 and 3.4) therefore provide concise illustrations of the velocity, acceleration and jerk vectors.

Chapter 4

Shape imposed kinematics

Having established a shape characterisation of tool path motion in the previous chapter, this chapter provides empirical evidence to support the corresponding shape schematics. By controlling the shape properties of a series of test tool paths, the imposed kinematics are controlled and the resulting motions are subsequently analysed to deduce the effects of shape.

The chapter begins by describing the test methodology employed to obtain the empirical evidence. This is then followed by an explanation of the apparatus and the techniques used to deduce the kinematics achieved for the specified tool path motions. This chapter then concludes by comparing the resulting kinematic profiles with the shape schematics of the characteristic model (chapter 3).

4.1 Methodology

4.1.1 General approach

Tool path shape is controlled to affect the kinematics imposed on a given machine. If these kinematics exceed the limits of the machine they cannot be realised in practice. Instead a motion with permissible kinematics will result from controller regulation. The differences between requested and achieved kinematics are studied. The resulting analysis may then be used to identify the maximum achievable kinematics for a tool path with given shape properties.

Many factors influence the kinematic properties produced by a given machine. Indeed, any natural phenomenon that causes the resultant force of a motion to change affects the kinematics achieved. For example, during machining the cutting forces, acting opposite to the direction of travel, can reduce the magnitude of the resultant force acting on a tool, thereby causing deceleration. This in turn causes the magnitude of velocity to decrease. It then follows that a smaller feed rate is observed. The desire is thus to isolate the effects of tool path shape on machine motion. However, not all factors can be controlled. For example, the magnitudes of the vibrations resulting from external influences may not be known or predictable. Actions are therefore taken to control testing conditions by minimising the effects of factors that can be controlled.

4.1.2 Testing conditions

For all tests, the mass loads on the axes are kept constant. Larger masses exert greater burdens on servomotors and affect achievable kinematics [13]. The masses of workpieces and cutting tools can vary depending upon the application for which the machine is being used. No workpiece or cutting tool is therefore fixed to the machine during testing. The main mass loads that the servomotors must overcome are the masses of the spindle and the axes. The spindle does not rotate and since there is no tool and workpiece, no material removal occurs, therefore no vibrations are induced from cutting. The axes are free to move without hindrance of surplus mechanical loads.

To increase the repeatability of the free motion tests, machine temperature is stabilised using a standard warming-up procedure [44]. From a *cold start* machine lubricant is distributed throughout the mechanical system. Some frictional energy is converted to heat. The resulting increase in temperature can cause thermal expansion of the mechanical components, in particular the machine's axes [45]. This thermally induced axis distortion can cause errors in the resulting motions [45]. Through conducting the warming-up procedure the rate at which temperature changes, with respect to time, decreases and begins to stabilise. This lessens the changes in the dimensions of the components. Smaller variability is therefore expected of the kinematics produced from repeated trials of a given test tool path.

4.1.3 Test tool paths

Circles are deemed appropriate test tool paths to identify the effects of shape on machine kinematics. Since circular tool paths are planar, only curvature needs to be manipulated. Torsion need not been considered ($\tau(s) = 0$). The shape of a given circle is described by a constant curvature, κ_c. Circles are also closed paths. Multiple traversals/revolutions can therefore be preformed without intermission, thus reducing time to perform tests and providing sufficient distance for a constant feed rate, $ds/dt = v_c$, to be achieved. From Eqs. (2.4), (2.5) and (2.7) it follows that the kinematic vectors imposed by tool path shape are of constant magnitude and their directions do not change relative to each other (Fig. 4.1). The analysis is simplified because in general acceleration and jerk may consist of two and three orthogonal components respectively, but at constant speed, each can be described by single component vectors (see chapter 2). Further, constant speed circular tool path motion may be characterised by the equations governing simple harmonic motion (SHM) [46]. This facilitates analysis of the tool path motion frequencies, undertaken in the following section.

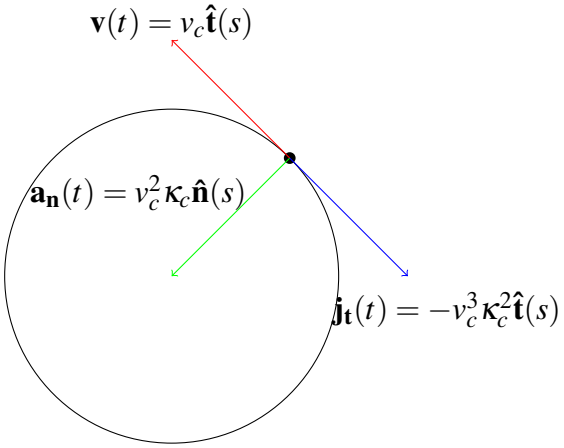

Figure 4.1: Shape imposed kinematics

4.2 Data aquisition

4.2.1 Test machines

As discussed in the introductory chapter, the specific nature of the motion control algorithms implemented by a given machine may not be known to the engineer. Further, the algorithms used by one machine need not be the same as those used by another. The test tool path motions are performed on three machines, the Hermle $C600U$, the Mazak $VCS430A$ and the Matsuura $LX1$, as a means of demonstrating that different machines may regulate a specified tool path motion according to their own specific motion control algorithms.

To ensure that the highest kinematic demands were enforced on each of the machines, the maximum feed rates were selected for each machine. Specifically, all the test tool paths had a commanded feed rate of $8m/min$, $35m/min$ and $90m/min$ on the Mazak, Hermle and Matsuura, respectively [47–49].

For all the machines, the circular motions are performed through simultaneous motion of two linear axes. For a given machine, the specific two linear axes chosen are immaterial since each linear axis is orthogonal to the other two and assuming each axis has the same kinematic capabilities, the kinematic properties of each axis form Cartesian components of the resultant kinematic properties of tool path motion. Technical data for each of the machines verifies that indeed all the axes of a machine have the same kinematic specification [47–49]. Further, preliminary testing suggests negligible difference in the motions produced between planes. The data presented in this thesis is therefore derived from motions in each of the machines' principal

xy planes.

4.2.2 Accelerometer

As shown by Eqs. (2.4), (2.5) and (2.7), to quantify the actual velocity, acceleration and jerk experienced on a given circular tool path, the achieved feed rate is required. Each of the controllers of the test machines provide a Digital Read-Out (DRO) of feed rate. This however, is not an independent source of measurement and as such can only be used as a preliminary indicator of the actual feed rate achieved in a given motion. An inertial sensor, specifically a tri-axial piezoresistive accelerometer, is used as an independent measurement source [50]. The sensor outputs the acceleration and time of a given motion. The achieved feed rate is then deduced from this acceleration profile. The actual velocity, acceleration and jerk experienced can then be found for each circular tool path from Eqs. (2.4), (2.5) and (2.7).

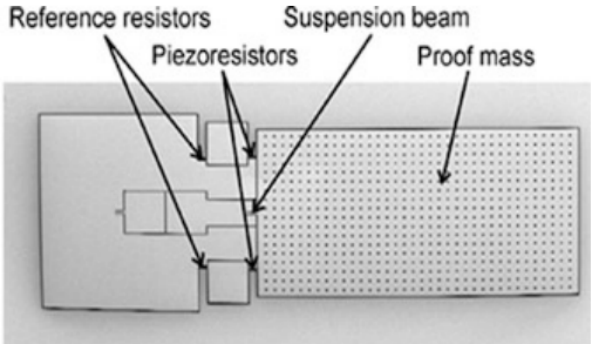

Figure 4.2: Diagram of a piezoresistive accelerometer [51]

The main principle on which the accelerometer operates is the piezoresistive effect [52]. This is a phenomenon whereby the application of mechanical stress causes a change in the electrical

Table 4.1: Accelerometer specification

Parameter	Value
Model	EGCS-50-QB
S/N	28 T6 JFG 3
Sensitivity (X/Y/Z)	$4.63 mV/g$
Input Imped (X/Y/Z)	$1116 ohms$
Output Imped (X/Y/Z)	$434 ohms$
Range	$\pm 50g$
Excitation	$15V$

resistivity of a semiconductor material [53]. When a resultant force causes the proof mass to accelerate, the piezoresistive elements are strained (Fig. 4.2). This strain in turn causes a change in resistance, which is amplified by the Wheatstone-bridge circuit configuration of the piezoresistors [54]. The resistance change causes an imbalance of the bridge and results in a change of voltage output that is proportional to the acceleration experienced by the proof mass and in turn the object that the sensor is attached to.

The specific piezoresistive accelerometer used was an Entran EGCS-50-QB. To ensure the sensor performed according to its specification (see table 4.1) and to provide meaning to its electrical outputs, each axis was calibrated using gravity. Each axis was rotated by $\pi/2$ radians in order to identify the voltages produced by the axes parallel and perpendicular to Earth's gravitational field. These values were then used to define the linear relationships between voltage and acceleration for each axis [53]. Further, a suitable data acquisition rate was chosen to ensure the accelerometer captured data at a sufficient rate in order to provide an appropriate representation of the acceleration experienced [53]. Preliminary testing revealed that a rate of $10,000\ Hz$ was more than sufficient to provide a representation of the actual acceleration experienced.

Other types of accelerometer were considered. For example, piezoelectric accelerometers were

trialled in preliminary testing. They exploit the vibrations of piezoelectric crystals to deduce accelerations. It was found that these accelerometers are more appropriate for applications involving higher frequency motions compared to the test tool path motions. For example, ballistics and engine testing [53].

In the case of the Hermle and Matsuura CNC machines, the accelerometer's axes are aligned with the given machine's axes and mounted, via an appropriate adhesive, to the flat vertical cladding of the corresponding z axis housings. Fig. 4.3 shows the accelerometer attached to the casing of the Hermle's coolant ducts. The assembly of the Mazak's axes is such that the x and y axes are independent of the z axis and so for this machine, the accelerometer was mounted to the machine's work table.

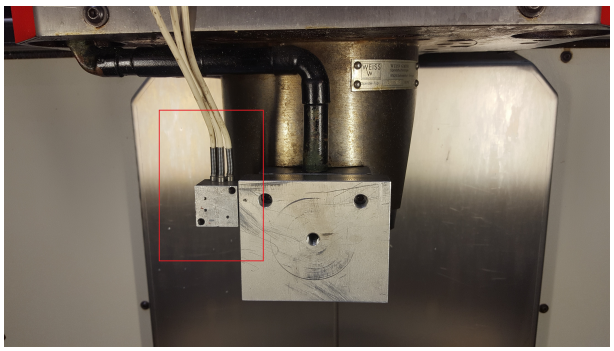

Figure 4.3: Tri-axial accelerometer

To draw signals from the accelerometer and process data a *SoMat eDAQ-lite* data acquisition system (Fig. 4.4) was used [55]. The interface through which setup, calibration and data retrieval was preformed was the *SoMat Test Control Environment* (TCE) software [56].

Figure 4.4: SoMat eDAQ-lite set up

4.2.3 Motion timings

Since the circular tool paths are closed, multiple revolutions were performed (5 revolutions) in succession. This enabled the tool to accelerate from rest to a terminal feed rate, the maximum achievable for the given curvature and decelerate back to rest at the end of the revolutions.

As explained in section 3.2 of chapter 3, the curvature of the tool path imposes a particular magnitude for the centripetal acceleration vector for a given commanded feed rate. If such a magnitude cannot be delivered by the machine's servomotors, motion regulation from the machine's controller produces a maximum permissible feed rate. It then follows that the remaining revolutions are performed at a constant feed rate, assuming the circumference of a given circular path is sufficiently long for the machine to accelerate from rest to the maximum permissible feed rate. Inspection of the acceleration profiles for all of the test tool path confirms that a constant feed rate is achieved after a single revolution and maintained until the final revolution. To remove the contributions of the accelerations from and to rest, the initial and final revolutions of a given test tool path are ignored from analysis. The circular tool paths may therefore be

considered to have been traversed at a constant feed rate.

For a given tool path motion, the time for one revolution can be obtained from the motion's corresponding acceleration profile. To reduce the effects of anomalous data, an average time, t_{av}, from three revolutions is taken, $t_{av} = (1/3)\sum_{i=0}^{2} t_i$. Since the circumference, $2\pi/\kappa_c$, of a test tool path is known, the average feed rate, v_{av}, achieved for a given curvature can be found, $v_{av} = 2\pi/\kappa_c t_{av}$. It then follows that the velocity, $\mathbf{v}_{time}(t)$, acceleration, $\mathbf{a}_{time}(t)$, and jerk, $\mathbf{j}_{time}(t)$, experienced during a given tool path motion can be found from the equations shown in Fig. (4.1). Similar approaches to quantify the kinematics of tool path motion have also been employed in industry [41–43].

4.2.4 Motion frequencies

The acceleration values from the acceleration profiles can also be exploited to quantify tool path motion kinematics. As stated at the end of section 4.1.3, a given tool path motion may be characterised as SHM. Since the circular motion is derived from the oscillations of two orthogonal linear axes, the curvature of the circular tool path corresponds to the frequency at which the linear axes oscillate. The greater the curvature of a circle, the greater the frequency of the axes oscillations.

Although the influences of factors other than shape on tool path motion have been minimised, they cannot be abolished entirely (see section 4.1.1). Each factor therefore contributes a component to the resultant acceleration profile. It can be shown that a given acceleration profile can be represented as a collection of sinusoids, where each sinusoid corresponds to a component ac-

celeration [57]. Since each sinusoid has an associated frequency, it follows that each frequency corresponds to a component acceleration and thus to a physical factor that influences tool path motion.

Performing Fourier analysis on each of the acceleration profiles decomposes them into their respective components and represents them in the frequency domain. The frequency, f_s, corresponding to tool path shape, specifically curvature, may then be identified from the frequency profile. The reciprocal of f_s denotes the time taken to complete one revolution of the tool path, T, $T = 1/f_s$. It then follows that the feed rate, v, at which traversal occurred is thus $v = 2\pi f_s/\kappa$. The velocity, acceleration and jerk experienced during a given tool path motion can then be found from the equations shown in Fig. (4.1).

To demonstrate the Fourier analysis procedure, consider the traversal of a circular path, of $1mm$ radius, at a commanded feed rate of $35m/min$, on the Hermle C600U CNC machine. Fig. 4.5 illustrates the axes acceleration profiles extracted from the accelerometer. To express a discrete axis acceleration signal, $a_\mu(t_i)$ where μ denotes the given axis, of N samples, in the frequency domain, $\hat{a}_\mu(f_i)$, the following transform is used.

$$\hat{a}_\mu(k) = \sum_{j=1}^{N} a_\mu(j) W_N^{(j-1)(k-1)} \ ,$$

where $W_N = e^{-\frac{2\pi i}{N}}$ is one of N roots of unity. The transform is applied to both axis components. The resulting profiles are shown in Fig. 4.6. Both profiles have the same dominant frequency. This suggests that each of the linear axes oscillated at the same rate, indicating constant feed

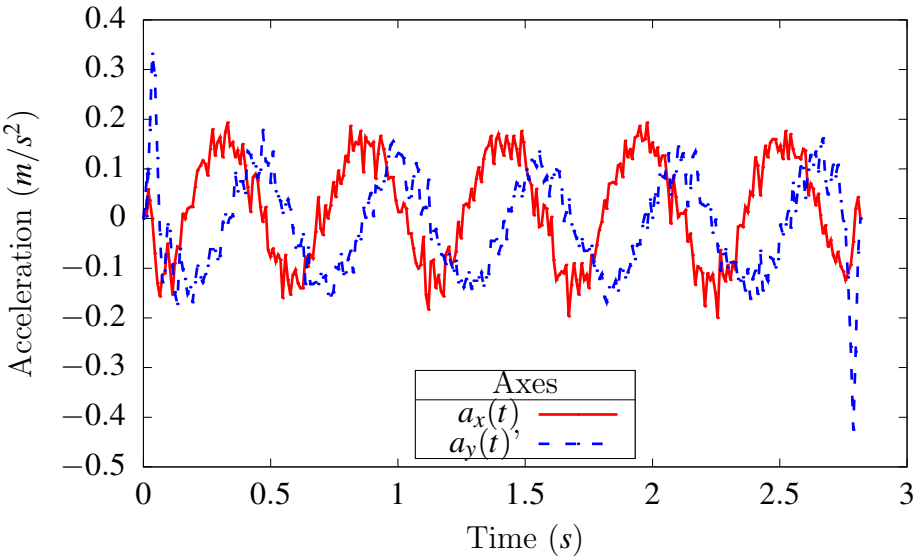

Figure 4.5: Axis accelerations (Radius $r = 1mm$)

rate travsersal of the circular tool path. It then follows that this feed rate may be quantified using the equations shown in Fig. (4.1). It then follows that the velocity, $\mathbf{v}_{freq}(t)$, acceleration, $\mathbf{a}_{freq}(t)$, and jerk, $\mathbf{j}_{freq}(t)$, experienced during a given tool path motion can be found from the equations shown in Fig. (4.1).

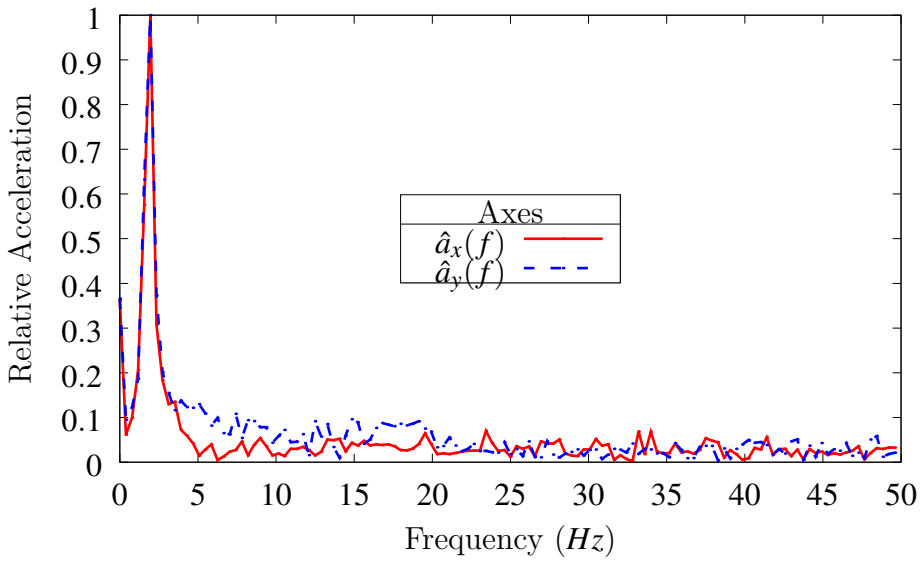

Figure 4.6: Spectral Energy

4.3 Motion analysis

This section presents the kinematic data derived from the acceleration profiles of each of the test tool path motions. Each of the values of the achieved kinematics, illustrated in the following graphs, are obtained by taking an arithmetic average of a kinematic value derived from the motion time and a value derived from the motion frequency. For example, an achieved velocity value, v_{av}, is obtained by taking an arithmetic average of the velocity value derived from the motion time, v_{time}, and a value derived from the motion frequency, v_{freq}, $v_{av} = (v_{time} + v_{freq})/2$. Using two measurement methods improves the reliability of the kinematic data presented.

4.3.1 Mazak VCS 430A

Consider first the Mazak $VCS430A$. Figs. 4.7 and 4.8 show the magnitudes of the kinematic vectors imposed on the machine by requesting it to traverse test tool paths of increasing curvature at the same commanded feed rate of $8m/min \equiv 0.1333m/s$. As described by the equations in chapter 3, Fig. 4.7 shows a linear increase in the required centripetal acceleration to traverse circular tool paths of increasing curvature. This linear increase in centripetal acceleration corresponds to a parabolic increase in jerk (see section 3.2), as shown by Fig. 4.8. Figs. 4.9 and 4.10 show that the imposed kinematics could be provided by the machine's servomotors.

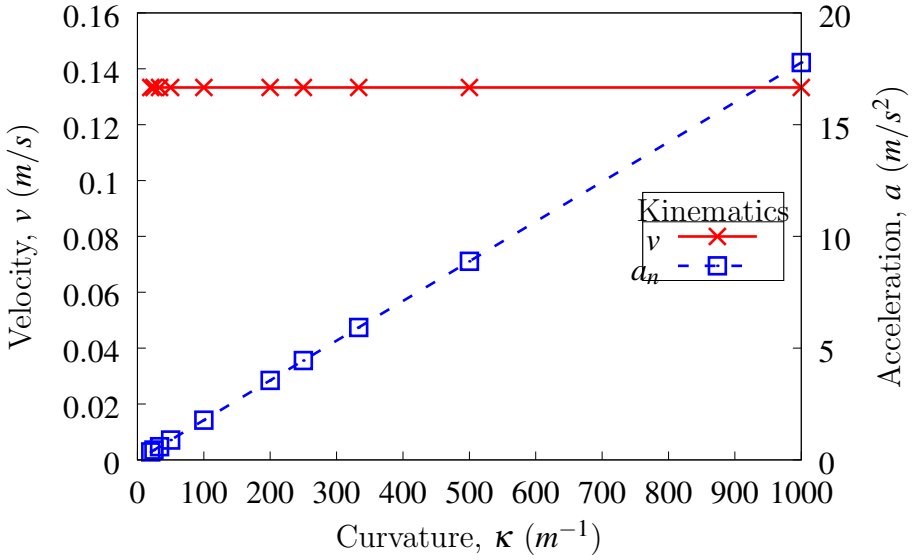

Figure 4.7: Shape imposed velocity and acceleration (Mazak *VCS*430*A*)

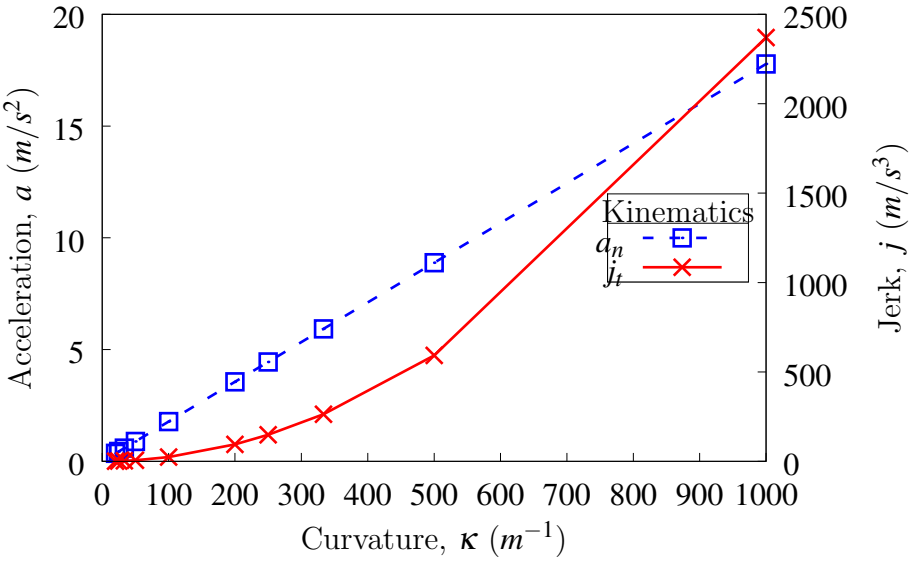

Figure 4.8: Shape imposed acceleration and jerk (Mazak *VCS*430*A*)

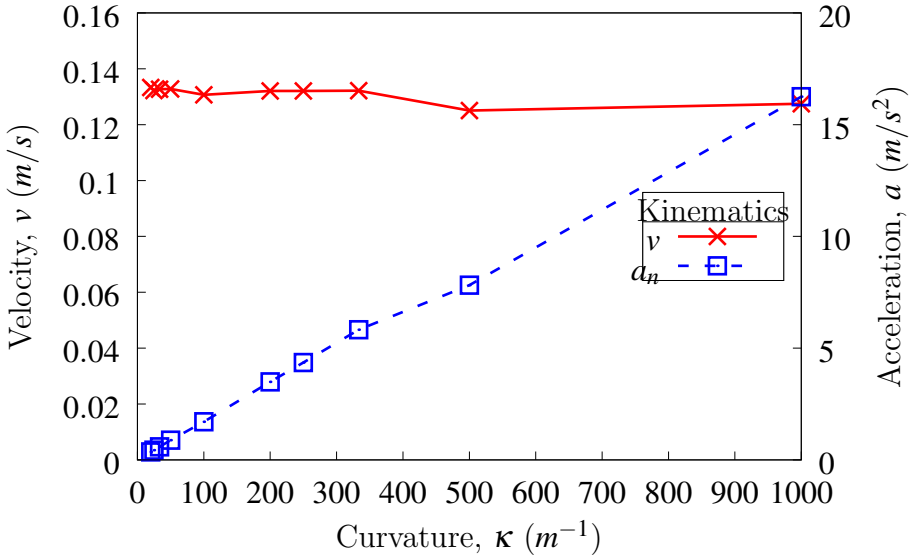

Figure 4.9: Achieved velocity and acceleration (Mazak *VCS*430*A*)

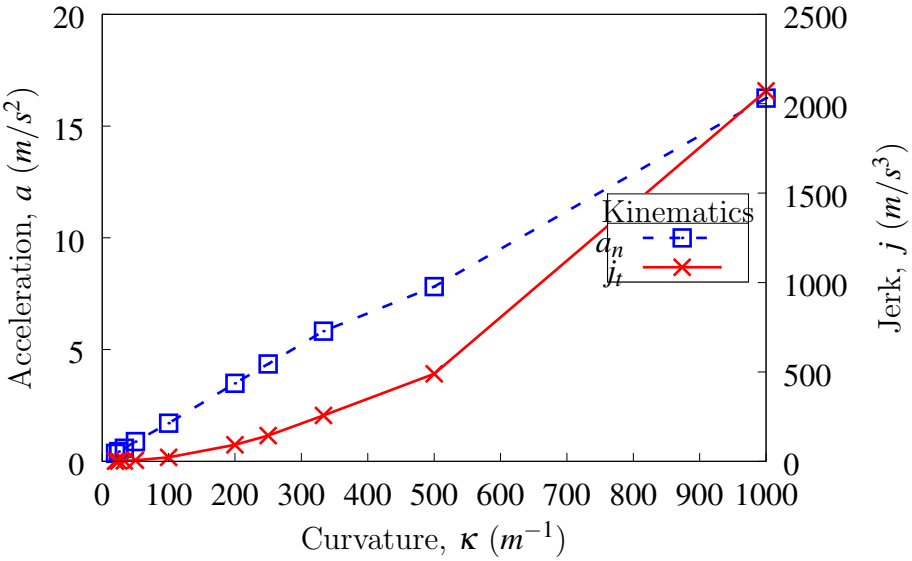

Figure 4.10: Achieved acceleration and jerk (Mazak *VCS*430*A*)

4.3.2 Matsuura LX1

The same tool paths were presented to the Matsuura LX1. However the machine's maximum feed rate of $90m/min \equiv 1.5m/s$ was set as the commanded feed rate for each of the tests. The same tool path shapes therefore imposed greater kinematic demands on the Matsuura $LX1$ than the Mazak $VCS430A$. Those specific kinematic demands are presented in Figs. 4.11 and 4.12. The machine was unable to provide these kinematic demands as shown in Figs. 4.13 and 4.14. Instead the servomotors provided alternative motions, deemed suitable approximations by the motion control algorithms. Indeed, the commanded feed rate was not achieved in any of the test tool path traversals. Fig. 4.13 shows an approximately constant centripetal acceleration was produced. As shown in chapter 3, such an acceleration profile corresponds to the characteristic decrease in the achieved feed rate as the curvature of each circular test tool path increases. Also, Fig. 4.14 shows the magnitude of the jerk vector increase parabolically as the test tool path curvatures increase. It follows that the empirical kinematic data profiles of the Matsuura $LX1$ resemble the characteristic features of the shape schematics developed in chapter 3.

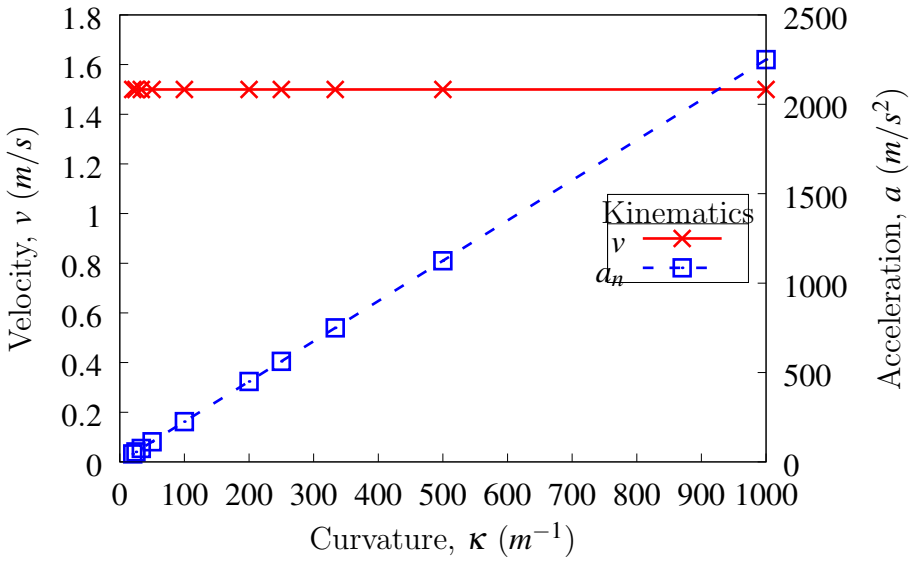

Figure 4.11: Shape imposed velocity and acceleration (Matsuura *LX*1)

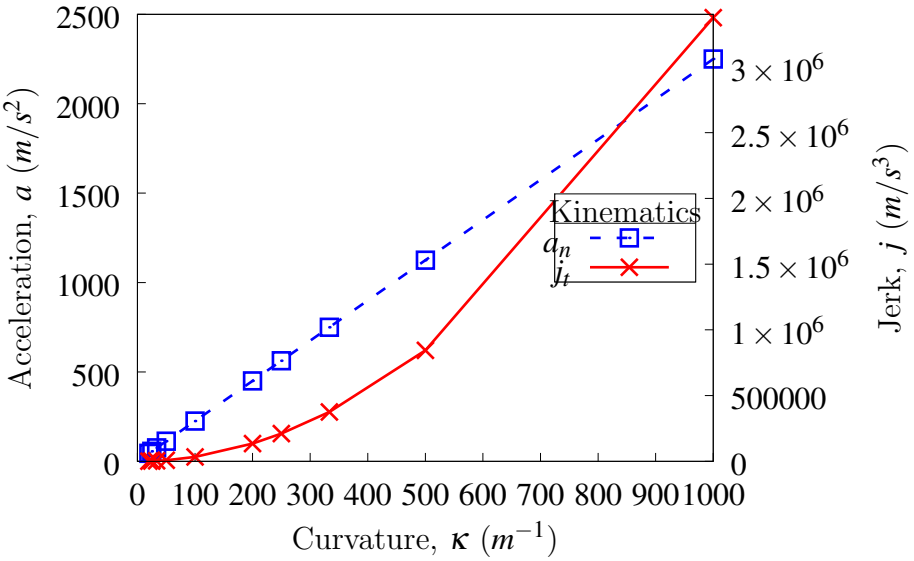

Figure 4.12: Shape imposed acceleration and jerk (Matsuura *LX*1)

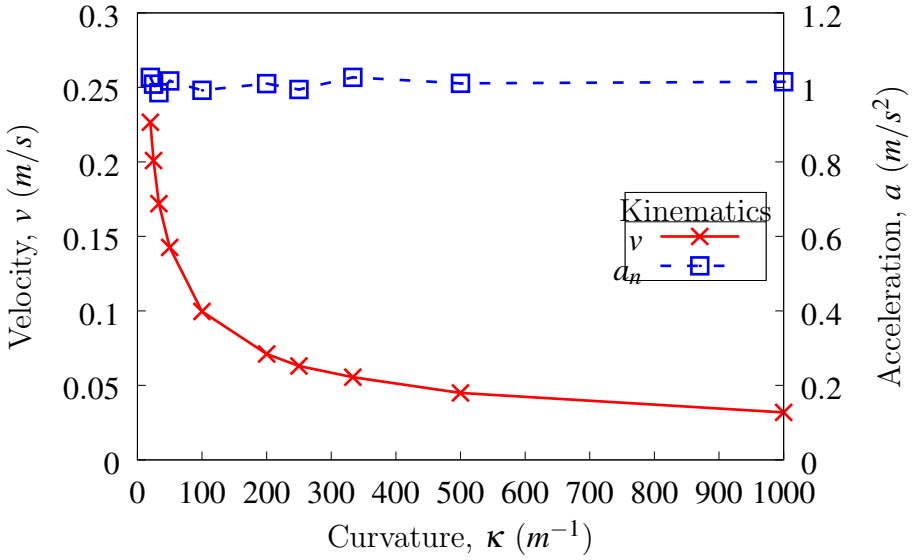

Figure 4.13: Achieved velocity and acceleration (Matsuura *LX*1)

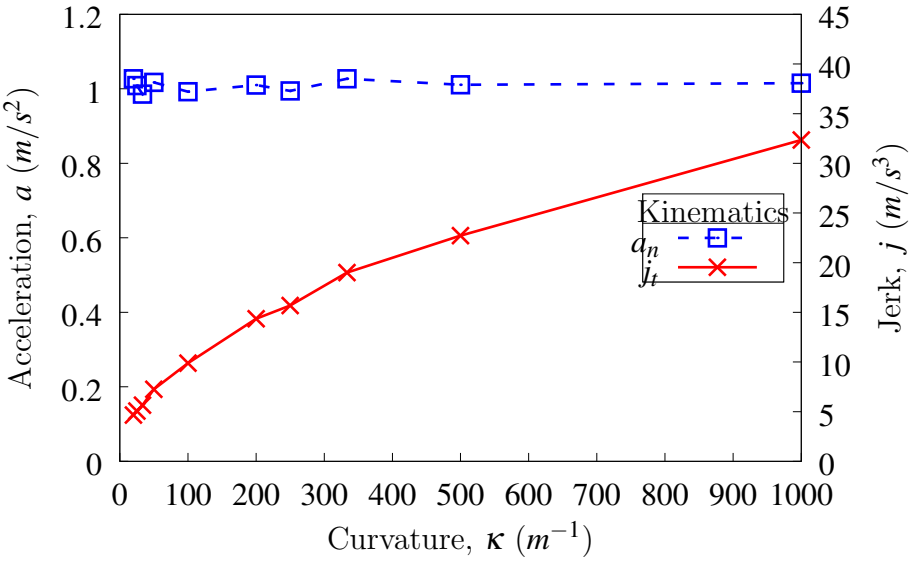

Figure 4.14: Achieved acceleration and jerk (Matsuura *LX*1)

4.3.3 Hermle C600U

Finally, the test tool paths were traversed on the Hermle $C600U$ with a commanded feed rate of $35m/min \equiv 0.5833m/s$. The variation in the magnitude of the centripetal acceleration, with respect to curvature, is considered negligible compared to the variation in achieved feed rate. The profiles then demonstrate the constant centripetal acceleration feature, upon which the characteristic model, given in chapter 3, is based. The shape imposed kinematics, shown in Figs. 4.15 and 4.16, were not realised. Figs. 4.17 and 4.18 show that the machine's centripetal acceleration limit had been exceeded and thus the requested kinematics were compromised.

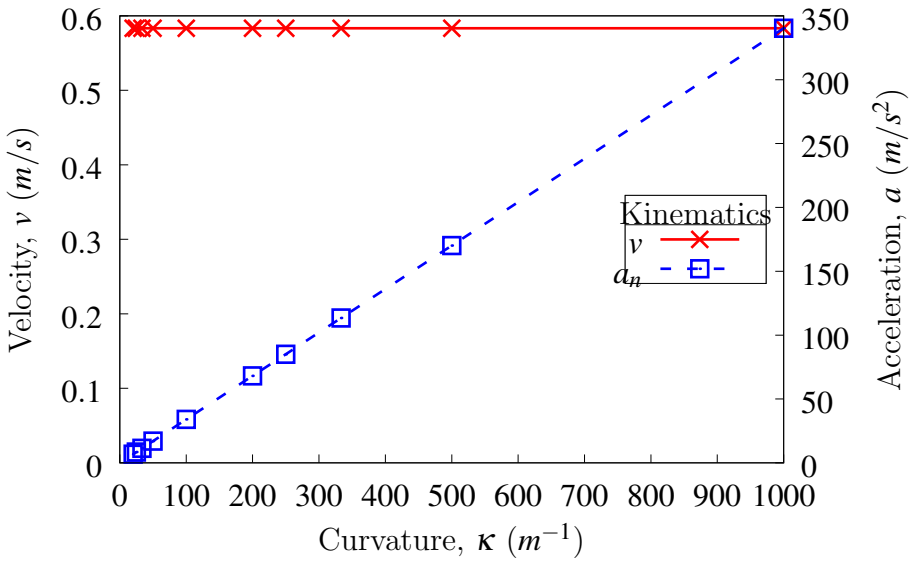

Figure 4.15: Shape imposed velocity and acceleration (Hermle C600U)

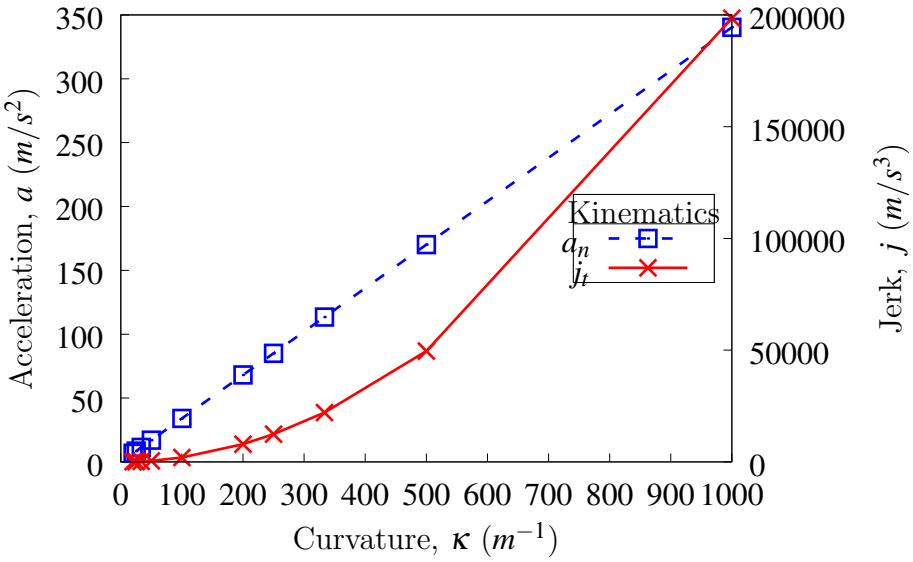

Figure 4.16: Shape imposed acceleration and jerk (Hermle C600U)

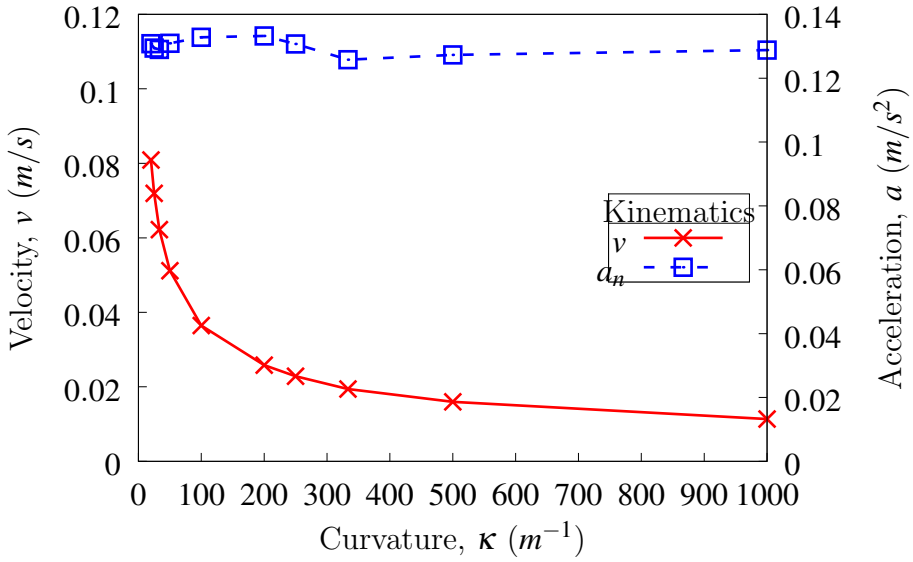

Figure 4.17: Achieved velocity and acceleration (Hermle C600U)

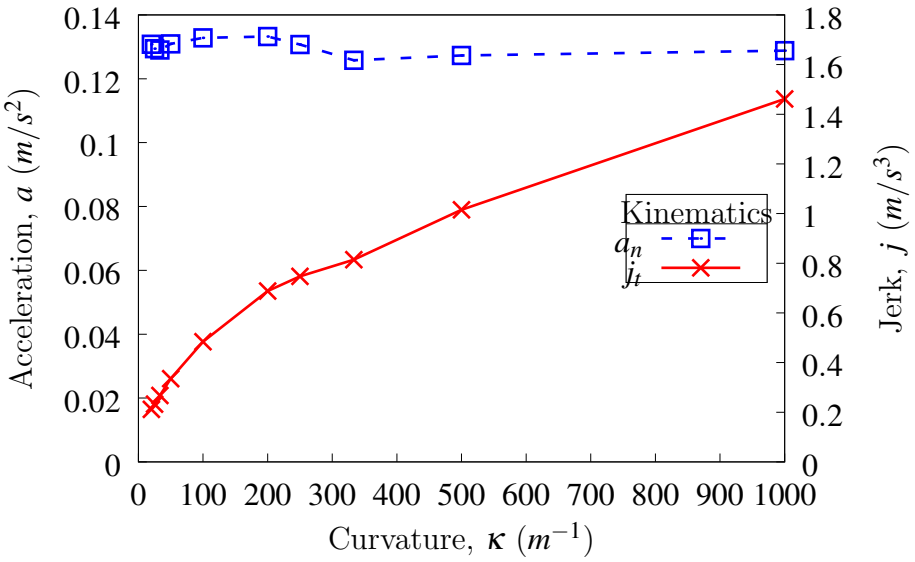

Figure 4.18: Achieved acceleration and jerk (Hermle C600U)

4.4 Chapter summary

This chapter has shown that the empirical evidence obtained from the Mazak *VCS*430*A*, the Matsuura *LX*1 and the Hermle *C*600*U* all support the characteristic model developed in chapter 3. For example, for the specified test tool paths, the motions produced by the Mazak *VCS*430*A* may be characterised by the velocity limited phase equations for velocity, acceleration and jerk. Both the Matsuura *LX*1 and the Hermle *C*600*U* were unable to provide their respective tool path motions. Controller regulation intervened as a consequence of the shape imposed centripetal accelerations exceeding the limits of each of the machines. Acceleration limited phase behaviour was thus observed. Fig. 4.19 compares the feed rates achieved by the Hermle (from Fig. 4.17) and Matsuura (from Fig. 4.13). Fig. 4.20 compares the centripetal accelerations achieved by the Hermle (from Fig. 4.17) and Matsuura (from Fig. 4.13). Fig. 4.21 compares the

jerks achieved by the Hermle (from Fig. 4.18) and Matsuura (from Fig. 4.14).

Despite different commanded feed rates being set, the maximum achieved feed rate on the Matsuura *LX*1 was less than the commanded feed rate specified for the Hermle *C*600*U* tests. This implies the same specified tool path motion can produce different achieved motions on the Matsuura *LX*1 and the Hermle *C*600*U* even if the defined parameters are with the specifications of both machines. The Hermle's lower centripetal acceleration limit (Fig. 4.20) resulted in lower attainable feed rates and jerks (Figs. 4.19 and 4.21) for tool paths of given curvatures.

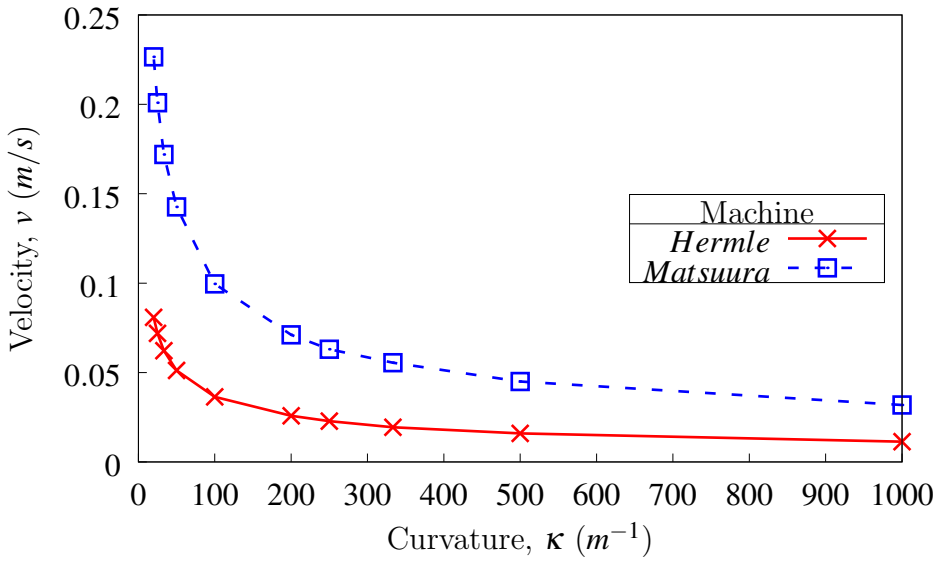

Figure 4.19: Hermle and Matsuura Feed rate Profile

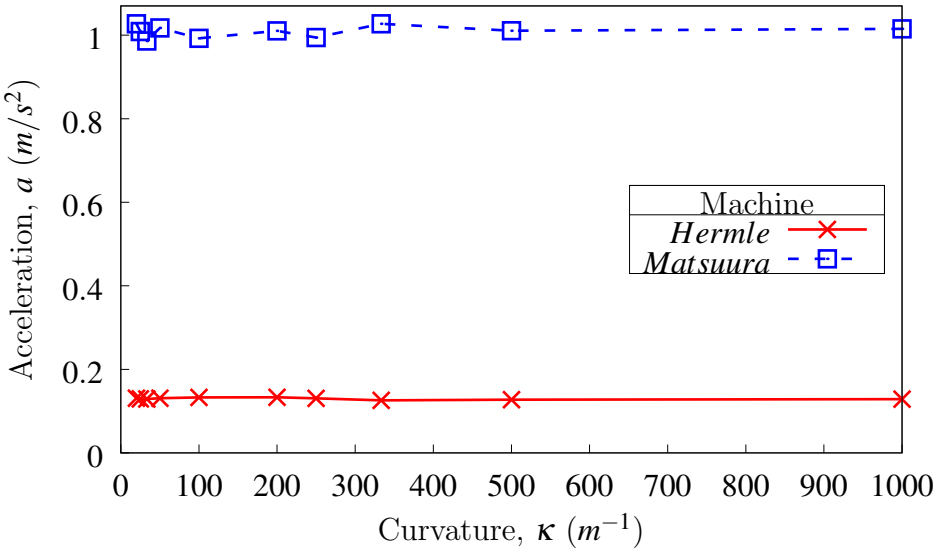

Figure 4.20: Hermle and Matsuura Acceleration Profile

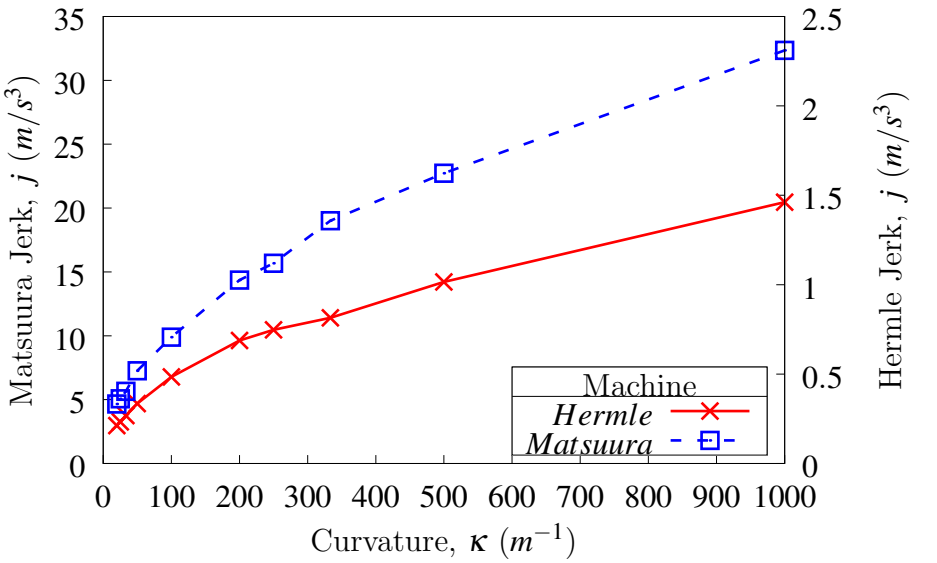

Figure 4.21: Hermle and Matsuura Jerk Profile

Having obtained, in this chapter, empirical evidence that supports the distinct phases of tool path motion described in chapter 3, the following chapter continues the investigation by testing for the other features of the shape characterisation model.

Chapter 5

Example tool path motions

This chapter continues the investigation by analysing experimental kinematic data from example tool paths, in order to provide supporting evidence for particular features of the shape characterisation of motion developed in chapter 3.

A distinguishing feature of the characterisation is that during the acceleration limited phase of motion, the achieved feed rate, v_a, is inversely proportional to the square root of the path's curvature, κ, $v_a \propto 1/\sqrt{\kappa}$. Indeed, Fig. 4.19, of chapter 4, suggests that both the Matsuura and Hermle behave in this manner when a path's curvature imposes a centripetal acceleration that exceeds their respective limits. However, since the Mazak demonstrated velocity limited phase behaviour it is omitted from the following analysis. This chapter therefore begins by adding further empirical weight to reinforce the validity of this feature, by demonstrating that it can be used to predict the times of circular tool path motions.

The chapter then considers transition curvature. The test tool paths, of chapter 4, are investigated again but with a lower commanded feed rate. Lowering the shape imposed kinematic demands serves to illustrate that tool path motion may be classified in two distinct phases. Specifically, a velocity and an acceleration limited phase.

Finally, the chapter concludes by considering the motion along a planar tool path of varying curvature. Fig. 3.2 shows that traversal of a path of varying curvature requires a tangential component of the acceleration vector. It is shown that tangential acceleration can cause an earlier phase change than that described by the transition curvature. The empirical kinematic data illustrates that transition curvature may be therefore be regarded as an upper bound on the value of the curvature at which tool path motion changes phase.

5.1 Motion timings

If a path's shape imposes kinematic demands that exceed a machine's limits, an alternative tool path motion to that specified in a NC file can be produced as a result of controller regulation [1]. Indeed, it was shown in chapter 4 that the Matsuura and the Hermle were both unable to traverse the circular test tool paths at their corresponding commanded feed rates (Figs. 4.13 and 4.17, respectively). Lower feed rates were achieved compared to those requested. Figs. 5.1 and 5.2 display the resulting differences between the requested and achieved motion times for the Hermle and the Matsuura, respectively.

To traverse a circular test tool path, of given length, s, at commanded feed rate, Ψ_1, requires a

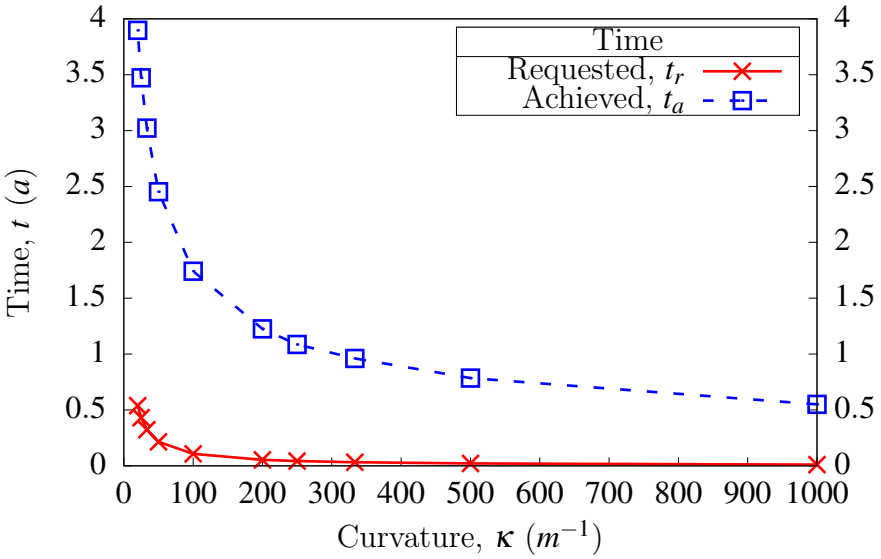

Figure 5.1: Requested and achieved motion timings (Hermle C600U)

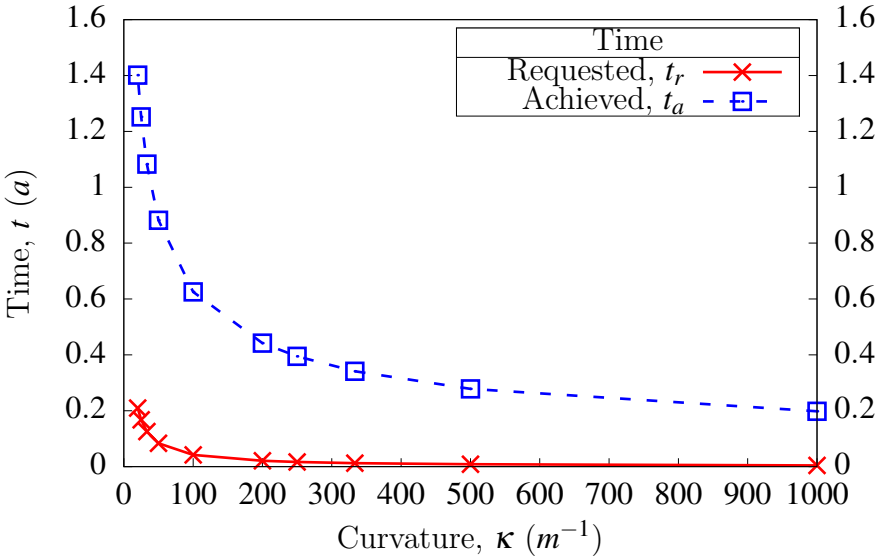

Figure 5.2: Requested and achieved motion timings (Matsuura LX1)

motion time, t_r, of

$$t_r = s/\Psi_1 \ . \tag{5.1}$$

However, Figs. 4.13 and 4.17 show that the commanded feed rates and therefore the requested motion times were not realised and further the profiles suggest that the actual achieved feed rates may be characterised by Eq. 3.4. The achieved feed rate, v_a, on a given circular test tool path may therefore be expressed as $v_a = \sqrt{\Psi_2/\kappa}$. The actual achieved time, t_a, is thus $t_a = s\sqrt{\kappa/\Psi_2}$. The length of the tool path may then be given as $s = t_a\sqrt{\Psi_2/\kappa}$. Substituting this expression for tool path length into Eq. 5.1 produces an equation relating the requested and achieved times for circular tool path motion,

$$t_a = \Psi_1\sqrt{\frac{\kappa}{\Psi_2}}t_r \ . \tag{5.2}$$

The above equation thus predicts the time taken to traverse a circular path of a given curvature, κ, at a particular commanded feed rate, Ψ_1, on machine with a specific centripetal acceleration limit, Ψ_2.

Employing Eq. 5.2 to predict the circular tool path motion times achieved on the Matsuura and the Hermle requires each machine's centripetal acceleration limit to be quantified. For each machine, an arithmetic average of all the deduced centripetal acceleration values, $\bar{\Psi}$, shown in Fig. 4.20, is used to obtain a value for Ψ_2,

$$\bar{\Psi} = \frac{1}{N}\sum_{i=1}^{N} \psi_i \ ,$$

where N is the number of samples, specifically, $N = 10$. Also, to indicate the variation within the empirical data, the standard deviation of each machine's centripetal acceleration values, σ_Ψ, is obtained using

$$\sigma_\Psi = \sqrt{\frac{1}{N}\sum_{i=1}^{N} \{\psi_i - \bar{\Psi}\}^2} \ .$$

The mean centripetal accelerations for each machine and their corresponding standard deviations are given in table 5.1. The smaller standard deviation associated with the Hermle's mean centripetal acceleration indicates less variability in measured values. Substituting the appropriate empirically derived centripetal acceleration limit into Eq. 5.2 produces predictions of the achieved motion times for each machine. The results for the Hermle and the Matsuura, are shown in Figs. 5.3 and 5.4 respectively. The error bars provide a graphical representation of the percentage error between the predicted and achieved motion times. In the case of the Hermle, the largest error of 1.45% occurred at a curvature of $250m^{-1}$. For the Matsuura, the largest error of 0.45% occurred at a curvature of $500m^{-1}$. The specific values for all the percentage errors are provided in appendix E.

The described approach to predict motion times is only applicable to circular motions on machines that exhibit the acceleration limited phase presented in chapter 3. The motivation for presenting the predictions is to reinforce the applicability of $v \propto 1/\sqrt{\kappa}$ for characterising feed

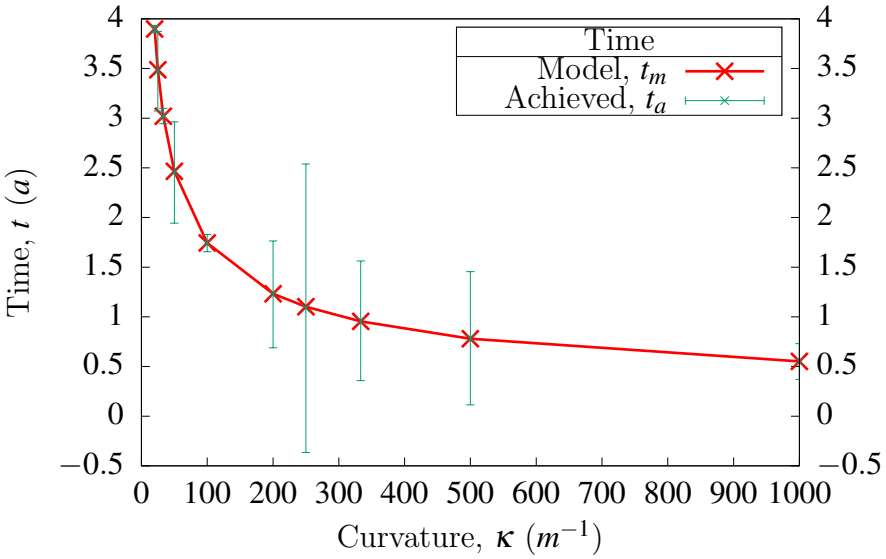

Figure 5.3: Comparing time model (Hermle C600U)

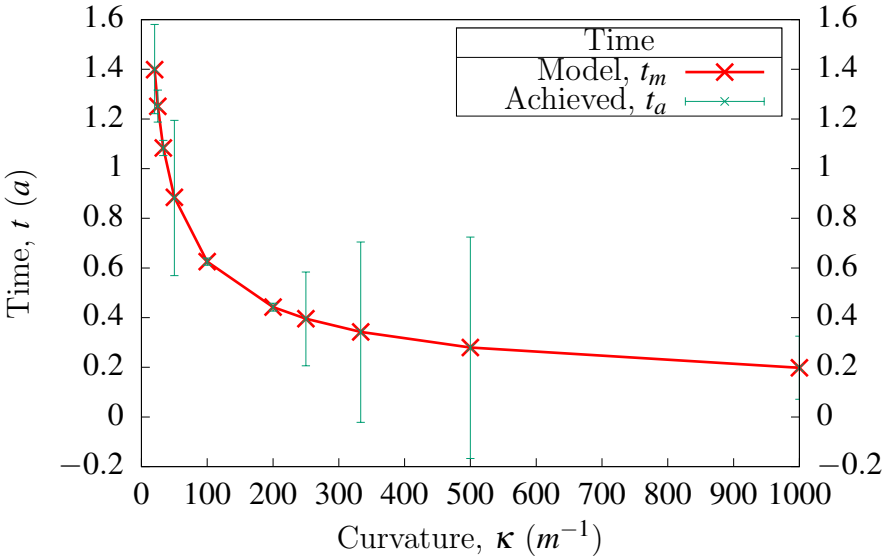

Figure 5.4: Comparing time model (Matsuura LX1)

Table 5.1: Empirical centripetal acceleration values

Machine	Average, $\bar{\Psi}$	Standard deviation, σ_Ψ
Hermle C600U	0.13	0.002
Matsuura LX1	1.009	0.0141

rate with respect to curvature, when motions occur under the constraint of a centripetal acceleration limit.

5.2 Transition Curvature

Chapter 3 described two distinct phases of tool path motion. The velocity limited phase described the kinematic properties resulting from tool path traversal at the commanded feed rate, Ψ_1. The acceleration limited phase described the kinematics produced as a result of an enforced constraint on the maximum centripetal acceleration, Ψ_2. These two phases are distinguished by the transition curvature, κ_α. This is the curvature at which tool path motion transitions between phases and may be quantified as $\kappa_\alpha = \Psi_2/\Psi_1^2$, as shown in section 3.2 of chapter 3. It then follows that when the path's curvature is less than the transition curvature, tool path traversal may be classified as velocity limited phase motion and when the path's curvature is greater than the transition curvature, tool path curvature may be classified as acceleration limited phase motion.

Consider the behaviour of the Hermle when it was used to traverse the circular test tool paths described in chapter 4. Figs. 4.17 and 4.18 suggest that the machine's motion may be classified as operating within the acceleration limited phase of motion. Since the commanded feed rate was specified as $\Psi_1 = 0.5833 m/s$ (see section 4.3.3) and the centripetal acceleration has been

found to be $\Psi_2 = 0.13m/s^2$ (see section 5.1) the transition curvature may therefore be given as $\kappa_\alpha = 0.382m^{-1}$. The lowest test tool path curvature was $\kappa_{min} = 20m^{-1}$, therefore $\kappa_\alpha << \kappa_{min}$. It then follows that all the centripetal accelerations imposed by the curvatures of the test tool paths exceed the machine's limit.

Lowering the commanded feed rate, increases the magnitude of the transition curvature. If $\Psi_1 = 0.05m/s$, the transition curvature becomes $\kappa_\alpha = 51.95m^{-1}$. This transition curvature is greater than the curvatures of 4 of the test tool paths, specifically $\kappa_\alpha > 20, 25, 33.\dot{3}$ and $50m^{-1}$. Traversal of the test tool paths with curvatures less than κ_α therefore require centripetal accelerations less than Ψ_2. It then follows that the commanded feed rate may be achieved for these paths, but not for paths whose curvatures exceed κ_α.

Figs. 5.5, 5.6 and 5.7 illustrate the achieved kinematic properties from traversing the test tool paths at the revised lower commanded feed rate. As suggested by the characterisation developed in chapter 3, κ_α separates the two distinct phases of motion. Velocity limited phase motion is experienced when the test curvatures, κ_i, lie within $0 \leq \kappa_i \leq \kappa_\alpha$ and acceleration limited phase motion is experienced when $\kappa_\alpha \leq \kappa_i \leq \kappa_{\max}$.

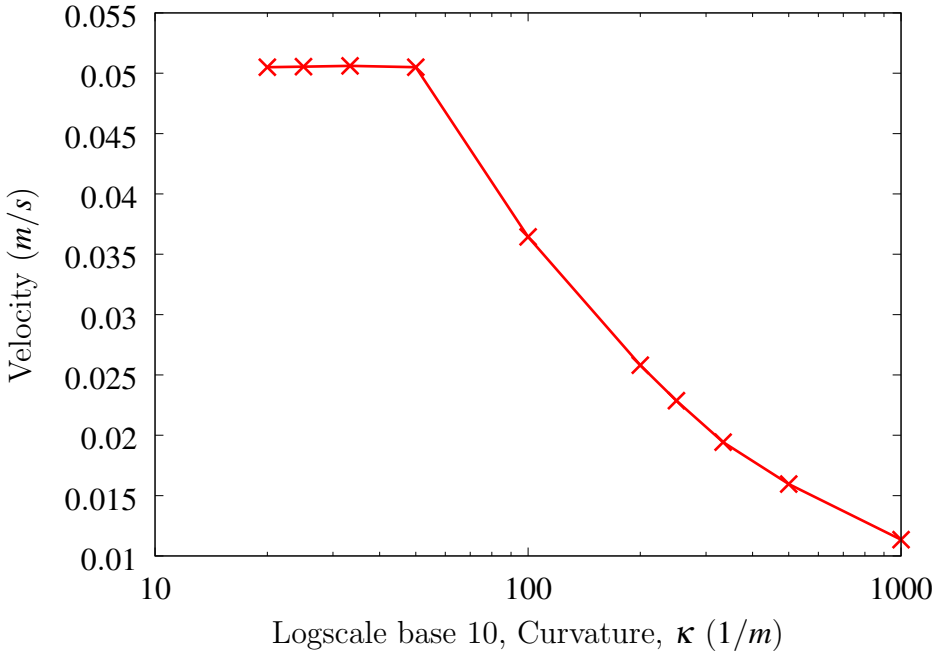

Figure 5.5: Transition curvature velocity profile

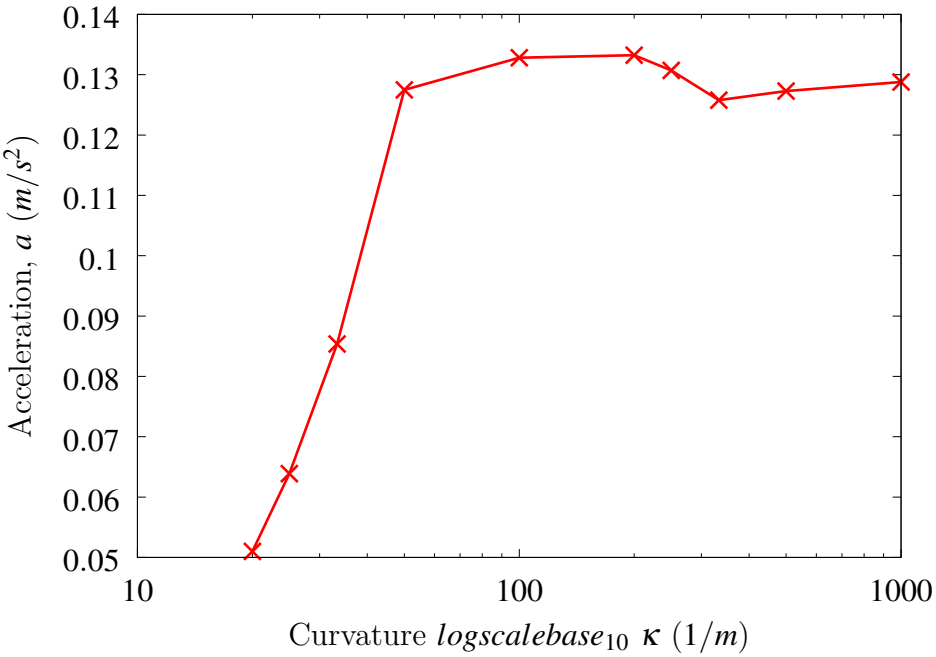

Figure 5.6: Transition curvature acceleration profile

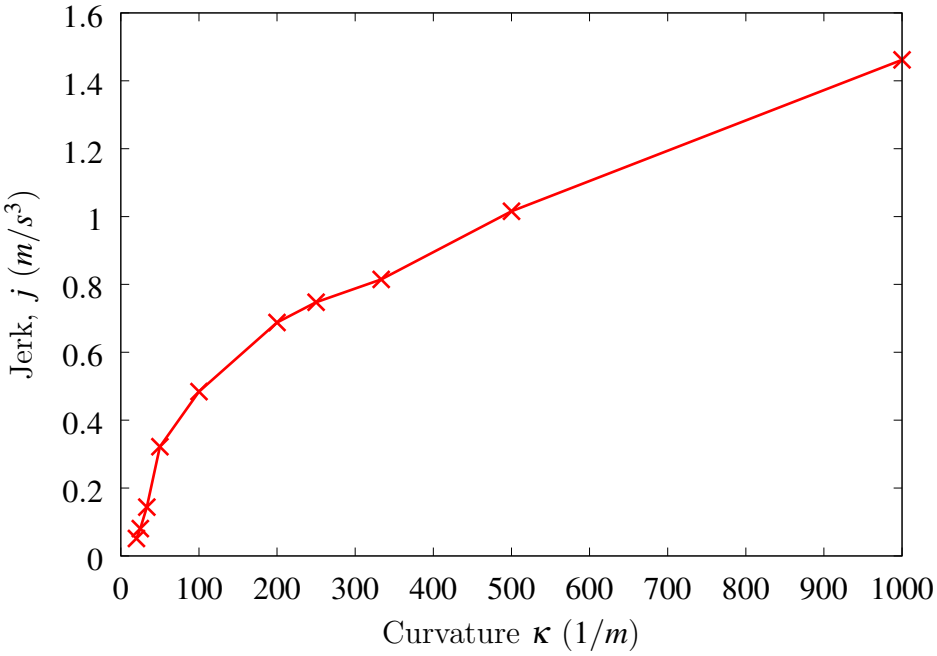

Figure 5.7: Transition curvature jerk profile

5.3 Premature phase transition

5.3.1 Spiral motion

The shape schematic, shown in Fig. 3.2 of chapter 3, shows that as the curvature of a tool path increases, the magnitude of the centripetal acceleration vector increases linearly until the machine's limit is reached. It is at this point, referred to as the transition curvature, that an instantaneous tangential acceleration is required in order to reduce the feed rate and thereby adhere to the centripetal acceleration limit. This instantaneous acceleration cannot be realised in practice [1]. It then follows from the discussion presented in section 3.3, of chapter 3, that

as a path's curvature increases, the actual curvature, κ_a, at which phase transition occurs is less than the theoretical transition curvature, κ_α, $\kappa_a < \kappa_\alpha$. This section therefore investigates the traversals of paths with varying curvature as a means of demonstrating this premature phase transition.

As described in chapter 3, a tool path with a monotonically increasing curvature profile imposes a set of kinematics vectors, on a given machine, that are characterised by the shape schematics presented in chapter 3 (Figs. 3.1, 3.2, 3.3 and 3.4). Such a path is the *Cornu spiral*. It is defined by a linear curvature profile $\kappa(s) = \alpha s + \beta$, $s \leq s \leq L$ and α, $\beta \in \mathbb{R}$ where L is the total tool path length, α refers to the gradient of the curvature profile and β refers to the initial curvature of the path [23].

To simplify the analysis of the resulting tool path motions, the tool path lengths, L, and the angle the path's final tangent vector, $\hat{\mathbf{t}}(s = L)$, subtends with the initial tangent vector, $\hat{\mathbf{t}}(s = 0)$, the winding angle, $\Omega = \int_0^L \kappa(s)ds$, are controlled to construct tool paths where the transition curvatures occur approximately half way through the motions, $\kappa_\alpha \approx \kappa(s = 1/2L)$. Preliminary testing revealed that traversing paths derived from the intrinsic equation $\kappa(s) = 2s$, $0 \leq s \leq 0.4m$, with a commanded feed rate of $0.5m/s \equiv 30m/min$, ensures the transition curvature, $\kappa_\alpha = \Psi_2/\Psi_1^2 \Rightarrow \kappa_\alpha = 0.52(m^{-1})$.

5.3.2 Path generation

Sampling period Precise representation of Cornu spiral tool paths cannot be achieved in NC files, since the analytical expressions for a given position require the evaluation of the Fresnel

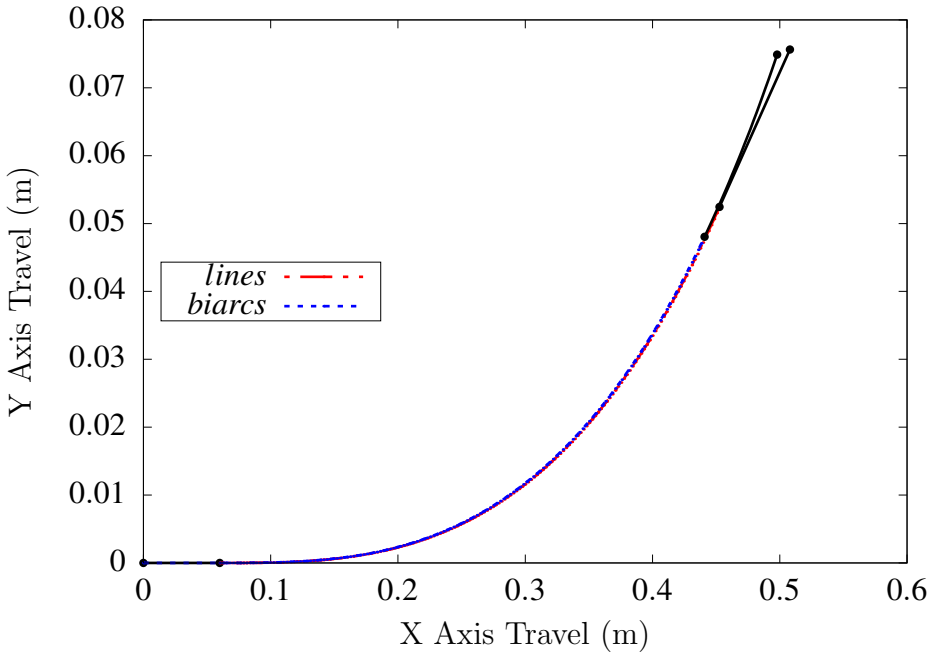

Figure 5.8: NC File Tool Paths

integrals [23]. These integrals are transcendental functions and thus require numerical methods for interrogation [58, 59]. The linear curvature profiles of Cornu spiral tool paths must therefore be approximated using paths of constant curvature, since such paths can be represented exactly [41–43, 47–49]. Linear and circular arc segmented tool paths are therefore used to form approximations to a Cornu spiral's linear curvature (Fig. 5.8).

As explained in the introductory chapter, the discretised nature of segmented tool paths requires the consideration of the effects of data starvation (see section 1.2). To facilitate this task the *sampling period* of the test machine may be identified using the methods employed in appendix C. Having quantified the machine's sampling period, the minimum length required for a given segment, s_{min}, can be defined and used to set the constant lengths of the linear and circular segments, L_{line} and L_{arc} respectively.

Linear segmentation Eqs. (5.3) and (5.4) show that positions on a Cornu spiral path $(x(s),\, y(s))$ can be expressed in terms of its curvature profile,

$$x(s) = x_0 + \int_0^s cos\left[\theta_0 + \frac{1}{2L}\{2\kappa_0 L\sigma + (\kappa_1 - \kappa_0)\sigma^2\}\right] d\sigma \ , \tag{5.3}$$

and

$$y(s) = y_0 + \int_0^s sin\left[\theta_0 + \frac{1}{2L}\{2\kappa_0 L\sigma + (\kappa_1 - \kappa_0)\sigma^2\}\right] d\sigma \ , \tag{5.4}$$

where (x_0, y_0) is the start of path, θ_0 is initial angle made by the path with x-axis, L is the total length of path and κ_0 and κ_1 are initial and final path curvatures respectively [23].

Since evaluation of these integrals requires numerical methods, some error may be present in each $x(s)$ and $y(s)$. The accuracy of each position cannot be stated since the true values for $x(s)$ and $y(s)$ are not knowable [58, 59]. Despite this, the error, between limits, s_{min} and s_{max}, may be bounded [58, 59]. Employing the trapezium rule to numerically evaluate Eqs. (5.3) and (5.4) simplifies the derivation and the resulting analysis of this error bound, ε_B. It is shown in appendix D that the error can be given as

$$\varepsilon_B = -\frac{(s_{max} - s_{min})^3\{\kappa_0 L + (\kappa_1 - \kappa_0)s_{max}\}^2}{12N^2L^2} \ ,$$

where N is the number of segments in the given interval. With a knowledge of the maximum

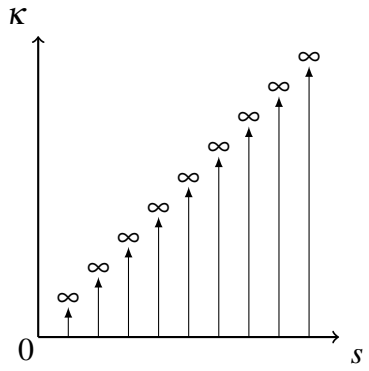

Figure 5.9: Piecewise impulse curvature profile

error of a given position, the closest representation of Cornu spiral path positions may be formed by ensuring that each position error is less than the positional accuracy of the given machine.

Linearly interpolating these positions forms a tool path whose shape is defined by a series of impulse curvatures, each at a distance L_{line} apart (Fig. 5.9) [1]. From Eq. (2.5) it can be seen that the curvature of such a path imposes an infinite acceleration, $|a_n(s)| = \infty$, normal to the direction of traversal of this position continuous path, G^0. Section 1.3 shows that such a path cannot be traversed at a feed rate greater than zero. To avoid high fluctuations in machine kinematics requires the tool to deviate from the specified tool path [16, 17].

Biarc segmentation Connecting two circular arcs with tangent continuity, G^1, forms a composite curve known as a *biarc* [60]. Approximating a Cornu spiral with a series of biarc segments produces a path with varying curvature (Fig. 5.10). The following scheme is used to generate such a path (Fig. 5.11) [1].

1. Rotate point $\mathbf{P}_i$ about centre $\mathbf{O}_i$ through angle $\theta_i = L_{arc}/r_i$.

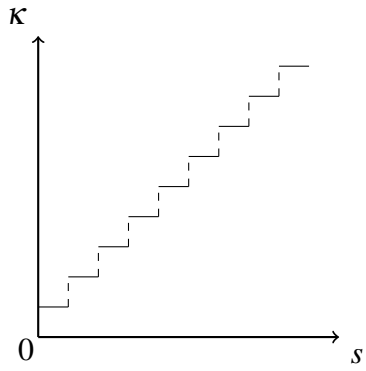

Figure 5.10: Piecewise constant curvature profile

2. Find new radius. $r_{i+1} = 1/(\alpha s_{i+1})$, where $s_{i+1} = s_i + L_{arc}$.

3. Find the new centre of rotation $\mathbf{O}_{i+1}$. $\mathbf{O}(r_{i+1}) = \mathbf{P}_{i+1} r_{i+1} + \mathbf{O}_i(\lambda - r_{i+1})$, where $\lambda = \|\mathbf{O}_i - \mathbf{P}_{i+1}\|$.

The result is a piecewise constant curvature series that approximates a Cornu spiral's linear curvature profile. The diagram shown in Fig. 5.10 illustrates the approximation. A step change in curvature corresponds to a point where two arc segments meet. Analysis of the resulting curvature profile shows that the magnitude of the curvature changes instantaneously from $1/r_i$ to $1/r_{i+1}$ at each segment. Eq. (2.7) shows that the shape of such a path imposes an infinite jerk in the normal direction to the path, $|j_n(s)| = \infty$. As with the linearly segmented spiral tool path, the biarc segmented spiral tool path requires a machine controller to comprise the requested motion and produce an alternative motion that its control algorithms deem appropriate [1].

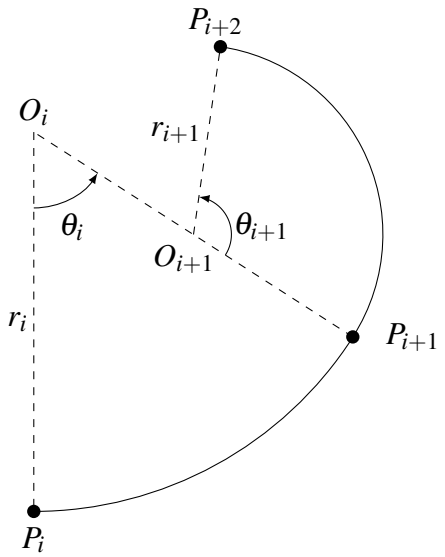

Figure 5.11: Biarc construction

5.3.3 Motion Analysis Methodology

Extra segments, $0.06m$ in length, are added to the ends of each path with the same level of geometric continuity achieved by the rest of the path. Specifically, G^0 for the linear segments approximation and G^1 for the biarc segments approximation. Practically, this will negate the influences of the accelerations from and to rest at the beginning and end of each motion.

The key attributes upon which the shape characterisation of motion provided in chapter 3 is based, are the commanded feed rate, Ψ_1, and the machine's centripetal acceleration limit, Ψ_2. Analysis of the spiral motion feed rates and centripetal accelerations will thus identify if the same characteristic behaviour is applicable.

Data extracted from the accelerometer presents acceleration in terms of machine axis components $\mathbf{a_x}(t) = a_x(t)\hat{\mathbf{x}}_\mathbf{m}$ and $\mathbf{a_y}(t) = a_y(t)\hat{\mathbf{y}}_\mathbf{m}$ [1]. Achieved axes velocities and displacements

are derived from axis acceleration profiles. Feed rate, normal acceleration and curvature can then be deduced [1]. To demonstrate the analysis procedure, Fig. 5.12 presents accelerations experienced by the Hermle's x and y axes.

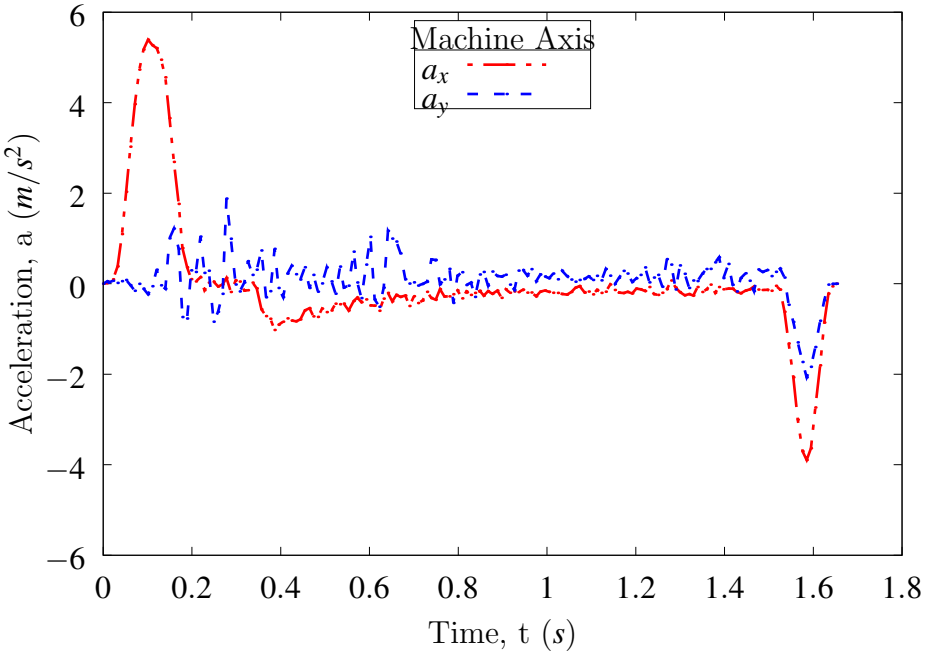

Figure 5.12: Biarc spiral acceleration profile

The velocities of the axes may be derived from integration of axes accelerations. Due to the empirical nature of the acceleration data, each value is likely to harbour some degree of error. This error can be preserved through integration and as a result misrepresents velocity [1]. The resulting x-axis velocities are shown in Fig. 5.13. *Forward* integration from beginning $t = 0$ to the end of the motion $t = t_N$ produces velocity denoted by v_f. *Backward* integration from $t = t_N$ to $t = 0$ produces velocity denoted by v_b. Profile v_f suggests the x-axis changes direction towards the end of the path and profile v_b suggests the axis started the motion not from rest.

Because of the cumulative nature of the integration process, the effects of the errors propagate

through the definite integrals and culminate at end limits of both the forward and backward integrations [1]. Inherent error present in the acceleration signals, is combated by performing a Hermite blend $H(v_f, v_b)$ of the resulting velocity profiles,

$$H(v_f, v_b) = v_f \left(1 - \frac{t}{t_N}\right) + v_b \left(\frac{t}{t_N}\right) .$$

$H(v_f, v_b)$ may be considered as a weighted average of v_f and v_b. The weight of v_f decreases at the same rate the weight of v_b increases. v_f and v_b therefore have a greater contribution to the start and end of the resulting profile v, respectively (Fig. 5.13). This reduces the effects of error propagation. For example, the motion described by v both starts and finishes at rest. In general, the error is not abolished entirely, but reduced to better illustrate the velocity experienced.

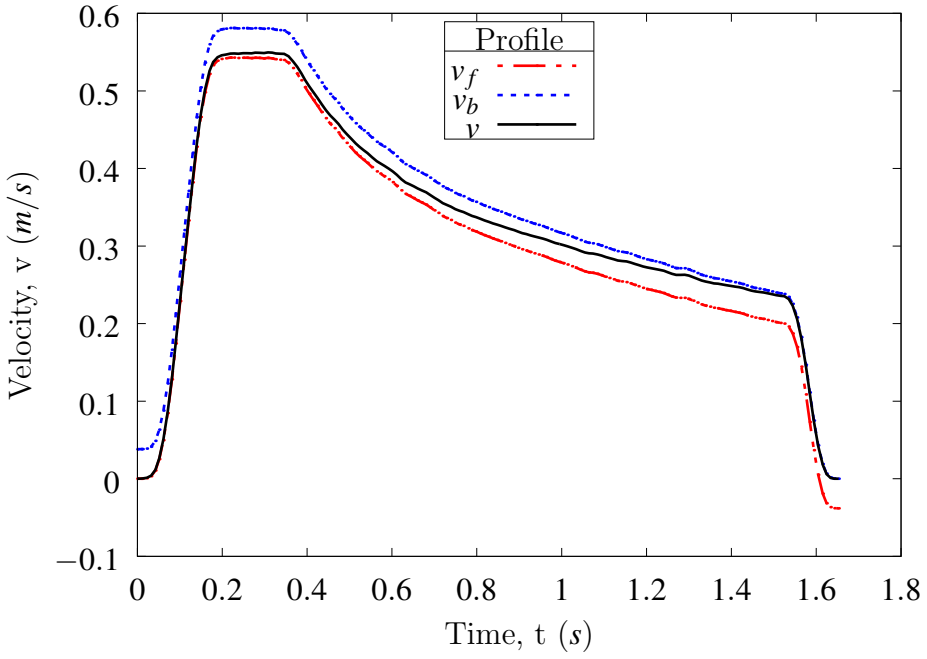

Figure 5.13: Blending

The euclidean norm of resulting axis velocities forms a representation of feed rate profile $v = \sqrt{v_x^2 + v_y^2}$ (Fig. 5.14).

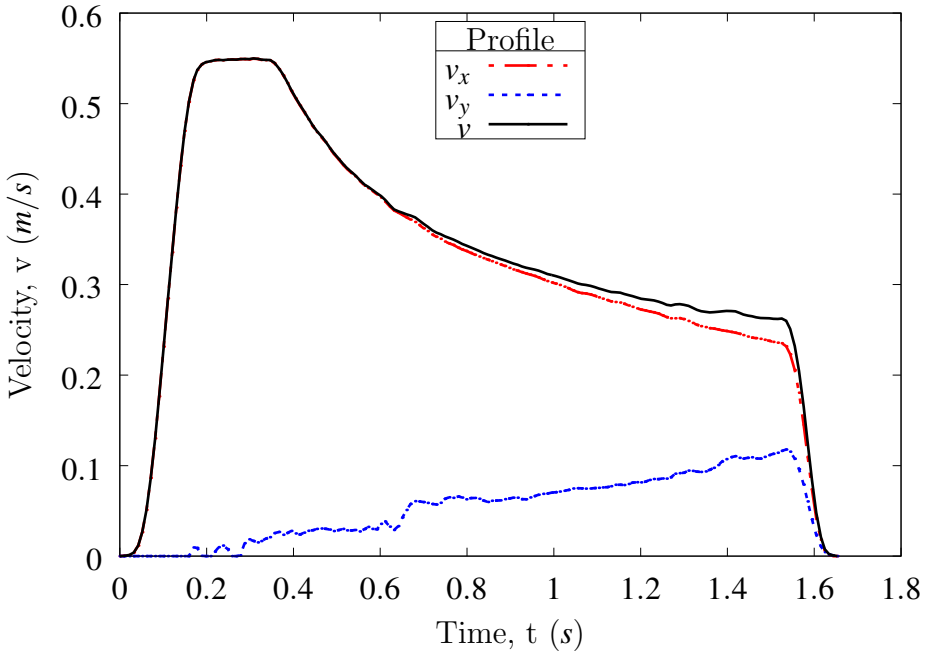

Figure 5.14: Axis velocities and feed rate

Axis displacements (Fig. 5.15) are derived by the same blending approach. From axis displacements arc length is found $s = \sqrt{s_x^2 + s_y^2}$. An approximation to curvature is formed by scaling arc length by the specified rate of change of curvature ($\alpha = 2 \Rightarrow \kappa(s) = 2s$).

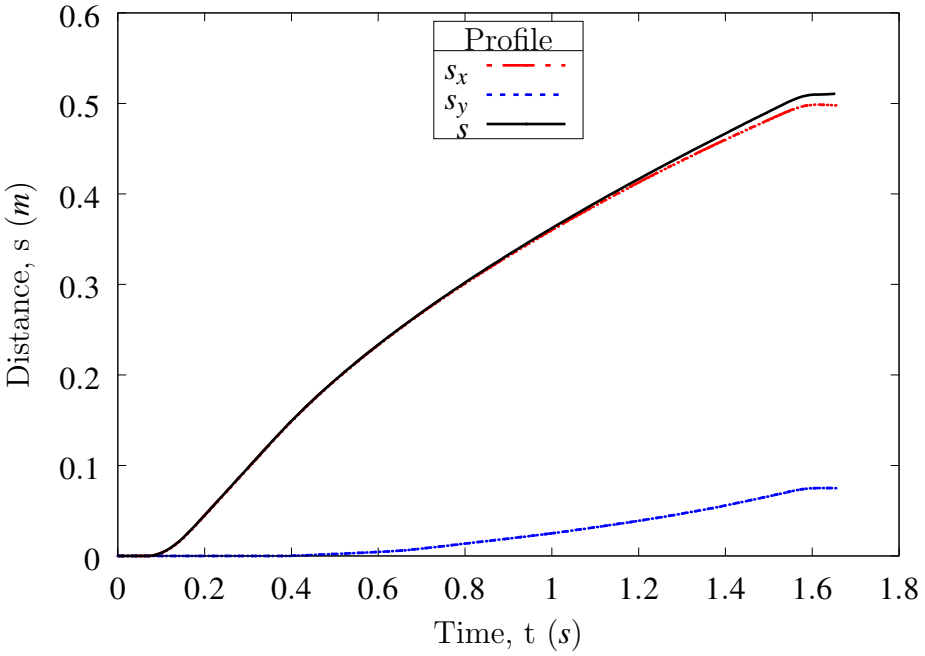

Figure 5.15: Axis displacements and arc length

5.3.4 Phase change

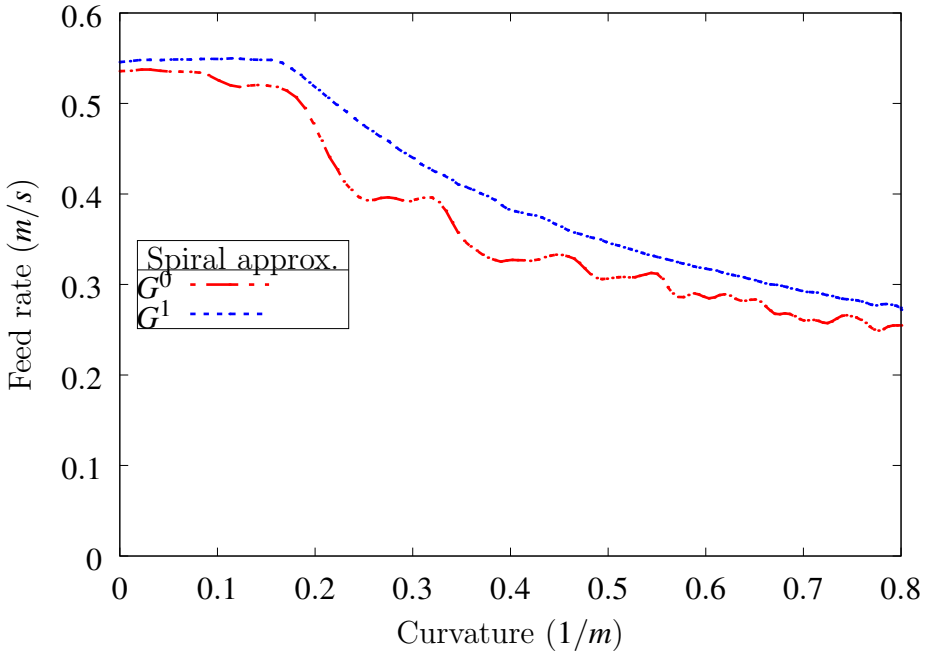

Figure 5.16: Feed rate

By substituting empirical feed rate values, from Fig. 5.16, and appropriately scaled arc lengths values into Eq. (2.5), a set of normal component acceleration values can be obtained. Fig. 5.17 shows normal components of acceleration vectors, resulting from each tool path motion. Both demonstrate a transition from velocity limited to acceleration limited behaviour.

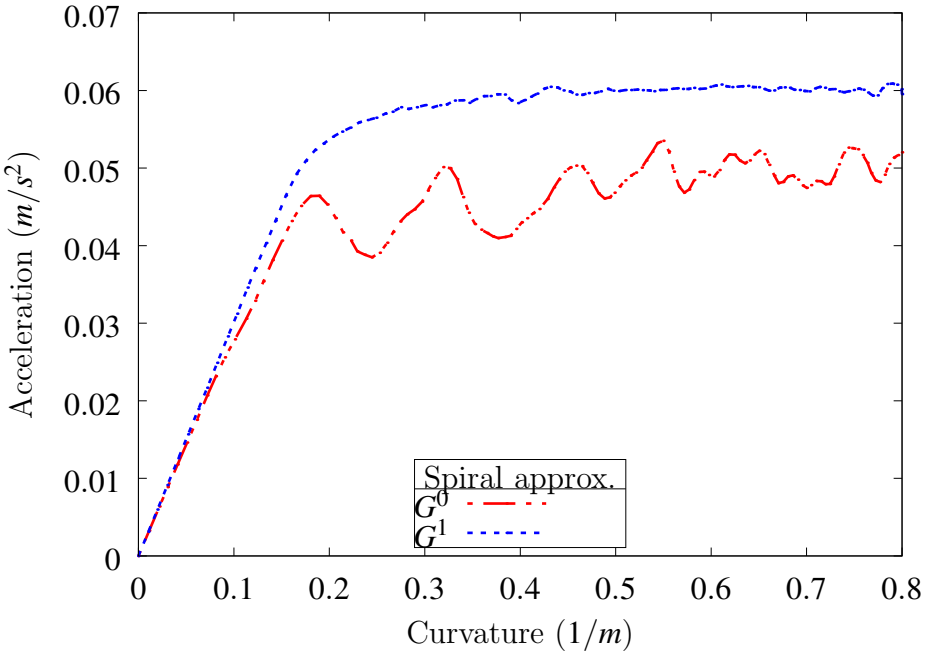

Figure 5.17: Normal acceleration component

Indeed, as argued in section 5.3.1 of this chapter, traversal of tool paths of varying curvature demonstrated a premature phase transition. Calculating the transition curvature from the commanded feed rate, Ψ_1, and the machine's centripetal acceleration, Ψ_2, gives the transition curvature as $\kappa_\alpha = 0.52(m^{-1})$. However, inspection of achieved feed rates and centripetal accelerations, with respect to curvature, reveals that the actual transition curvature, κ_a, $\kappa_a \approx 0.18(m^{-1})$ (See Figs. 5.16 and 5.17 respectively). Between $0 \leq \kappa(s) \leq \kappa_a$, both the linearly and the biarc segmented paths enabled the commanded feed rate to be achieved. Once the path's curvature had exceeded κ_a, $\kappa(s) \geq \kappa_a$, the magnitude of the achieved feed rates began to decrease. Fig. 3.2, of chapter 3, shows that this decrease occurs as a result of tangential deceleration. Although the schematic suggests that this deceleration is discontinuous, in practice this discontinuity refers to the discrete time period where the machine transitions into the acceleration

limited phase of motion [1]. In order to ensure that the centripetal acceleration limit is adhered to this transition period must occur before $\kappa(s) = \Psi_2/\Psi_1^2$. κ_α may therefore be seen as an upper bound on the curvature at which motion changes from the velocity to the acceleration limited phase [1]. The primary reason for the premature transition is that the characteristic model assumes instantaneous acceleration and deceleration from rest. In practice these discontinuities are not realised. They therefore refer to the discrete time period where the machine transitions from one limited phase to another. The actual curvature at which this transition begins must therefore be less than the theoretical transition curvature. Further, the machine's motion algorithms are unknown. The reasons for this specific difference between κ_α and κ_a for the given tests, on the example machine, may therefore not be known. Many mechanical systems employ safety factors to allow for emergency situations, unexpected loads, misuse, or degradation [10]. Perhaps the premature transition may also occur as a result of a kinematic safety factor stated in the control algorithms in order to protect the machine's servomotors.

5.4 Chapter summary

This chapter served to reinforce the applicability of the motion characterisation presented in chapter 3. This was achieved by considering 3 separate examples, each of which considered a particular feature of the characterisation.

The first example used the acceleration limited phase behaviour of feed rate with respect to curvature, $v \propto 1/\sqrt{\kappa}$, to predict the traversal times of circular tool path motions. The predictions thus accounted for a given machine's centripetal acceleration limit by considering the

magnitudes of the kinematics imposed by tool path shape.

This was then followed by an example that illustrated the two distinct phases of motion. Analysis of a machine's transition curvature for a given feed rate was used to lower the shape imposed kinematic demands of tool path motion. This then demonstrated the velocity and acceleration limited phases of the characterisation described in chapter 3.

The chapter then concluded by investigating traversals of paths with varying curvature. As a result of the necessary tangential component of acceleration, it was shown that a premature phase transition was required in order to adhere to a given machine's kinematic limits. The transition curvature described by $\kappa_\alpha = \Psi_2/\Psi_1^2$, may therefore be considered as the upper bound curvature at which the commanded feed rate is not achieved.

Chapter 6

Discussion

Having provided, in chapters 4 and 5, empirical evidence that supports the shape characterisation of motion, this chapter returns to some of the key ideas upon which the characterisation is based.

The chapter begins by discussing the overall purpose of the thesis. Key findings and outcomes from the previous chapters are highlighted in order to demonstrate how the research aim has been achieved.

The chapter then considers the contributions of shape to tool path motion. It is argued that it is desirable to minimise the kinematic demands of a specified tool path motion, as this in turn may improve the likelihood of those kinematics being achieved.

The following section then describes distinctive features of the shape characterisation model.

Features fundamental to the nature of the characterisation are identified and discussed. It is shown how the approaches employed in this thesis may be utilised to derive alternative shape characterisations of motions, since a given machine need not demonstrate the same behaviour as that presented by those in this thesis.

This chapter concludes by examining the kinematic properties resulting from the spiral tool path experiments conducted in chapter 5. It is shown that higher levels of geometric continuity between consecutive segments, of a given path, resulted in more stable and predictable kinematic properties.

6.1 Characterisation methodology

As stated in section 1.4 of chapter 1, the aim of the thesis was to present a methodology for assessing the kinematic capabilities of any CNC machine, in terms of a tool path's intrinsic shape properties.

A review of current methods for describing tool path motion, provided in section 1.3 of chapter 1, identified that many methods depend upon the algorithms implemented in a machine's controller. Either a method proposes novel algorithms or requires knowledge of the algorithms currently implemented in a controller. These methods are therefore limited to specific machines. Further, because the algorithms are often the intellectual property of the machine and controller manufacturers they are difficult to access.

Chapter 3 showed that by enforcing constraints on the general kinematic vector equations

(Eqs. (2.4), (2.5) and (2.7)), a characterisation of tool path motion may be given simply in terms of a tool path's intrinsic shape properties and a machine's kinematic limits. Provided the constraints enforced on the equations are appropriate for the given machine, the resulting schematics may be used to assess whether a proposed tool path motion is likely to achieved given the kinematic capabilities of the machine. Further, knowledge of the particular machine's kinematic capabilities, in terms of shape, may be used to generate an achievable tool path motion. The resulting schematics may help to identify geometric constraints that can be employed to design a new tool path.

The kinematic constraints employed in chapter 3 may seem intuitive since they enable the maximum magnitudes of kinematics vectors to be produced by a machine at any given instance in a motion. However a given machine need not behave in this manner. Different machines can respond differently to an imposed breach of its kinematic limits, therefore chapter 4 detailed free motion tests that can be used on any CNC machine in order to identify the maximum magnitudes of kinematic vectors given the shape of a tool path. As detailed in sections 4.1.1 and 4.1.2 of chapter 4 the approach attempts to isolate the contribution of a tool paths shape properties to the actual kinematics produced in a given motion. The resulting empirical data may then be used to enforce kinematic constraints on the vector equations to produce a shape characterisation of tool path motion suitable for any given test machine.

6.2 Contributions of shape

The shape properties of a tool path impose a particular set of kinematic demands on a given machine as a result of traversal [28]. It was shown in chapter 2 that curvature is intrinsically linked to the velocity, acceleration and jerk vectors. It then follows that curvature may be controlled in order to affect tool path motion, as shown in chapters 4 and 5.

Consider the analogous task of planning an aircraft's flight path. Two key issues need to be considered: minimising the risk of mid air collision and fuel consumption. To ensure a safe flight, an aircraft is required to fly over a number of intermediate checkpoints [61]. Also, fuel consumption is predominantly dependent upon the aircraft's acceleration [62]. Eq. 2.5, of chapter 2, shows that acceleration at a given point is proportional to the path's curvature. Thus assuming all other contributing factors are unchanged, decreasing the curvature, decreases the acceleration and so decreases the amount of fuel consumed. It then follows that an aircraft must interpolate the departure and arrival positions, whilst minimising the curvature of the resulting flight path. The task may therefore be viewed as one of geometric design opposed to logistics. Within the context of tool path motion, it then follows that minimising the curvature of the path minimises the imposed tool path kinematics.

Any of the many fairing techniques could thus be used to optimise, whilst adhering to design constraints, the tool path shape in order to minimise the corresponding kinematic demands [28]. It has been shown in chapter 4 that the permissible kinematics of a given machine are limited by the physical capabilities of the machine's servomotors. Fairing a tool path's shape therefore increases the likelihood of the commanded feed rate being achieved since the path's

shape imposes the minimal set of kinematics on a machine's servomotors.

6.3 Characteristic features of motion

The purpose of the characterisation is to describe features of motion that result from tool path shape. The purpose is not to precisely quantify the magnitude of a given kinematic vector, at a given instance in time. Indeed, many models have been proposed that are able to predict tool path motion time to a relatively high degree of precision [11, 18, 20, 21]. However, these models often presume a knowledge of the control algorithms implemented by a machine's controller. In practice, the specifics of these control algorithms are not generally accessible (chapter 1). By enforcing constraints on the general kinematic vector equations, derived in chapter 2, motion is described simply in terms of the kinematic limits of a given machine and the shape properties of the tool path.

The resulting equations show that tool path motion may be classified into two separate phases. The velocity limited phase describes the behaviour of the kinematic vectors when a tool path's specified commanded feed rate is achieved. This phase may therefore be viewed as the ideal phase of motion, since the commanded feed rate is often specified in order to achieve particular machining parameters (for example, material removal rates and cutting forces). The acceleration limited phase is defined by tool path motion with a constant magnitude for the centripetal acceleration vector. In order to maintain this kinematic constraint the actual feed rate must deviate from the commanded feed rate. The desired tool path motion is therefore compromised in the acceleration limited phase.

It was argued in section 3.4, of chapter 3, that the characteristic equations describing the phases are not the most intuitive or insightful. For example, Eq. 3.10, corresponding to the tangential component of the jerk vector during the acceleration limited phase, contains the second derivative of curvature with respect to arc length, $d^2\kappa(s)/ds^2$. There are however kinematic vectors that depend only upon the existence of curvature at a given arc length. Specifically, they are the acceleration vector, $\mathbf{a}(t) = \Psi_1^2\kappa(s)\hat{\mathbf{n}}(s)$ and the tangential jerk vector, $\mathbf{j}_t(t) = -\Psi_1^3\{\kappa(s)\}^2\hat{\mathbf{t}}(s)$, during the velocity limited phase and the velocity vector, $\mathbf{v}(t) = \sqrt{\frac{\Psi_2}{\kappa(s)}}\hat{\mathbf{t}}(s)$, during the acceleration limited phase. If at a given point on a tool path the curvature becomes zero, the contribution of shape to these kinematics also vanishes. These vectors are thus deemed to be fundamental features of the presented characterisation.

The nature of the constraints enforced on the general kinematic vector equations ensures that a given machine provides the maximum kinematic performance permissible by its servomotors. For example, it was shown in section 3.2, of chapter 3, that when a path's curvature imposes a centripetal acceleration that exceeds a machine's limits, the machine will continue to provide the maximum permitted centripetal acceleration despite curvature imposing a greater magnitude. Yet this behaviour need not occur for every machine, for a given machine's motion has some dependence on its own mechatronic attributes [1]. However, by using the methods employed in chapter 4, it is possible to identify the maximum velocity, acceleration and jerk, for a given curvature. The resulting profiles can then be used to enforce appropriate constraints on the general kinematic vectors (chapter 2) and thus derive an alternative shape characterisation of motion.

6.4 Shape quality

Cornu spiral tool path traversal was investigated in chapter 5 as a means of demonstrating premature transition from the velocity to the acceleration limited phase of motion. It was shown that the Cornu spiral could not be represented exactly and thus was approximated by linearly and biarc segmented tool paths. This section discusses the effects of the geometric continuity of each of the paths on the resulting properties of tool path motion.

The same commanded feed rate was specified for each spiral tool path. However, different levels of geometric continuity were achieved in each path. It then follows that each path imposed a different set of kinematic demands on the machine's servomotors. Fig. 5.9 shows a series of impulse curvatures, indicating that the linear segments joined with position continuity, G^0. Eq. 2.5, of chapter 2, shows each junction of consecutive linear segments imposes an infinite acceleration in the normal direction to the path. Fig. 5.10 shows a series of constant curvatures. It follows that at each junction the curvature changes instantaneously. The rate of change of curvature is thus undefined at each junction. The normal component of Eq. 2.7 shows that an infinite normal jerk is required at each junction. Both tool paths impose impractical kinematic demands on the machine. However, the tangent discontinuities may be considered to impose greater kinematic demands on machine motion than the curvature discontinuities, since a lower order time derivative is undefined in the associated set of kinematic functions [1]. Regulation from the machine's controller was therefore required. The resulting feed rate and centripetal acceleration are presented in Figs. 5.16 and 5.17.

As the curvature of both paths increased, the feed rate decreased (see Fig. 5.16). This may per-

haps be intuitive. However, relationships between tool path shape and machine motion can be further refined [1]. Both the feed rate and acceleration profiles illustrate the machine's transition from the velocity to the acceleration limited phase. the feed rate may therefore be considered to be inversely proportional to the square root of curvature. Further, both tool path motions were able to provide initial periods where centripetal acceleration rises linearly with curvature to maintain a constant feed rate. As the machine transitions into the limited acceleration phase, acceleration no longer increases linearly and submits to the centripetal acceleration limit [1]. Fig. 5.16 and 5.17 also show that less kinematic fluctuation occurred on the path with a higher level of geometric continuity, specifically the biarc spiral path. Less fluctuation implies greater stability [1]. The kinematics resulting from the biarc spiral motion are more predictable in the sense that they greater resemble the schematics derived in chapter 3. Whether the fluctuations, resulting from the linearly segmented spiral tool path, are significant, is dependent on the application for which the motion is implemented [1].

6.5 Chapter summary

The chapter began by suggesting that it is desirable to control the shape of a given tool path such that the effects of the kinematics of the tool motion imposed on the machine's servomotors are minimised. It was argued that minimising the kinematic demands of a specified tool path motion, improves the likelihood of those kinematics being realised in practice.

This was then followed by an examination of the shape characterisation model. The kinematic vectors that were solely dependent upon curvature were classified as fundamental features of

the characterisation. It was shown that if at a given point on a tool path, the curvature becomes zero, the contribution of shape to the actual tool path motion also becomes zero.

The chapter then concluded by considering the kinematic properties resulting from the spiral tool path experiments conducted in chapter 5. The effects of geometric continuity were discussed. The empirical data suggests that free form paths constructed from a series of biarc segments as opposed to linear segments can produce more stable and predictable motion. The term stable in this context refers to the magnitudes of the local perturbations of the kinematics vectors. Further, biarc G^1 segments are considered to produce more predictable motions since the kinematic profiles for the biarc spiral in Figs. 5.16 and 5.17 better resemble the schematics, Figs. 3.1 and 3.2, shown in chapter 3.

Chapter 7

Conclusions

The main aim of this thesis was to demonstrate *a priori* shape characterisation of tool path motion. Through the empirical evidence presented in chapters 4 and 5, such a characterisation has been achieved without knowledge of the control algorithms implemented by a given machine's controller.

This chapter begins by presenting an overview of the research tasks undertaken. This is then followed by discussions of the contributions and limitations of the investigation. The thesis then concludes by describing a possible avenue for future research.

7.1 Overview

The thesis began by providing an overview of CAD/CAM, specifically within the context of milling. A tool path and its role within CAD/CAM were then defined and discussed. This was then followed by a review of the current approaches employed by machine controllers to regulate motion, with an emphasis throughout, on the effects of shape on tool path motion. This then laid the foundation for an explicit statement of the research aim and the corresponding objectives required to achieve it.

Chapter 2 established the foundations of the mathematical theory required, in chapter 3, in order to derive the shape characteristic model. In particular, the kinematic properties, velocity, acceleration and jerk, were related to a tool path's intrinsic shape properties, curvature and torsion.

In chapter 3, constraints were then enforced upon these relations in order to provide a description of tool path motion that accounted for a machine's kinematic limits. Two distinct phases of motion originated as a result of deriving the shape characteristic model. It was shown that the velocity limited phase described motion at the commanded feed rate and the acceleration limited phase described motion with a constant magnitude for the centripetal acceleration vector.

Having established the shape characteristic model, chapter 4 provided empirical evidence to support the corresponding shape schematics. Kinematic data obtained from the Mazak VCS430A, the Matsuura LX1 and the Hermle C600U all supported the characteristic model. For the specified test tool paths, the motions produced by the Mazak VCS430A described the velocity lim-

ited phase of the model. Further, it was shown that the Matsuura LX1 and the Hermle C600U were unable to provide their respective tool path motions. As a consequence of the shape imposed centripetal accelerations exceeding the limits of each of the machines, acceleration limited phase behaviour was observed.

Finally, chapter 5 continued the investigation by analysing particular features of the model. In particular, the relationship between feed rate and curvature during the accelerated limited phase of motion, $v \propto 1/\sqrt{\kappa}$, was employed to predict tool path motion times. This served to add further empirical weight to reinforce the applicability of this feature of the model. Circular tool path motion was then employed to illustrate that a given machine's tool path motion may be classified in the velocity and acceleration limited phases. The chapter then concluded by investigating traversals of paths with varying curvature. As a result of the necessary tangential component of acceleration, it was shown that a premature phase transition was required in order to adhere to a given machine's kinematic limits. The transition curvature described by $\kappa_\alpha = \Psi_2/\Psi_1^2$, may therefore be considered as the upper bound curvature at which the commanded feed rate is not achieved.

7.2 Contributions

For any given CNC machine, this thesis has presented a methodology for assessing its kinematic capabilities in terms of shape. A key advantage of the method, over current methods of describing tool path motion, is that it is independent of a machine's motion control algorithms. As a result of performing the free motion tests, detailed in chapter 4, constraints may be enforced

on the general kinematic vectors (Eqs. 2.4, 2.5 and 2.7) in order to obtain a characterisation of tool path motion that is solely dependent on the intrinsic shape properties of the path and the machine's kinematic limits. The resulting schematics may be used in at least two ways. Firstly, a proposed tool path motion may be checked to see whether its shape imposed kinematics are likely to be achieved on a given machine. Secondly, having identified the maximum magnitudes of the kinematics vectors achievable by the machine, given the shape of the tool path, the commanded feed rate and desired tool path shape may be adapted in order to accommodate the machine's kinematic limits.

The characteristic model presented in this thesis may be used to inform the heuristic and iterative modification of the machining parameters associated with cutting tool and workpiece movements. This in turn can help to reduce the material and energy resources being consumed and thus improve the efficiency and productivity of the manufacturing process. Since the model provides a description of motion that is independent of a given machine's motion control algorithms, the characteristic equations may be employed in a pre-processing manner to inform the selection of parameters without the need for physical machining.

7.3 Limitations

The kinematic discontinuities inherent to the shape characterisation model and illustrated in the schematics of Figs. 3.1, 3.2, 3.3 and 3.4, arise from the idealised assumption of removing acceleration and deceleration from and to rest. In practice these discontinuities are not realised. They therefore refer to the discrete time period where the machine transitions from one limited

phase to another. The actual curvature at which this transition begins must therefore be less than the theoretical transition curvature. Indeed, this premature transition was shown to occur along the spiral tool paths investigated in section 5.3 of chapter 5. Perhaps future research could account for these discontinuities by modelling and incorporating the given machine's acceleration and deceleration behaviour from and to rest.

Also, this thesis has considered only the effects of curvature on tool path motion. In effect, torsion was equated to zero, $\tau(s) = 0$. From Eq. 2.7, of chapter 2, it follows that the binormal component of the jerk vector becomes zero, $j_b(t)\hat{\mathbf{b}}(s) = 0$. The resultant jerk vector, $\mathbf{j}(t)$, is thus limited to describing the rate of change of acceleration, with respect to time, in a given plane. The jerk vector is thus unable to describe the rate at which a given tool path *twists* out of the osculating plane [14, 31].

7.4 Future Research

Considering torsion effects may extend the investigation to tool paths in higher dimensions, as implied above. From Eq. 2.7, of chapter 2, it follows that the jerk vector would gain a binormal component. The vector would then be able to describe the jerk experienced on a non planar tool path.

Further, corresponding incorporation of the binormal vector into the shape characteristic model, may provide a means of describing the characteristic nature of motions where a tool's orientation may be allowed to change with respect to the workpiece [63, 64]. If the rotational axis of

a given tool is aligned with the binormal vector, or at least enforced to maintain a fixed offset angle, the motion of the path's Frenet frame, in particular the motion of the binormal vector, could be used to describe the motion of the tool. This then motivates investigating the motions of a machine's rotational axes. In practice, derivation of the rotational kinematic properties from the linear axes of an accelerometer would require consideration of the specific assembly of the given machine's axes.

References

[1] L. Chanda and R. J. Cripps. Characterising the effects of shape on tool path motion. *International Journal of Machine Tools and Manufacture*, 132:17–35, 2018.

[2] X T. Yan, B. Eynard, and C. Jiang. *Advanced Design and Manufacture to Gain a Competitive Edge, New Manufactring Techniques and their Role in Improving Enterprise Performance*. Springer, 2008.

[3] M. P. Groover and E. W. Zimmers. *CAD/CAM Computer-Aided Design And Manufacturing*. Prentice-Hall Inc., 1984.

[4] Dasault Systemes SolidWorks Coporation. *SOLIDWORKS*. [Online]. Available from: `http://www.solidworks.co.uk/`. [Accessed 21st December 2017].

[5] Autodesk Inc. AutoCAD. *AutoCAD*. [Online]. Available from: `https://www.autodesk.co.uk/products/autocad/overview`. [Accessed 21st December 2017].

[6] D. F. Rogers and J. A. Adams. *Mathematical Elements for Computer Graphics*. McGraw Hill, 1989.

[7] L. Chen, H. Kang, and W. Hung. Effects Of Desing Features On Automobile Styling Perceptions. *International Association Of Design Research on Manufacturing Research*, 2007.

[8] Gerald Farin. *Curves and Surfaces for CAGD*. Morgan Kaufmann Publishers, 2002.

[9] Autodesk Inc. *PowerMILL*. [Online]. Available from: `https://www.autodesk.com/products/powermill/overview`. [Accessed 21st December 2017].

[10] S. Suh, S. Chung, and I. Stroud. *Theory and Design of CNC Systems*. Springer, 2008.

[11] Y. Jin, Y. He, J. Fu, Z. Lin, and W. Gan. A fine-interpolation-based parametric method with a novel real-time look-ahead algorithm. *Computer-Aided Design*, 55:37–48, 2014.

[12] S.J. Yutkowitz. Apparatus and method for smooth cornering in a motion control system, May 23 2001. EP Patent App. EP20,000,204,087.

[13] R. T. Farouki, Y. Tsai, and C. S. Wilson. Physical constraints on feedrates and feed accelerations along curved tool paths. *Computer Aided Geometric Design*, 17:337–359, 2000.

[14] Martin M. Lipschutz. *Differential Geometry*. McGraw-Hill, 1969.

[15] S. H. Schot. Jerk: The time rate of change of acceleration. *American Journal of Physics*, 46:1090–1094, 1978.

[16] S. Tulsyan and Y. Altintas. Local toolpath smoothing for five-axis machine tools. *International Journal of Machine Tools and Manufacture*, 96:15–26, 2015.

[17] X. Pessoles, Y. Landon, and W. Rubio. Kinematic modelling of a 3-axis NC machine tool in linear and circular interpolation. *International Journal of Advanced Manufacturing Technology*, 47:639–655, 2010.

[18] M. T. Lin, M. S. Tsai, and H. T. Yau. Development of a dynamics-based NURBS interpolator with real-time look-ahead algorithm. *International Journal of Machine Tools and Manufacture*, 47:2246–2262, 2007.

[19] S. Tajima and B. Sencer. Kinematic corner smoothing for high speed machine tools. *International Journal of Machine Tools and Manufacture*, 108:27–43, 2016.

[20] M. K. Jouaneh, Z. Wang, and D. A. Dornfield. Trajectory planning for coordinated motion of a robot and a positioning table. part 1. path specification. *IEEE Transactions on Robotics and Automation*, 6:735–745, 1990.

[21] K. Erkorkmaz and Y. Altintas. High speed CNC system design. part I: jerk limited trajectory generation and quintic spline interpolation. *International Journal of Machine Tools and Manufacture*, 41:1323–1345, 2001.

[22] M. K. Jouaneh, Z. Wang, and D. A. Dornfield. Trajectory planning for coordinated motion of a robot and a positioning table. part 2. optimal trajectory specification. *IEEE Transactions on Robotics and Automation*, 6:746–759, 1990.

[23] J. M. Ali, R. M. Tookey, J. V. Ball, and A. A. Ball. The generalised Cornu spiral and its application to span generation. *Journal of Computational and Applied Mathematics*, 107:37–47, 1999.

[24] A. W. Nutbourne, P. M. McLellan, and R. M. L. Kensit. Curvature profiles for planes curves. *Computer Aided Design*, 4:176–184, 1972.

[25] B. Sencer, K. Ishizaki, and E. Shamoto. A curvature optimal sharp corner smoothing algorithm for high-speed feed motion generation of NC systems along linear tool paths. *International Journal of Advanced Manufacturing Technology*, 76:1977–1992, 2015.

[26] H. Zhao, L. Zhu, and H. Ding. A real-time look ahead interpolation methodology with curvature-continuous b-spline transition scheme for CNC machining of short line segments. *International Journal of Machine Tools and Manufacture*, 65:88–98, 2013.

[27] V. Pateloup, E. Duc, and P. Ray. B-spline approximation of circle arc and straight line for pocket machining. *Computer Aided Design*, 42:817–827, 2010.

[28] L. Chanda and R. J. Cripps. Toolpath Geometry and High Speed Machine Axis Motion. *Proceedings of the 14th International Conference on Manufacturing Research*, 3:7–12, 2016.

[29] F. R. Gantmacher. *Curves and Surfaces for CAGD*. Chelsea Publishing Company, 1977.

[30] A. W. Nutbourne and R. R. Martin. *Differential Geometry Applied To Curve And Surface Design*. Ellis Horwood Limited, 1991.

[31] T. F. Bancoff and S. T. Lovett. *Differential Geometry of Curves and Surfaces*. CRC Press, 2010.

[32] B. N. Taylor and A. Thompson. *NIST SP 330 - The International System of Units (SI)*. International Bureau of Weights and Measures, 2008.

[33] M. R. Spiegel. *Theory And Problems Of Vector Analysis and an Introduction to Tensor Analysis*. McGraw-Hill, 1988.

[34] I. Newton. *Philosophiae Naturalis Principia Mathematica*. Benjamin Motte, 1687.

[35] D. Eager, A. Pendrill, and N. Reistad. Beyond velocity and acceleration: jerk, snap and higher derivatives. *European Journal of Physics*, 37:1–11, 2016.

[36] P-B. Barre, R. Bearee, P. Borne, and E. Dumetz. Influence of a Jerk Controlled Movement Law on the Vibratory Behaviour of High-Dynamics Systems. *Journal of Intelligent and Robotic Systems*, 42:275–293, 2005.

[37] S. Tajima and B. Sencer. Global tool-path smoothing for CNC machine tools with uninterrupted acceleration. *International Journal of Machine Tools and Manufacture*, 121:81–95, 2017.

[38] Z. Jia, D. Song, J. Ma, G. Hu, and W. Su. A NURBS interpolator with constant speed at feedrate-sensitive regions under drive and contour-error constraints. *International Journal of Machine Tools and Manufacture*, 116:1–17, 2017.

[39] Y. Wang, D. Yang, R. Gai, S. Wang, and S. Sun. Design of trigonometric velocity scheduling algorithm based on pre-interpolation and look-ahead interpolation. *International Journal of Machine Tools and Manufacture*, 96:94–105, 2015.

[40] S. H. Schot. Aberrancy: Geometry of the third derivative. *Mathematics Magazine*, 51:259–275, 1978.

[41] C. Cadwallader. *Delcam incorporates machine DNA profiler into PowerMill 2013*. Machinery, 2012.

[42] S. W. Mackman, W. Strother, and S. Hobbs. Method and system for testing a machine tool GB patent, May 02 2012. GB Patent App. GB1204908.6.

[43] S. W. Mackman, W. Strother, and S. Hobbs. Method and system for testing a machine tool US patent, November 14 2013. US Patent App. US9625897B2.

[44] ISO/DIS10791-6. Test code for machine tools-Part 1: geometric accuracy of machines operating under no-load or quasi-static conditions. *ISO*, 2012.

[45] X. Thiem, B. Kauschinger, and S. Ihlenfeldt. Structure model based correction of thermally induced motion errors of machine tools. *17th Machining Innovations Conference for Aerospace Industry*, 14:128–135, 2017.

[46] J. R. Taylor. *Classical Mechanics*. University Science Books, 2005.

[47] Yamazaki Mazak UK Ltd. *Mazak series brochure*. Mazak, 2014.

[48] AG. Hermle. *Hermle C600 series brochure*. Gosheim Germany, 1999.

[49] Matsuura Machinery Ltd. *Matsuura LX series brochure*. Matsuura, 1999.

[50] StrainSense Limited. *Entran-Accelerometers*. [Online]. Available from: `http://www.strainsense.co.uk/products/entran-accelerometers`. [Accessed 3rd January 2018].

[51] E Jesper Eklund and Andrei M Shkel. Single-mask fabrication of high- g piezoresistive accelerometers with extended temperature range. *Journal of Micromechanics and Microengineering*, 17(4):730–740, 2007.

[52] C. S. Smith. Piezoresistance effect in germanium and silicon. *Physical Review*, 94:42–49, 1954.

[53] K. J. Vinoy, G. K. Ananthasuresh, R. Pratap, and S. B. Krupanidhi. *Mirco and Smart Devices and Systems*. Springer, 2014.

[54] T. R. Padmanabhan. *Industrial Instrumentation: Principles and Design*. Springer, 2000.

[55] HBM Test and Measurement. *eDAQ-lite System*. [Online]. Available from: https://www.hbm.com/en/5502/daq-data-acquisition-systems. [Accessed 15th November 2017].

[56] HBM Test and Measurement. *SoMat Test Control Environment Software*. [Online]. Available from: https://www.hbm.com/en/1996/software/. [Accessed 15th November 2017].

[57] E M. Stein and G. Weiss. *Introduction to Fourier Analysis on Euclidean Spaces*. Princeton University Press, 1971.

[58] W. H. Press, S. A. Teukolsky, W. T. Vetterling, and B. P. Flannery. *Numerical Recipes in C, The art of scientific computing*. Cambridge University Press, 1994.

[59] D. Kincaid and W.Cheney. *Numerical Analysis: Mathematics of Scientific Computing*. Brooks/Cole, 1996.

[60] K. M.Bolton. Biarc curves. *Computer-Aided Design*, 7:89–92, 1975.

[61] L. Simpson, D. Bashioum, and E. Carr. Computer Flight Planning in the North Atlantic. *Journal of Aircraft*, 2:337–346, 1965.

[62] L. Simpson, D. Bashioum, and E. Carr. Estimation of aircraft fuel consumption. *Journal of Aircraft*, 19:969–975, 1982.

[63] R. J. Cripps and G. Mullineux. Constructing 3D motions from curvature and torsion profiles. *Computer-Aided Design*, 11:379–387, 2012.

[64] R. J. Cripps and G. Mullineux. Using geometric algebra to represent and interpolate tool poses. *International Journal of Computer Integrated Manufacturing*, 29:406–423, 2016.

Appendix A

Machine axis limits

The power, P, required to produce a given torque, Υ, and angular velocity, ω from the shaft of a rotating servomotor can be expressed as [46]

$$P = \Upsilon\omega \ . \tag{1.1}$$

Similarly, Υ may be expressed in terms of the servomotor's inertia, I, and the shaft's angular acceleration, α, as [46]

$$\Upsilon = I\alpha \ . \tag{1.2}$$

The relationships between the angular and linear kinematic properties associated with circular

tool path motion can be expressed as,

$$a = \frac{v^2}{r} \ , \tag{1.3}$$

$$\alpha = \frac{a}{r} \ , \tag{1.4}$$

and

$$\omega = \frac{v}{r} \ , \tag{1.5}$$

where v and a are the linear velocity and acceleration respectively, and r is the radius of a given circular tool path motion [46].

Substituting Eq. 1.2 into Eq. 1.1 generates an alternative expression for power,

$$P = I\alpha\omega \ . \tag{1.6}$$

Also, an expression relating angular acceleration and linear velocity can be formed by substi-

tuting Eq. 1.3 into Eq. 1.4,

$$\alpha = \frac{v^2}{r^2} \ . \tag{1.7}$$

Substituting Eqs. 1.5 and 1.7 into Eq. 1.6 produces,

$$P = I\frac{v^3}{r^3} \ . \tag{1.8}$$

Making v the subject of the above equation and letting $v = v_{max}$ and $P = P_{max}$ provides an expression for the maximum achievable traversal speed using servomotors with a given maximum power,

$$v_{max} = \left(\frac{P_{max}}{I}\right)^{\frac{1}{3}} r \ . \tag{1.9}$$

An alternative expression for torque can be found by substituting Eq. 1.7 into Eq. 1.2,

$$\Upsilon = I\frac{v^2}{r^2} \ . \tag{1.10}$$

Making v the subject of the above equation and letting $v = v_{max}$ and $\Upsilon = \Upsilon_{max}$ provides an expression for the maximum achievable traversal speed using servomotors with a given maximum

torque,

$$v_{max} = \left(\frac{\Upsilon_{max}}{I} \right)^{\frac{1}{2}} r \, . \tag{1.11}$$

Appendix B

Jerk vector derivation

Taking the derivative of Eq. (2.5) with respect to time, provides an expression for the jerk vector:

$$\mathbf{j}(t) = \frac{d}{dt}\left[\frac{d^2s}{dt^2}\hat{\mathbf{t}}(s) + \left\{\frac{ds}{dt}\right\}^2 \kappa(s)\hat{\mathbf{n}}(s)\right]$$

$$= \frac{d}{dt}\left[\frac{d^2s}{dt^2}\hat{\mathbf{t}}(s)\right] + \frac{d}{dt}\left[\left\{\frac{ds}{dt}\right\}^2 \kappa(s)\hat{\mathbf{n}}(s)\right] .$$

Let

$$\xi_0(t) \equiv \frac{d}{dt}\left[\frac{d^2s}{dt^2}\hat{\mathbf{t}}(s)\right]$$

and

$$\xi_1(t) \equiv \frac{d}{dt}\left[\left\{\frac{ds}{dt}\right\}^2 \kappa(s)\hat{\mathbf{n}}(s)\right] .$$

It then follows that,

$$\xi_0(t) = \frac{d^3s}{dt^3}\hat{\mathbf{t}}(s) + \frac{ds}{dt}\frac{d^2s}{dt^2}\frac{d\hat{\mathbf{t}}(s)}{ds}.$$

Substituting Eq. (2.1) into the above equation gives

$$\xi_0(t) = \frac{d^3s}{dt^3}\hat{\mathbf{t}}(s) + \frac{ds}{dt}\frac{d^2s}{dt^2}\kappa(s)\hat{\mathbf{n}}(s) . \tag{2.1}$$

Also,

$$\xi_1(t) = 2\frac{ds}{dt}\frac{d^2s}{dt^2}\kappa(s)\hat{\mathbf{n}}(s) + \left\{\frac{ds}{dt}\right\}^3 \frac{d}{ds}\left[\kappa(s)\hat{\mathbf{n}}(s)\right]$$

$$= 2\frac{ds}{dt}\frac{d^2s}{dt^2}\kappa(s)\hat{\mathbf{n}}(s) + \left\{\frac{ds}{dt}\right\}^3 \frac{d\kappa(s)}{ds}\hat{\mathbf{n}}(s) + \left\{\frac{ds}{dt}\right\}^3 \kappa(s)\frac{d\hat{\mathbf{n}}(s)}{ds} .$$

Substituting Eq. (2.2) into the above equation gives

$$\begin{aligned}\xi_1(t) = 2\frac{ds}{dt}\frac{d^2s}{dt^2}\kappa(s)\hat{\mathbf{n}}(s) + \left\{\frac{ds}{dt}\right\}^3\frac{d\kappa(s)}{ds}\hat{\mathbf{n}}(s) \\ - \left\{\frac{ds}{dt}\right\}^3\{\kappa(s)\}^2\hat{\mathbf{t}}(s) + \left\{\frac{ds}{dt}\right\}^3\tau(s)\kappa(s)\hat{\mathbf{b}}(s)\ .\end{aligned} \tag{2.2}$$

Summing Eq. 2.1 and Eq. 2.2 produces the equation given below,

$$\mathbf{j}(t) = j_t(t)\hat{\mathbf{t}}(s) + j_n(t)\hat{\mathbf{n}}(s) + j_b(t)\hat{\mathbf{b}}(s)\ ;$$

where

$$j_t(t) = \frac{d^3s(t)}{dt^3} - \left\{\frac{ds(t)}{dt}\right\}^3\{\kappa(s)\}^2\ ,$$

$$j_n(t) = 3\frac{ds(t)}{dt}\frac{d^2s(t)}{dt^2}\kappa(s) + \left\{\frac{ds(t)}{dt}\right\}^3\frac{d\kappa(s)}{ds}\ ,$$

and

$$j_b(t) = \left\{\frac{ds(t)}{dt}\right\}^3\kappa(s)\tau(s)\ .$$

Appendix C

Sampling Period

Sampling period, T_s, is the time interval in which a controller receives position feedback from servo loops. Since the purpose of the investigation is to study the effects of shape on tool path motion, care has been taken to ensure that tool path motions do not require processing speeds greater than the controller's processing capability.

The greater the number of points used to define a tool path, the greater the processing speed required from the controller. Consider a planar linear tool path defined by N equally spaced points. If the commanded feed rate is achieved, the distance between consecutive points does not require a sampling period greater than the controller's limit. By incrementally increasing the number of equally spaced points until the commanded feed rate is not achieved, the controller sampling period can be identified.

A planar linear path has no curvature and no torsion, so shape has no affect. The length of the

line does however affect the achieved feed rate. The length of the line should be sufficiently long such that the machine can accelerate to the commanded feed rate from rest and decelerate from the commanded feed rate to rest.

The specific values of feed rate and line length chosen are immaterial. In general, the greater the commanded feed rate, the greater the distances required for acceleration and deceleration and so the longer the line needed. However, for a line of a given length, the greater the commanded feed rate, the fewer equally spaced points required to observe a difference between the commanded and achieved feed rates.

The Hermle's maximum permissible feed rate, F_{max}, $(0.6m/s)$ is therefore set as the commanded feed rate in the linear tool path motion tests. The tool path length is set to $0.5m$, as preliminary testing showed such a length is sufficiently long to enable the commanded feed rate to be achieved. By incrementally increasing the density of the equally spaced points, it is found that the threshold number of points, N_t, at which the specified feed rate is still achieved is 214 (Fig. C.1). From this, the minimum distance between consecutive points can be found, $s_{min} = L/N_t$. It then follows that $T_s = s_{min}/F$.

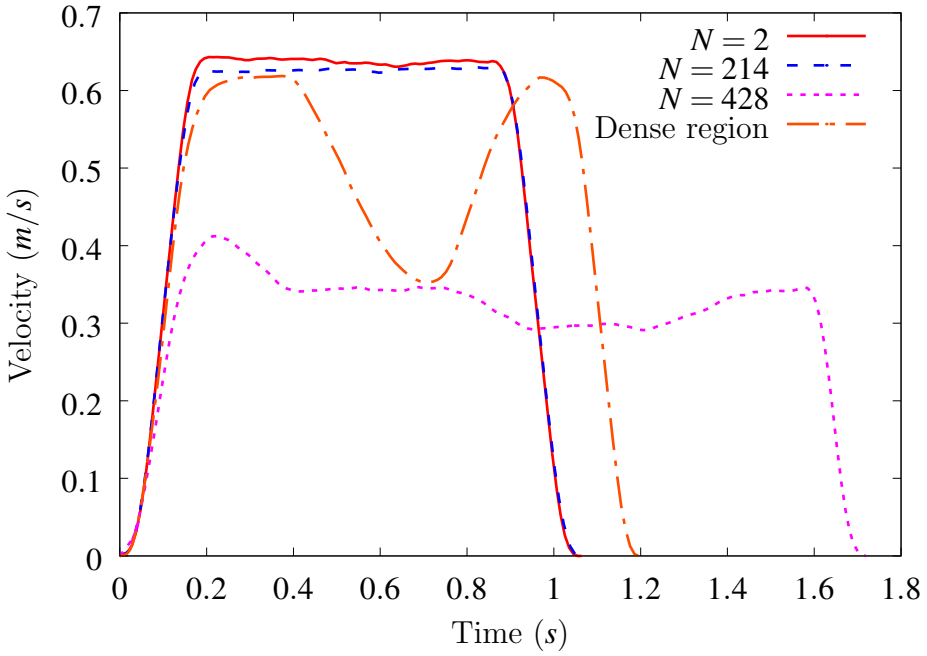

Figure C.1: Feed rate profiles for different point densities

To verify the threshold number of points does not affect motion, a comparison is made to a motion produced for $N = 2$ points (start and end points of the line). Fig. C.1 suggests negligible difference between the two motions. Doubling the threshold number of points to 428, halves the distance between consecutive points and the achieved feed rate is approximately halved (Fig. C.1). Further, the line is then divided into three sections, the first and last sections contain points minimally spaced and the middle section contains points that are spaced with half the minimal distance. From the figure it can be seen that the achieved feed rate drops to approximately half in the middle dense region as the sampling period phenomenon takes effect.

Appendix D

Numerical integration error bound

For a given interval $[s_{min}, s_{max}]$, the total error ε_T of numerical integration, using the trapezoidal rule, can be given as

$$\varepsilon_T = -\frac{(s_{max} - s_{min})^3}{12N^2} \frac{\sum_{i=0}^{N-1} f''(\zeta_i)}{N} ,$$

where N is the number of segments in the interval and $f''(\zeta_i)$ is the second derivative of the integrand evaluated at some point ζ_i, $s_{min} \leq \zeta_i \leq s_{max}$ [59]. The expression

$$\frac{\sum_{i=0}^{N-1} f''(\zeta_i)}{N} ,$$

can be considered as an approximate average value of the second derivative in the specified

interval. At some point, the second derivative will take its average value ζ_{avg}, assuming it is continuous. In the case of the integrands given in Eqs. (5.3) and (5.4), it is shown below in Eqs. (4.3) and (4.4) and Fig. D.1 that the second derivatives are indeed continuous. Therefore let,

$$\zeta_{avg} = \frac{\sum_{i=0}^{N-1} f''(\zeta_i)}{N} \ .$$

The total error may then be expressed as

$$\varepsilon_T = -\frac{(s_{max} - s_{min})^3}{12N^2} \zeta_{avg} \ .$$

It is not known where ζ_{avg} lies in the interval. By replacing ζ_{avg} with $max(|f''(\zeta_i)|)$, an upper bound ε_B on the total error for the given interval can be found. It then follows that,

$$\varepsilon_B = -\frac{(s_{max} - s_{min})^3}{12N^2} max(|f''(\zeta_i)|) \ . \tag{4.1}$$

The above equation shows that to identify error bounds of the Cornu spiral positions, resulting from Eqs. (5.3) and (5.4), evaluation of the second derivatives of the corresponding integrands is required. This can be achieved by rewriting Eqs. (5.3) and (5.4) as [23]

$$x(s) = x_0 + \int_0^s f_x(\sigma) d\sigma \ ,$$

and

$$y(s) = y_0 + \int_0^s f_y(\sigma) d\sigma \ ,$$

where $f_x(\sigma) = cos(\alpha(\sigma))$, $f_y(\sigma) = sin(\alpha(\sigma))$ and

$$\alpha(\sigma) = \theta_0 + \frac{1}{2L}\{2\kappa_0 L\sigma + (\kappa_1 - \kappa_0)\sigma^2)\} \ . \tag{4.2}$$

The first and second derivatives of the integrand $f_x(\sigma)$ are

$$\frac{df_x(\sigma)}{d\sigma} = -\frac{d\alpha(\sigma)}{d\sigma} sin(\alpha(\sigma)) \ ,$$

and

$$\frac{d^2 f_x(\sigma)}{d\sigma^2} = -\left[\frac{d^2\alpha(\sigma)}{d\sigma^2} sin(\alpha(\sigma)) + \left\{\frac{d\alpha(\sigma)}{d\sigma}\right\}^2 cos(\alpha(\sigma))\right] \ , \tag{4.3}$$

respectively. Similarly,

$$\frac{df_y(\sigma)}{d\sigma} = \frac{d\alpha(\sigma)}{d\sigma} cos(\alpha(\sigma)) \ ,$$

and

$$\frac{d^2 f_y(\sigma)}{d\sigma^2} = \frac{d^2\alpha(\sigma)}{d\sigma^2} cos(\alpha(\sigma)) - \left\{ \frac{d\alpha(\sigma)}{d\sigma} \right\}^2 sin(\alpha(\sigma)) \ . \tag{4.4}$$

From Eq. (4.2) it follows that,

$$\frac{d\alpha(\sigma)}{d\sigma} = \frac{1}{L}\{\kappa_0 L + (\kappa_1 - \kappa_0)\sigma\} \ ,$$

and

$$\frac{d^2\alpha(\sigma)}{d\sigma^2} = \frac{\kappa_1 - \kappa_0}{L} \ .$$

$|cos(\alpha(\sigma))|$ and $|sin(\alpha(\sigma))| \leq 1, \forall\ \sigma$, $d^2(\alpha(\sigma))/d\sigma^2$ is constant, and $\{d\alpha(\sigma)/d\sigma\}^2 = O(\sigma^2)$ since,

$$\left\{ \frac{d\alpha(\sigma)}{d\sigma} \right\}^2 = \frac{1}{L^2}\{\kappa_0 L + (\kappa_1 - \kappa_0)\sigma\}^2 \ . \tag{4.5}$$

It then follows that the magnitude of $\{d\alpha(\sigma)/d\sigma\}^2$ increases monotonically and so its maximum value occurs at s_{max} for the interval $[s_{min}, s_{max}]$. As illustrated by Fig. D.1, as $\sigma \to \infty$, $\{d\alpha(\sigma)/d\sigma\}^2$, denoted $(\alpha')^2$ in Fig. D.1, begins to envelope both second derivative terms (Eqs. (4.3) and (4.4)). By substituting Eq. (4.5) into Eq. (4.1) an alternative expression for the error bound can be formed

$$\varepsilon_B = -\frac{(s_{max} - s_{min})^3 \{\kappa_0 L + (\kappa_1 - \kappa_0) s_{max}\}^2}{12N^2L^2} .$$

The number of segments required, for a given interval, to obtain a suitable magnitude of error can then be identified,

$$N = \sqrt{\frac{(s_{max} - s_{min})^3 \{\kappa_0 L + (\kappa_1 - \kappa_0) s_{max}\}^2}{12|\varepsilon_B|L^2}} .$$

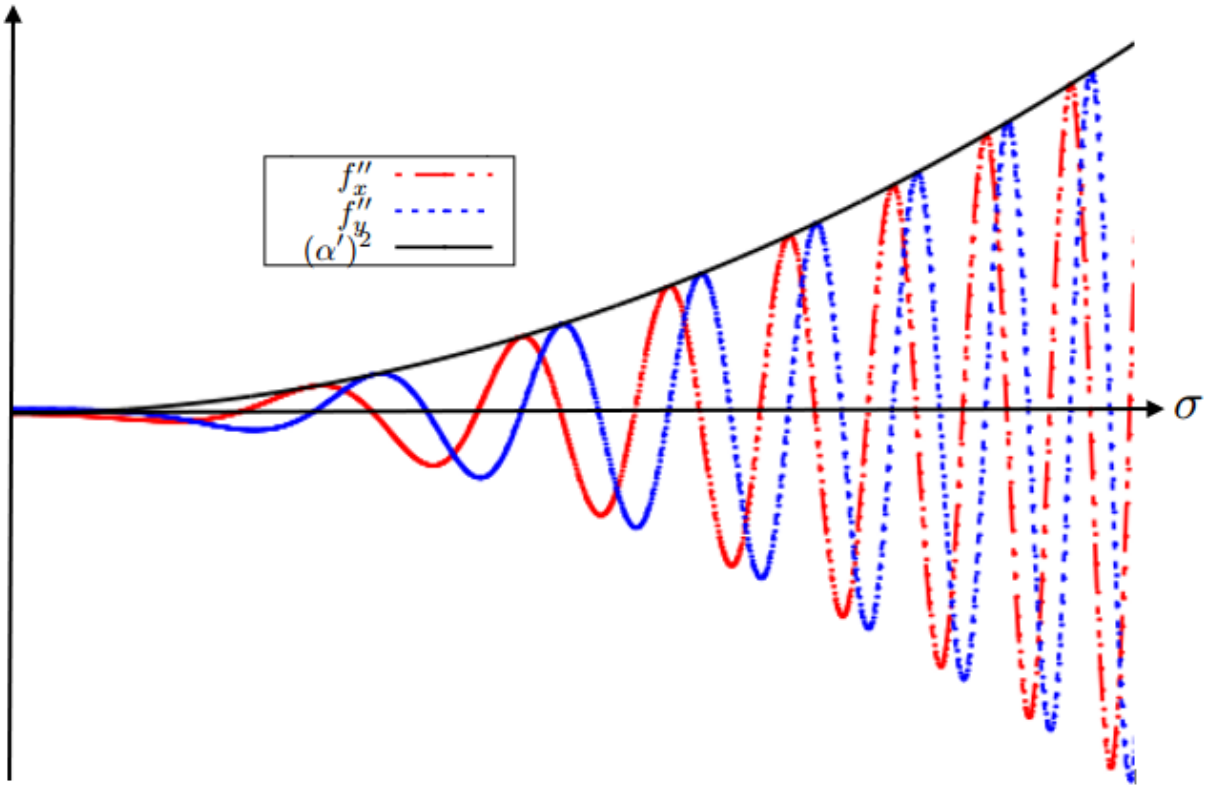

Figure D.1: Error bound

Appendix E

Motion timing percentage errors

Table E.1: Hermle motion timings

Predicted time, $t_p(s)$	Achieved time, $t_a(s)$	Error, %
0.551	0.55	0.179
0.78	0.785	0.671
0.955	0.961	0.602
1.103	1.087	1.453
1.233	1.226	0.538
1.743	1.742	0.087
2.466	2.453	0.51
3.02	3.022	0.077
3.487	3.473	0.4
3.898	3.897	0.037

Table E.2: Matsuura motion timings

Predicted time, $t_p(s)$	Achieved time, $t_a(s)$	Error, %
0.551	0.55	0.179
0.78	0.785	0.671
0.955	0.961	0.602
1.103	1.087	1.453
1.233	1.226	0.538
1.743	1.742	0.087
2.466	2.453	0.51
3.02	3.022	0.077
3.487	3.473	0.4
3.898	3.897	0.037

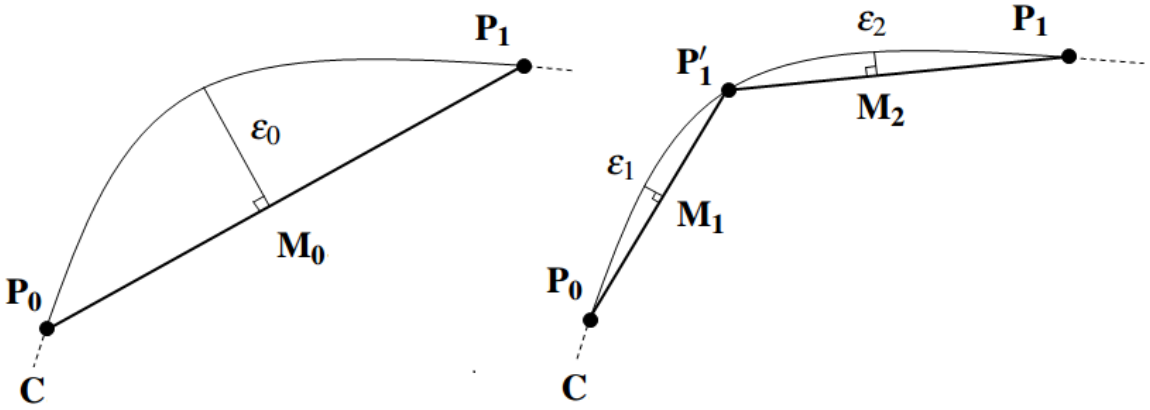

Figure 1.4: Interpolation error, ε

$\mathbf{P}_0$ to $\mathbf{P}_1$ the desired path is approximated by a single chord, $\overline{\mathbf{P}_0\mathbf{P}_1}$. The error of this type of interpolation, ε_0, may be defined as the length of a perpendicular line segment connecting the midpoint, $\mathbf{M}_0$, of the chord, $\overline{\mathbf{P}_0\mathbf{P}_1}$, to the tool path, $\mathbf{C}$. By selecting another point, $\mathbf{P'}_1$, on $\mathbf{C}$ between $\mathbf{P}_0$ and $\mathbf{P}_1$ two chords, $\overline{\mathbf{P}_0\mathbf{P'}_1}$ and $\overline{\mathbf{P'}_1\mathbf{P}_1}$, form an alternative linear approximation to the portion of the desired tool path, $\mathbf{C}$. Points $\mathbf{M}_1$ and $\mathbf{M}_2$ denote the midpoints of $\overline{\mathbf{P}_0\mathbf{P'}_1}$ and $\overline{\mathbf{P'}_1\mathbf{P}_1}$ respectively. Given the direction of the desired path, $\mathbf{C}$, changes monotonically between points $\mathbf{P}_0$ and $\mathbf{P}_1$ the error of each chord, ε_1 and ε_2 respectively, is less that the error of the original single chord, ε_0; $\varepsilon_1, \varepsilon_2 < \varepsilon_0$.

The greater the number of positions selected, the smaller the interpolation error for a given chord and so the closer the shape of the discretised tool path is to the desired continuous tool path. A greater number of positions also decreases the distances between consecutive positions. If the time taken to process and execute a cutting tool's movement between consecutive positions, T_m, is less than the controller's minimum processing time, T_p, the tool will rest at the end position and wait or *dwell* for the next motion command to be generated by the controller. When $T_m < T_p$, the machine's servomotors are effectively deprived of motion data. This phe-

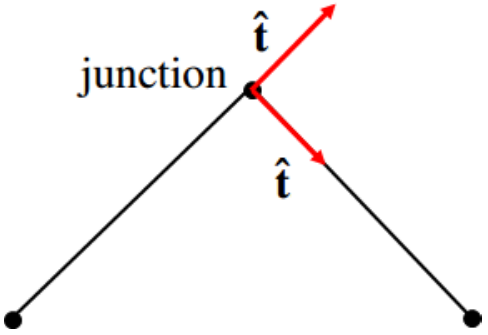

Figure 1.5: Undefined tangent vector

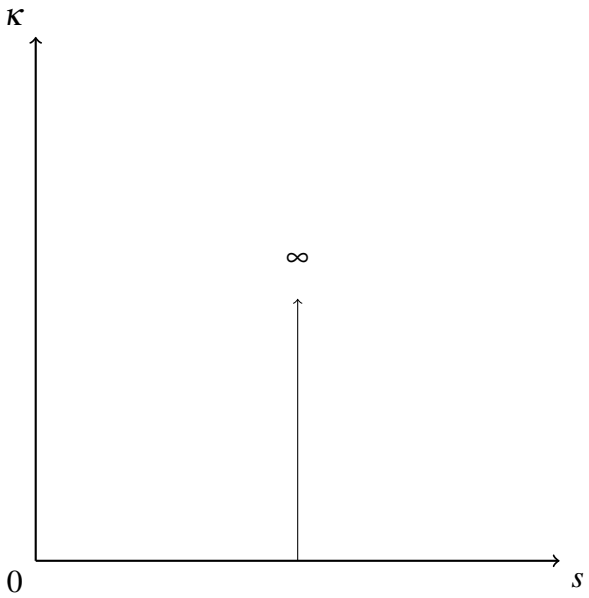

Figure 1.6: G^0 linear segments. Piecewise impulse curvature profile

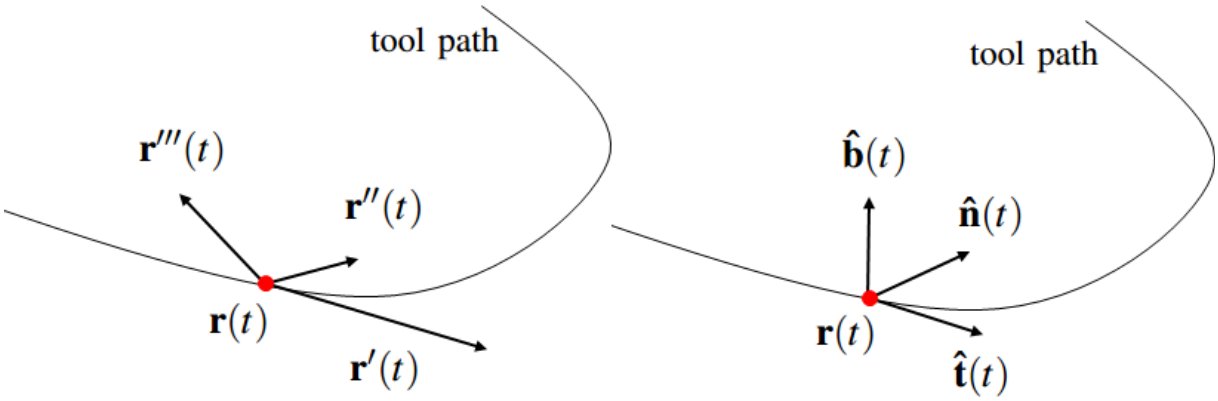

Figure 2.1: Local affine system (left) and Frenet frame (right) [8]

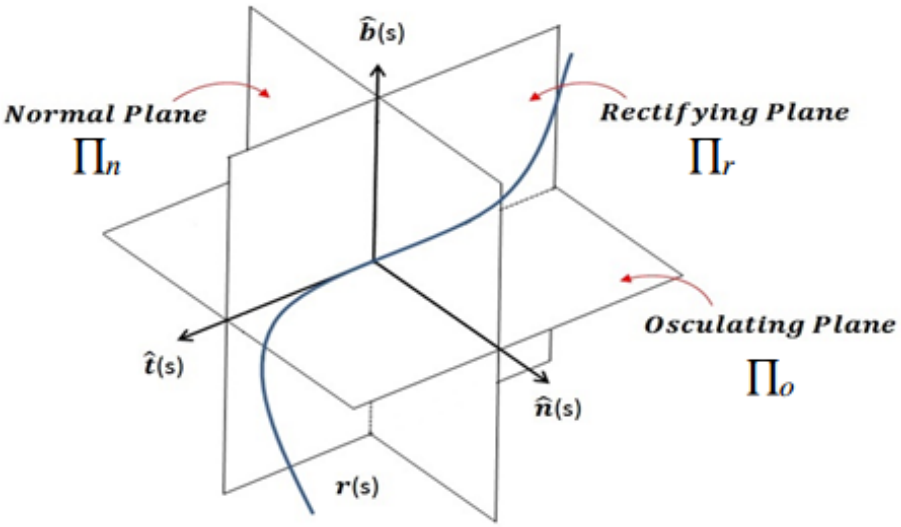

Figure 2.2: The local planes

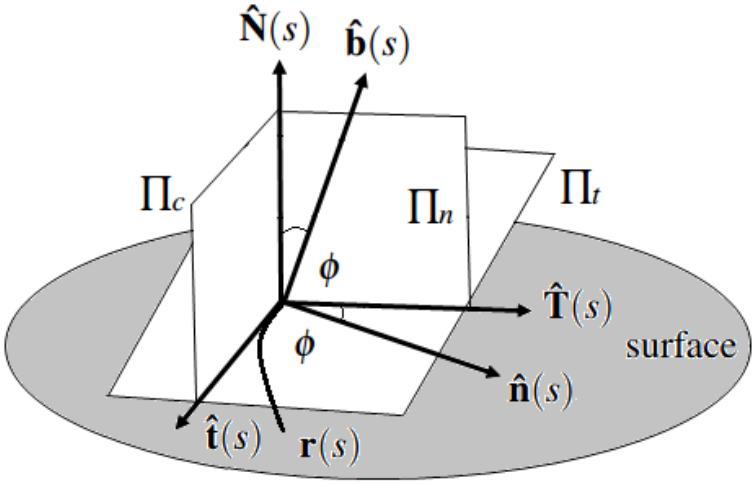

Figure 2.3: Surface Frame [30]

the surfaces of the original CAD model [3]. Indeed, in the finishing stages, the desired tool paths are derived from the surfaces on which they lie (see section 1.2). The following section therefore describes the relationships between the shape properties of the CAD model surfaces and the desired tool paths used in the corresponding machining process.

2.2 Tool paths on surfaces

Consider a tool path lying on a surface. In addition to the Frenet frame, $\mathbf{F}_1(s)$, it is possible to assign another frame, the Darboux frame, $\mathbf{F}_2(s)$, at each point on the tool path (Fig. 2.3) [30]. At a given point there is only one unit surface normal vector, $\hat{\mathbf{N}}(s)$, and an infinity of tangent vectors. These tangent vectors lie in the tangent plane that is orthogonal to $\hat{\mathbf{N}}(s)$. The tool path's unit tangent vector and the surface's unit normal vector can together be used to form a vector that is orthogonal to both, referred to in this thesis as the bi-tangent vector, $\hat{\mathbf{T}}(s)$, $\hat{\mathbf{T}}(s) = \hat{\mathbf{N}}(s) \wedge \hat{\mathbf{t}}(s)$ [30].

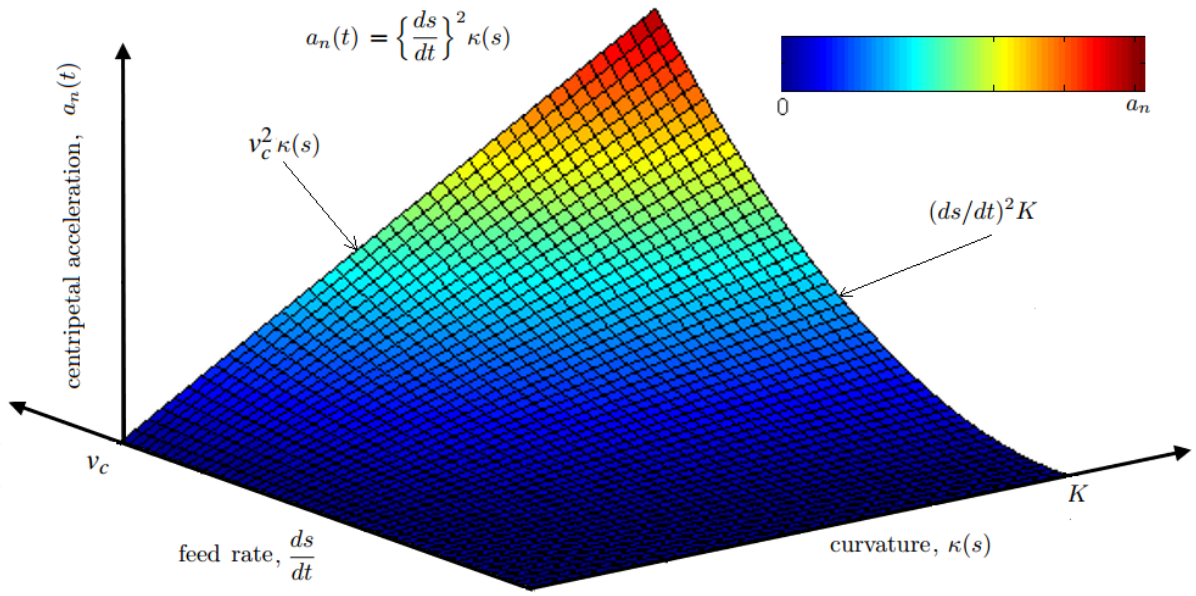

Figure 2.4: Centripetal acceleration surface

osculant, whose derivatives, up to and including order two, agree with those of the path [14]. Subsequently, normal acceleration is commonly referred to as centripetal acceleration [33].

From Eq. (2.5) it follows that normal acceleration consists of time and shape dependent elements, feed rate, ds/dt, and curvature, $\kappa(s)$, respectively. The surface, shown in Fig. (2.4), illustrates the effect of each element on centripetal acceleration, $a_n(t)$. The surface is mathematically expressed explicitly in terms of ds/dt and $\kappa(s)$, $a_n(t) = (ds/dt)^2\kappa(s)$. Centripetal acceleration (Fig. 2.5) increases linearly with curvature, $a_n(t) = v_c^2\kappa(s)$, for a constant feed rate, v_c. Centripetal acceleration increases parabolically with feed rate, $a_n(t) = (ds/dt)^2 K$, for a constant curvature, K.

xy planes.

4.2.2 Accelerometer

As shown by Eqs. (2.4), (2.5) and (2.7), to quantify the actual velocity, acceleration and jerk experienced on a given circular tool path, the achieved feed rate is required. Each of the controllers of the test machines provide a Digital Read-Out (DRO) of feed rate. This however, is not an independent source of measurement and as such can only be used as a preliminary indicator of the actual feed rate achieved in a given motion. An inertial sensor, specifically a tri-axial piezoresistive accelerometer, is used as an independent measurement source [50]. The sensor outputs the acceleration and time of a given motion. The achieved feed rate is then deduced from this acceleration profile. The actual velocity, acceleration and jerk experienced can then be found for each circular tool path from Eqs. (2.4), (2.5) and (2.7).

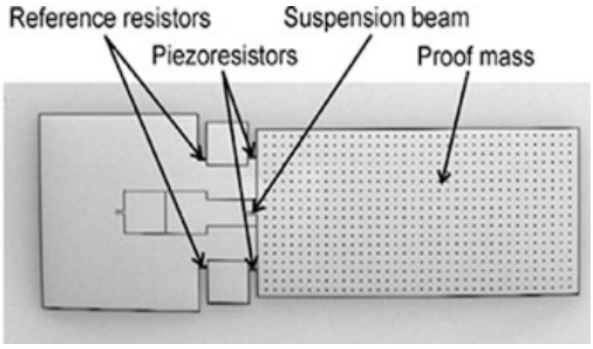

Figure 4.2: Diagram of a piezoresistive accelerometer [51]

The main principle on which the accelerometer operates is the piezoresistive effect [52]. This is a phenomenon whereby the application of mechanical stress causes a change in the electrical

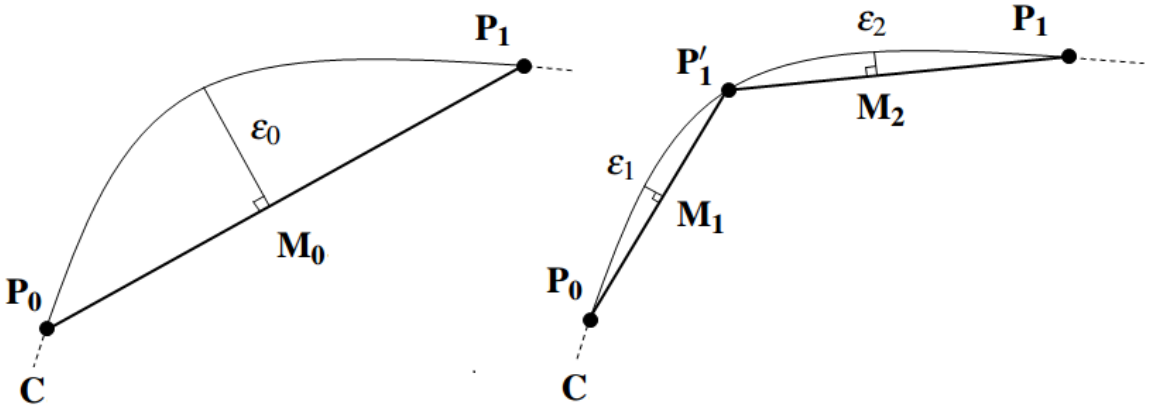

Figure 1.4: Interpolation error, ε

$\mathbf{P}_0$ to $\mathbf{P}_1$ the desired path is approximated by a single chord, $\overline{\mathbf{P}_0\mathbf{P}_1}$. The error of this type of interpolation, ε_0, may be defined as the length of a perpendicular line segment connecting the midpoint, $\mathbf{M}_0$, of the chord, $\overline{\mathbf{P}_0\mathbf{P}_1}$, to the tool path, $\mathbf{C}$. By selecting another point, $\mathbf{P'}_1$, on $\mathbf{C}$ between $\mathbf{P}_0$ and $\mathbf{P}_1$ two chords, $\overline{\mathbf{P}_0\mathbf{P'}_1}$ and $\overline{\mathbf{P'}_1\mathbf{P}_1}$, form an alternative linear approximation to the portion of the desired tool path, $\mathbf{C}$. Points $\mathbf{M}_1$ and $\mathbf{M}_2$ denote the midpoints of $\overline{\mathbf{P}_0\mathbf{P'}_1}$ and $\overline{\mathbf{P'}_1\mathbf{P}_1}$ respectively. Given the direction of the desired path, $\mathbf{C}$, changes monotonically between points $\mathbf{P}_0$ and $\mathbf{P}_1$ the error of each chord, ε_1 and ε_2 respectively, is less that the error of the original single chord, ε_0; $\varepsilon_1, \varepsilon_2 < \varepsilon_0$.

The greater the number of positions selected, the smaller the interpolation error for a given chord and so the closer the shape of the discretised tool path is to the desired continuous tool path. A greater number of positions also decreases the distances between consecutive positions. If the time taken to process and execute a cutting tool's movement between consecutive positions, T_m, is less than the controller's minimum processing time, T_p, the tool will rest at the end position and wait or *dwell* for the next motion command to be generated by the controller. When $T_m < T_p$, the machine's servomotors are effectively deprived of motion data. This phe-

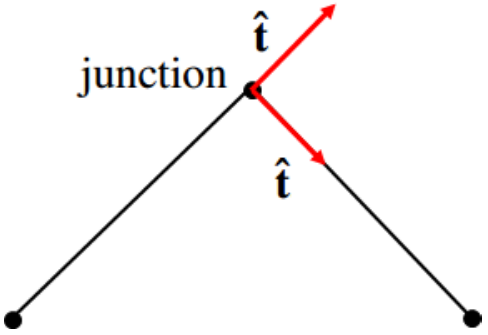

Figure 1.5: Undefined tangent vector

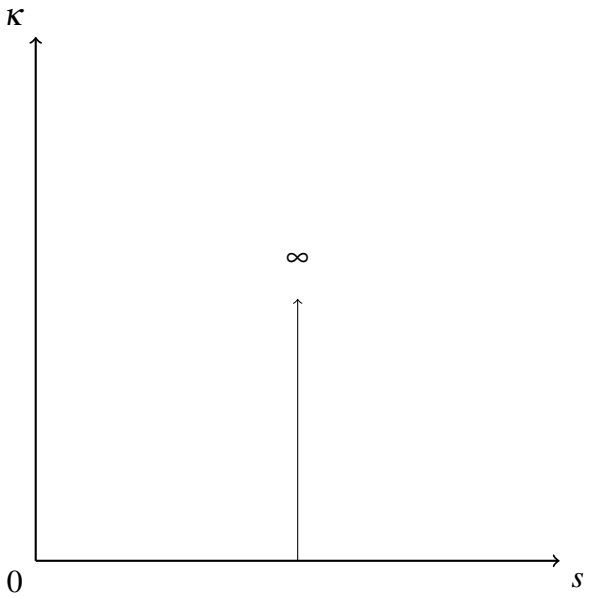

Figure 1.6: G^0 linear segments. Piecewise impulse curvature profile

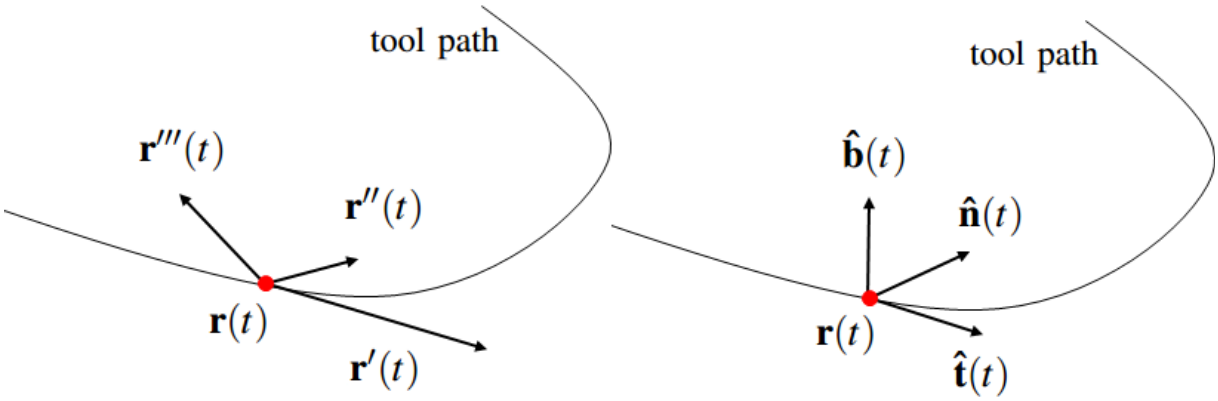

Figure 2.1: Local affine system (left) and Frenet frame (right) [8]

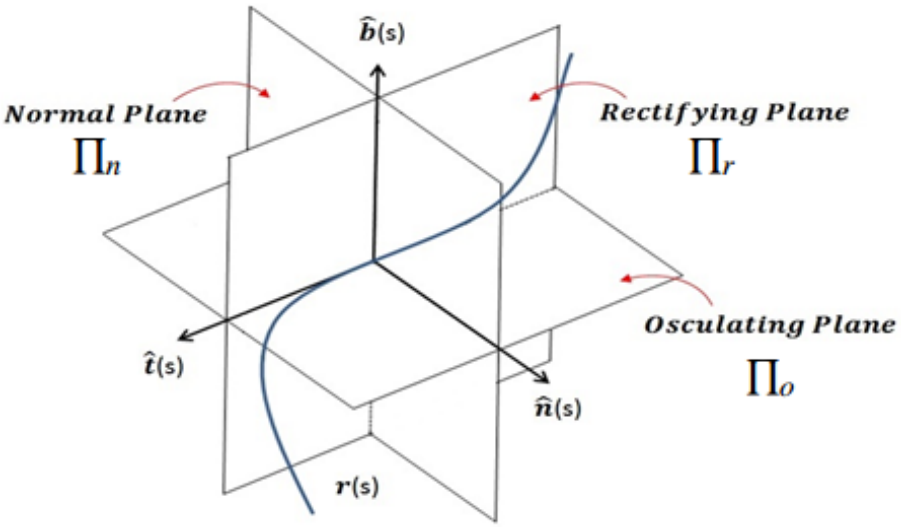

Figure 2.2: The local planes

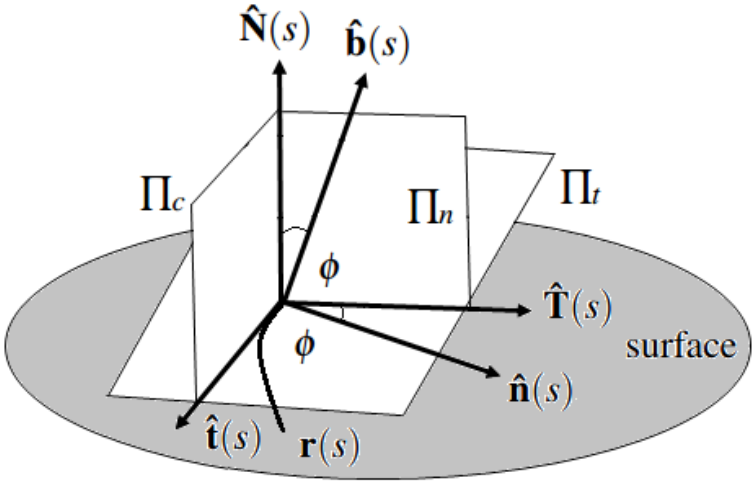

Figure 2.3: Surface Frame [30]

the surfaces of the original CAD model [3]. Indeed, in the finishing stages, the desired tool paths are derived from the surfaces on which they lie (see section 1.2). The following section therefore describes the relationships between the shape properties of the CAD model surfaces and the desired tool paths used in the corresponding machining process.

2.2 Tool paths on surfaces

Consider a tool path lying on a surface. In addition to the Frenet frame, $\mathbf{F}_1(s)$, it is possible to assign another frame, the Darboux frame, $\mathbf{F}_2(s)$, at each point on the tool path (Fig. 2.3) [30]. At a given point there is only one unit surface normal vector, $\hat{\mathbf{N}}(s)$, and an infinity of tangent vectors. These tangent vectors lie in the tangent plane that is orthogonal to $\hat{\mathbf{N}}(s)$. The tool path's unit tangent vector and the surface's unit normal vector can together be used to form a vector that is orthogonal to both, referred to in this thesis as the bi-tangent vector, $\hat{\mathbf{T}}(s)$, $\hat{\mathbf{T}}(s) = \hat{\mathbf{N}}(s) \wedge \hat{\mathbf{t}}(s)$ [30].

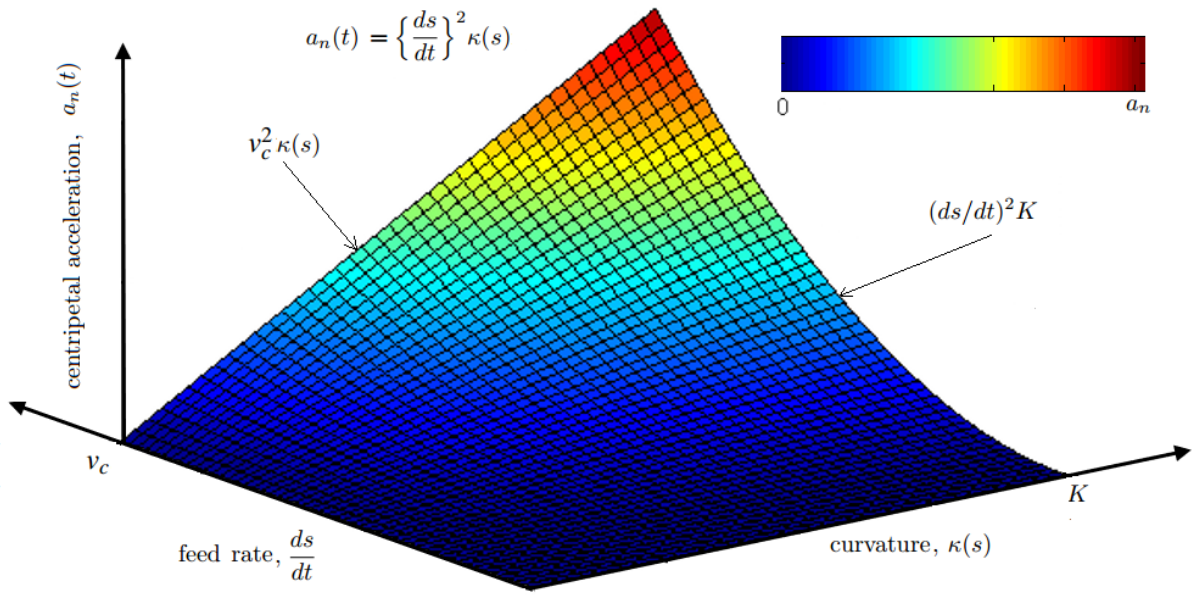

Figure 2.4: Centripetal acceleration surface

osculant, whose derivatives, up to and including order two, agree with those of the path [14]. Subsequently, normal acceleration is commonly referred to as centripetal acceleration [33].

From Eq. (2.5) it follows that normal acceleration consists of time and shape dependent elements, feed rate, ds/dt, and curvature, $\kappa(s)$, respectively. The surface, shown in Fig. (2.4), illustrates the effect of each element on centripetal acceleration, $a_n(t)$. The surface is mathematically expressed explicitly in terms of ds/dt and $\kappa(s)$, $a_n(t) = (ds/dt)^2\kappa(s)$. Centripetal acceleration (Fig. 2.5) increases linearly with curvature, $a_n(t) = v_c^2\kappa(s)$, for a constant feed rate, v_c. Centripetal acceleration increases parabolically with feed rate, $a_n(t) = (ds/dt)^2 K$, for a constant curvature, K.

xy planes.

4.2.2 Accelerometer

As shown by Eqs. (2.4), (2.5) and (2.7), to quantify the actual velocity, acceleration and jerk experienced on a given circular tool path, the achieved feed rate is required. Each of the controllers of the test machines provide a Digital Read-Out (DRO) of feed rate. This however, is not an independent source of measurement and as such can only be used as a preliminary indicator of the actual feed rate achieved in a given motion. An inertial sensor, specifically a tri-axial piezoresistive accelerometer, is used as an independent measurement source [50]. The sensor outputs the acceleration and time of a given motion. The achieved feed rate is then deduced from this acceleration profile. The actual velocity, acceleration and jerk experienced can then be found for each circular tool path from Eqs. (2.4), (2.5) and (2.7).

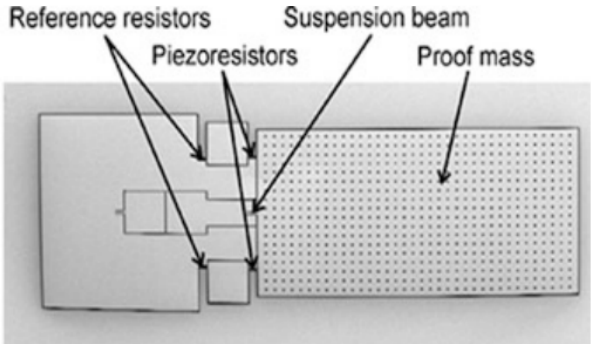

Figure 4.2: Diagram of a piezoresistive accelerometer [51]

The main principle on which the accelerometer operates is the piezoresistive effect [52]. This is a phenomenon whereby the application of mechanical stress causes a change in the electrical